

High resolution aerial and field mapping of thermal features in Ragged Hills, Yellowstone National Park

Juliane Becker, September 2004





High resolution aerial and field mapping of thermal features in Ragged Hills, Yellowstone National Park

DIPLOMA THESIS

Juliane Becker

SUPERVISED BY

Prof. Dr. Broder Merkel

Prof. Dr. Irmgard Niemeyer

Dipl.-Geol. Britta Planer-Friedrich

Freiberg, September 2004

“Change has always characterized the thermal features located in the Norris Geyser Basin.”

(Lewis 1964)



Front page: Aerial overview of the mapping area Ragged Hills, Norris Geyser Basin

Eidesstattliche Erklärung

Hiermit versichere ich, dass ich die vorliegende Diplomarbeit ohne unzulässige Hilfe Dritter und ohne Benutzung anderer als der angegebenen Hilfsmittel angefertigt habe; die aus fremden Quellen direkt oder indirekt übernommenen Gedanken sind als solche kenntlich gemacht.

Freiberg, 24.09.2004

Juliane Becker

LIST OF CONTENTS

| | |
|--|-----------|
| List of contents..... | I |
| Abbreviations..... | III |
| Abstract..... | 5 |
| 1 Objectives and deliverables..... | 7 |
| 1.1 Objectives..... | 7 |
| 1.2 Deliverables..... | 8 |
| 2 Remote sensing from low flying platforms..... | 9 |
| 2.2 Balloon aerial photography..... | 10 |
| 2.3 Kite aerial photography..... | 12 |
| 2.4 Airship aerial photography..... | 15 |
| 2.5 Model airplane and helicopter..... | 19 |
| 2.6 Single-engine light aircraft..... | 22 |
| 2.7 Camera models..... | 23 |
| 2.8 Camera control methods..... | 24 |
| 2.9 Federal Aviation Regulations..... | 25 |
| 3 Mapping area Yellowstone National Park..... | 27 |
| 3.1 Geology..... | 28 |
| 3.1.1 Precambrian to Mesozoic..... | 28 |
| 3.1.2 Cenozoic volcanism..... | 29 |
| 3.1.3 Glaciations..... | 33 |
| 3.2 Hydrogeology..... | 34 |
| 3.2.1 Hydrothermal features..... | 36 |
| 3.2 Norris Geyser Basin..... | 38 |
| 3.2.1 Geology..... | 39 |
| 3.2.2 Hydrogeology..... | 41 |
| 4 Methods applied..... | 47 |
| 4.1 Design of equipment..... | 47 |
| 4.1.1 The airplane..... | 47 |
| 4.1.2 The balloon..... | 48 |
| 4.2 Field work..... | 49 |
| 4.2.1 Ground control points..... | 49 |
| 4.2.2 Aerial survey..... | 53 |
| 4.2.2.1 Survey from the balloon..... | 53 |

| | | |
|-----------|---|------------|
| 4.2.2.2 | Survey from the Cessna | 55 |
| 4.2.3 | Ground survey..... | 56 |
| 4.2.3.1 | Mapping..... | 56 |
| 4.2.3.2 | Water chemistry - Sampling | 57 |
| 4.2.4 | Thermal photography..... | 59 |
| 4.3 | Digital Atlas..... | 62 |
| 4.3.1 | Geographical Information Systems..... | 62 |
| 4.3.2 | TNTmips..... | 63 |
| 4.3.2.1 | Creating the overview map | 63 |
| 4.3.2.2 | Digitizing the geobjects and Importing data | 68 |
| 4.3.2.3 | Creating the digital atlas | 68 |
| 4.3.3 | Geomatica | 70 |
| 5 | Results and discussion | 73 |
| 5.1 | Digital atlas | 73 |
| 5.1.1 | Working with the atlas | 74 |
| 5.1.1.1 | Navigation..... | 74 |
| 5.1.1.2 | Important tools..... | 75 |
| 5.1.2 | The groups and layers | 76 |
| 5.1.2.1 | Getting started..... | 76 |
| 5.1.2.2 | Individual layers..... | 77 |
| 5.1.2.2.1 | Groups of the overview layout..... | 77 |
| 5.1.2.2.2 | Groups of the detailed layout..... | 79 |
| 5.2 | Methods evaluation..... | 83 |
| 5.2.1 | Ground survey..... | 83 |
| 5.2.2 | Aerial survey..... | 85 |
| 5.2.3 | Digital atlas | 87 |
| 5.3 | Interpretation of mapping results | 89 |
| 5.3.1 | Morphological changes | 89 |
| 5.3.2 | Interpretation of hydrochemistry data..... | 95 |
| 5.3.2.1 | Water types | 96 |
| 5.3.2.2 | Thermography and gas activity..... | 99 |
| 5.3.2.3 | Time series of water chemistry | 101 |
| 6 | Recommendations..... | 109 |
| 7 | Acknowledgement..... | 111 |
| 8 | References..... | 113 |
| 9 | Appendix..... | 119 |

ABBREVIATIONS

| Abbreviation | Meaning |
|--------------|---|
| AAS | Atomic Absorption Spectroscopy |
| C/A – code | Clear/Access – code |
| CCD | Charge Coupled Device |
| DEM | Digital Elevation Model |
| DMAA | Dimethylated Arsenic Acid |
| EGNOS | European Geostationary Navigation Overlay System |
| EPRODESERT | Evaluation of Processes Leading to Land Degradation and Desertification Under Extensified Farming Systems in North-East Spain |
| GCP | Ground Control Point |
| GIS | Geographical Information System |
| GPS | Global Positioning System |
| IC | Ionic Chromatography |
| ICP-AES | Inductively Coupled Plasma-Atomic Emission Spectrometry |
| ICP-MS | Inductively Coupled Plasma-Mass Spectrometry |
| INEEL | Idaho National Engineering and Environmental Laboratory |
| KAP | Kite aerial photography |
| Landsat TM | Landsat Thematic Mapper |
| LCD | Liquid Crystal Display |
| MMAA | Monomethylated Arsenic Acid |
| MOGUL | Large-scale Monitoring of Gully Erosion in Semi-Arid Landscapes |
| NAVSTAR | Navigation Satellite Timing and Ranging |
| NESPAL | National Environmentally Sound Production Agriculture Laboratory |
| P – code | Precise – code |
| PE | Polyethylen |
| RPV | Remotely Piloted Vehicle |

| Abbreviation | Meaning |
|--------------|---|
| RTMC | Radio Technical Commission for Maritime Service |
| TIC | Total Inorganic Carbon |
| TOC | Total Organic Carbon |
| U.S.G.S. | United States Geological Survey |
| WAAS | Wide Area Augmentation System |
| WLAN | Wireless Local Area Network |
| YNP | Yellowstone National Park |
| YNPRH | Yellowstone National Park Ragged Hills |

ABSTRACT

High resolution aerial images taken in a cost and time effective way from low-flying platforms were used to map a hydrothermal area in the Yellowstone National Park. The mapping area called Ragged Hills is located in the Norris Geyser Basin, a major hydrothermal basin of the Park famous for its great diversity and number of thermal features. Because of an increasing thermal activity since the early 1990s numerous hydrothermal features of different sizes developed in Ragged Hills. Various changes in size and chemistry of the thermal features were observed during sporadic ground surveys. No detailed maps of the thermal inventory existed because of the difficulties in mapping this rapidly changing area by standard ground survey methods. Mapping the features in a short time to get a status quo of the feature's form and size was the goal of the present work.

Two different low-flying platforms were used during this project – a helium filled balloon and a single engine airplane (Cessna 172). To be able to georeference the aerial photos later a grid of ground control points was laid out and the points were surveyed by differential GPS as well as by theodolite. Deviations between both methods were on average 37 cm (Northing) and 61 cm (Easting). The overflights with the airplane were more cost intensive, requiring aircraft rental and trained pilots. Because the obtained images were in most cases blurred, they were served as overview only. Nevertheless the pixel resolution was quiet good with an average of 6 cm. Besides the true color images taken by a digital camera, also thermal pictures were taken from the airplane with a spatial resolution of 1.2 m. The balloon survey provided a cost-effective and easy-to-handle alternative. Major restrictions are only the transport of the helium bottles to the study site, and the requirements for calm wind conditions. From an altitude of 50 to 80 m sharp and high resolution images were obtained. About 45 pictures were used to create a mosaic of the whole study area with a pixel resolution of 2.5 cm. No high-resolution thermal pictures could be taken from the balloon because the weight of the camera (3.9 kg) exceeded the balloon's lifting capacity (1.5 kg). The created high-resolution aerial overview was included in a digital atlas together with topography and geological maps, older low-resolution aerial pictures, and hydrochemical data.

The following diploma thesis gives an overview about available low-flying platforms and their individual advantages and disadvantages, describes the methods used in detail and evaluates them regarding expenditure and time it took to realize the individual working steps. Furthermore an interpretation of mapping and hydrochemical data is presented.

1 OBJECTIVES AND DELIVERABLES

Yellowstone National Park (YNP) in Wyoming, USA, is known for its geothermal activity with more than 10,000 hot springs, fumaroles, geysers and mud pots. The thermal activity of that area is attributed to a hotspot situated below the National Park. In the Park, areas can be found where the geothermal activity has not changed since several years but also regions that undergo significant changes over short periods of time. The Norris Geyser Basin in the northwestern part of the Park is such an area. Especially Ragged Hills, located in the northwestern part of the basin, attracted attention by an increasing thermal activity since the early 1990's. Lots of new hydrothermal features with different sizes from centimeter to meter range arose and are still developing.

Since the 1970's, geology and hydrogeology were investigated repeatedly, but one problem still exists. Till now it takes too much time mapping the huge number of geothermal features in a relative short period of time to get the status quo of form and size of the geothermal structures and detect possible general trends.

This diploma thesis that is equivalent to an international master shows one possibility to solve those problems by creating a high resolution digital atlas that bases on aerial photographs of the geothermal area Ragged Hills in the Yellowstone National Park.

1.1 OBJECTIVES

For the ground mapping of the geothermal features a parameter catalogue with information on location, shape, mineral precipitation, gas activity, turbidity and others was designed to characterize the structures in a standardized way. Aerial mapping of the features with a resolution in the centimeter range was done by

- Establishing a ground survey grid with two permanent and 102 temporary marked ground control points in an area of 530m x 250m
- Surveying these points with Differential Global Positioning System (DGPS) and theodolite
- Testing a custom made construction to mount a digital camera to the single-engine airplane (Cessna 172) and a construction to mount a digital camera to a helium filled latex balloon

- Aerial survey from the airplane (from approximately 700 m altitude) and the balloon (from approximately 50 to 80 m altitude)

Thermal ground and aerial pictures from the Ragged Hills area were taken by Dr. Earl Mattson and Dr. Mitchell Plummer from the Idaho National Engineering and Environmental Laboratory (INEEL). Hydrogeochemical sampling (pH, conductivity, temperature, redox potential, Fe(II), total Fe, S²⁻, SiO₂, As(III), As(V), mono- and dimethylated As) was done at 17 geothermal features. On site parameters were additionally measured at 28 sites.

The results were processed by

- Combining the single aerial pictures to one overview mosaic with the Geographical Information System (GIS) software TNTmips version 6.8 (MicroImages),
- Presenting survey, thermal and hydrogeochemistry data in a multi-layer digital GIS atlas,
- Comparing older aerial photos with the overview mosaic,
- Analyzing the survey and sampling results.

Optimized procedures were documented.

1.2 DELIVERABLES

- Establishing a cost effective, fast and easy to handle method to get high resolution aerial photos with the help of a low flying platform
- Creating a high resolution map of the Ragged Hills area state September 2003 as a basis for further observations of changes of the geothermal features
- Providing a multi-layer digital atlas combining information from previous and the present projects
- Investigating a regional correlation between geometry of the hot springs, heat flow and hydrogeochemistry
- Drawing up a timetable for building the constructions, field work, mosaicking, arranging the digital atlas including a cost estimation regarding the equipment

2 REMOTE SENSING FROM LOW FLYING PLATFORMS

Since a helium balloon and a single engine airplane (Cessna 172) were used to obtain high resolution aerial images of a geothermal area during this project, this chapter initially introduces the process of remote sensing from low flying platforms.

Small format aerial photography from unmanned or manned low flying platforms performed with 35- or 70-mm film cameras or compact digital cameras (Warner et al. 1996) is needed for all applications that require high resolution images of particular objects and small study site's investigations. Conventional aerial photography works with large-format cameras and is normally taken from airplanes in 3050 to 6100 m (10,000 to 20,000 ft) altitude. With a photo scale ranging from 1:10,000 to 1:40,000 the vertically taken photo sequences have a standard resolution of 1 to 2 m (Aber 2004e). Usually they are updated only every few years for mapping or monitoring purposes of a region. Remote sensing from low flying platforms can close the gap between terrestrial photography and conventional airborne aerial photography (Ries and Marzloff 2003). Details can be shown that will not be recognized on the ground or in conventional airphotos and satellites images (Aber 2004e). Typical altitudes for low flying platforms range from a few meters up to several hundred meters. Photos can be taken from manned or unmanned platforms by means of color, black-white and infrared films or with digital sensors. The aerial shots may be taken high or low oblique to get a general overview of the survey site, or vertically for detailed survey and mapmaking purposes (Fig. 2.1). To transform the original, uncorrected images into orthogonal photos the x-, y- and z-coordinates of ground control points have to be used and the camera's interior orientation (camera characteristics, defined by calibration) should be known. The height information could be derived from Digital Elevation Models (DEM) that has been calculated from stereophotos for instance.

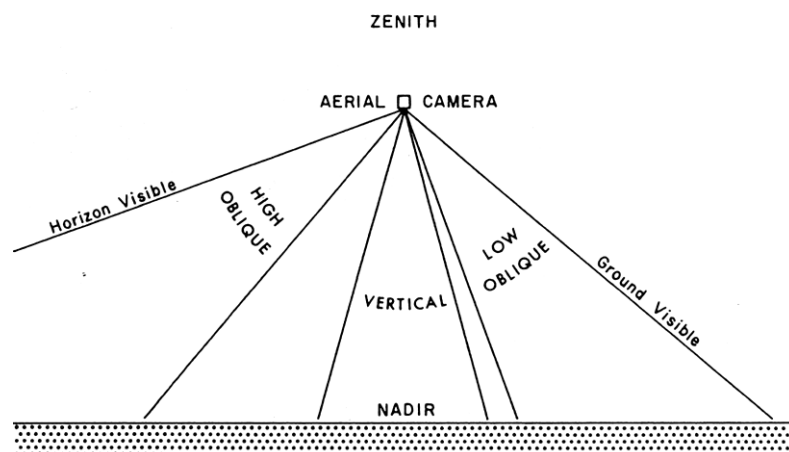


Fig. 2.1 Illustration of different views possible to take from a low flying platform (Aber et al. 1999)

As it is shown in the following sections aerial photography from low flying platforms offers many possibilities to get high resolution images for various purposes. Four of the today generally used unmanned and one manned low flying platforms and their characteristics will be described in a short overview. Additional to the individual descriptions the last three sections will inform about possible camera models, about the problem how to control the camera from the ground, and the aviation regulations that might have to be considered.

2.2 BALLOON AERIAL PHOTOGRAPHY

The first aerial photos were taken from manned, hot air balloons. In 1858, Gaspar Felix Tournachon also known as "Nadar" (Fig. 2.2) photographed the houses of the French village Petit Bicetre (Aerial Arts 2004). In 1860 James Wallace Black took the oldest existing aerial photos from Boston from a balloon. The balloon aerial photography developed fast and getting photos from a balloon got easier. When the U.S. Army recognized the advantages of aerial photography for reconnaissance, a Balloon Corps Unit was founded and aerial photography was used widely during the American Civil War (Hawkes 2004). Later it was replaced by aerial photography from airplanes.



Fig. 2.2 "Nadar" taking photos from a balloon (Burtch 2004)

Today, aerial photography from unmanned, gas filled balloons is used for example in areas where the use of helicopter or planes is too expensive and logistically difficult. Boike and Yoshikawa (2003) applied balloon aerial photography in the Arctic for geometric analysis of ice-wedge networks, quantification of patterned ground, and mapping water and vegetation, Palacio-Prieto and López-Blanco (1994) in Mexico for gully erosion evaluation.

The basic equipment for balloon photography consists of the balloon, lines, a spool, the camera (section 2.7), possibly film material, the rig for the camera cradle and its suspension. Different types of balloons can be used for aerial photography depending on the results required and maximum lifting capacity needed. Normal latex and weather latex

balloons can be distinguished. Weather balloons are designed to transport meteorological instruments upon a special altitude to get information mostly about the upper atmospheric conditions. Reaching the altitude, the balloon expands and bursts because of the low air pressure, and the instruments are transported to the ground by a parachute. Accidental premature bursting could be very risky for the photography technique. Thus, it is recommended to use heavy-duty, robust and long-lasting latex balloons that are normally tethered to the ground and recovered by pulling the tether lines down (Aber 2004a).

To get the balloon lifted it has to be filled with a gas that is lighter than air. Methan and hydrogen are not practical because they are flammable and explosive. Therefore, today, the safe noble gas helium is the most frequently used balloon gas. The amount of helium depends on the maximum load. As rule of thumb 1 L helium lifts 1 gram weight (Aber 2004d). Because of the diffusive loss of helium through the latex cover it is recommended to fill the balloon only at the survey site. Depending on the accessibility of the survey site the transport of helium in several steel cylinders is more or less difficult. Thus, it is important to reduce the weight of rig, tether lines and camera to an absolute minimum to need as little helium as possible to lift the whole construction into the air.

To operate the balloon a minimum of one person is necessary. But being controlled by one tether line the balloon with the camera can rotate and controlled navigation is impossible. Consequently, a second tether line is recommended for better maneuverability. Boike and Yoshikawa (2003) mentioned the possibility of attaching two or three additional lines to the camera suspension to improve the camera stabilization. But they also point out the difficulty managing lines and persons during the survey and the increased risk of sudden line movements and thus blurred images.

However, one crucial factor for the balloon aerial photography is the wind condition. Only calm wind conditions or very light winds allow a stable flight of the balloon. Already with wind exceeding 3 mph the balloon will get out of control and will be pushed downwards to the ground as a result of being tethered (Aber 2004d). Thus, balloon operations are generally done when winds are still calm, for example early in the morning (Palacio-Prieto and López-Blanco 1994). All in all, the handling and camera positioning with an unmanned balloon is easier than that of kite platforms described in the next section (Boike and Yoshikawa 2003).

2.3 KITE AERIAL PHOTOGRAPHY

Kite aerial photography began in the late 19th century. There are different information about the year and the person who started kite aerial photography. One of these first attempts was done by the Frenchman Arthur Batut who took aerial photos from a kite in 1888. That kite consisted of wooden bars, was covered with paper and released by a burning fuse. There are also reports about the British meteorologist E. D. Archibald who has allegedly taken aerial photos already in 1882 and 1887 (Aber 2004b). From that time on to the early 20th century continuous progress led to the development of mechanical and electrical triggers, more advanced kites, better cameras and rigs. The kites were used for many purposes - military investigation, disaster estimation and scientific survey. In the 1930s, the wide expansion of kite aerial photography was pushed back by the development of powered flight (Aber et al. 1999). Only since the 1970s and '80s its comeback slowly began. Today, kite aerial photography is again a very common and far developed method to get high resolution, large-scale aerial images at low costs with simple equipment easy to transport and to operate in the field over a wide range of weather conditions.

Kite photography is and was successfully used for various scientific investigations. Boike and Yoshikawa (2003) applied it in the Arctic where the application of helicopter or planes is too expensive and logistically difficult (section 2.2). Aber et al. (2003) have done microstructural (1:100 to 1:1000 scale) mire and vegetation investigations in Estonia. Different color and texture zones of vegetation communities within the bogs, bog microtopography, surface water, and other features were mapped. To get high-resolution, frequent imagery for environmental site investigations in Kansas Aber et al. (1999) used the kite aerial photography as cost-effective technique. During this project two different sites were studied. Complex, small, meandering stream channels were mapped and potholes within the drainage channel were located with the help of vertical kite aerial photography. The complex geometry of the stream channels and their cover by brushy vegetation excluded investigations from the ground or conventional air photos. Furthermore, the detailed structure of an upland deciduous forest was investigated by oblique kite aerial photography. This project was related to a larger study regarding forest growth where Landsat Thematic Mapper images were used to develop vegetation indices for comparison with climatic and tree-ring records. Besides other results it was concluded that Landsat TM vegetation index values under-represent the leaf-coverage or biomass within the forest canopy because of their low resolution. In 2000 a project on large-scale

monitoring of gully erosion in the frequently windy savannahs of the Sahel of Burkina Faso started (Marzloff et al. 2002, MOGUL project). Gully erosion is a well known phenomenon in arid and semi-arid regions so far supported with few quantitative data only. The images produced covered areas of 200 mm² to 4.5 ha and enabled the rectification, georeferencing and mapping of gully extent and morphology. Stereo photography allowed stereoscopic interpretation of gully morphology and erosion processes.

The basic equipment for the kite aerial photography consists of the kite, a line, a spool, the camera (section 2.7), maybe film material, the rig for the camera cradle and its suspension. There is a wide range of kites but mainly soft and rigid kites are distinguished (Fig. 2.3). Soft kites have no rigid structure and inflate with wind pressure to form an airfoil profile. Their advantages are the very low weight-to-surface ratio, the extremely easy preparing and launching and the easy transport to the survey area. Problematic is their tendency to collapse when the wind reduces. Rigid kites have a hard framework that gives form and shape to the kites. Traditionally the framework was made of wood and bamboo. Today, the most modern kites consist of graphite rods and fiberglass poles. Their ability to fly stable under light (4-7 mph) and moderate (8-12 mph) wind conditions without the danger of deflating and crashing is the advantage compared to soft kites (Aber 2004c). Disadvantages are their greater weight-to-surface ratio and the more difficult transport.

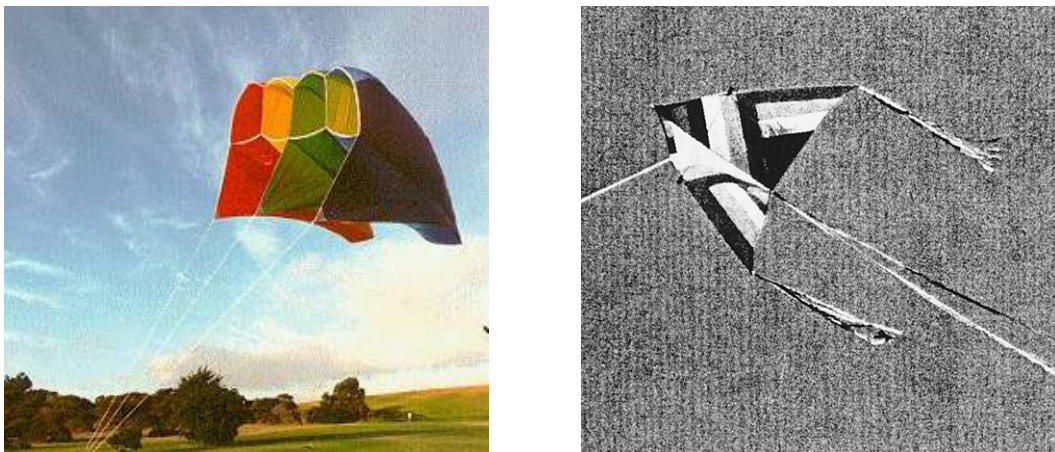


Fig. 2.3 Two main types of kites; left: soft kite (Benton 2004); right: delta-rigid kite (Aber 2001b)

Considering the main requirements of weight and bulk size, easy handling especially in cold weather conditions and stability, Boike and Yoshikawa (2003) recommended the rigid delta kite for light to moderate wind conditions and a soft parafoil kite for moderate to strong (> 6 m/s) winds. For average rigs with a weight of 1 to 1 ½ kg Aber et al. (2001) recommended a kite of 2.8 to 3.3 m² (30-36 ft²) lifting surface for moderate wind speeds of

10-15 mph. Smaller kites are used for stronger winds to lift the same load. For lighter wind, a pair of two large kites attached to the same tether line is suggested.

To avoid personal injuries the kite line should only be handled with gloves. It is also possible to attach the kite to the waist. Strongest wind conditions (> 12 m/s) force the use of a ground anchor with a figure eight ring to allow the retrieval of the kite (Boike and Yoshikawa 2003). Marzloff et al. (2002) anchored the kite to a motor vehicle because it pulled up to 400 kg in good wind conditions (Fig. 2.4). The rig and the camera (section 2.7) should be relatively small, robust and light-weighted. Dual and single camera rigs are possible to use. Dual rigs are necessary when taking infrared photos to obtain a parallel true color photo for later identification of the site (Aber et al. 2001), for stereographic photography and when operating with different focal lengths. Generally, the suspension that attaches the camera to the kite is not directly connected to the kite but flexibly attached by an additional line some meters below it. Marzloff et al. (2002) used a second line to pull a sledge-like gondola with the fixed camera along the kite line (Fig. 2.4).

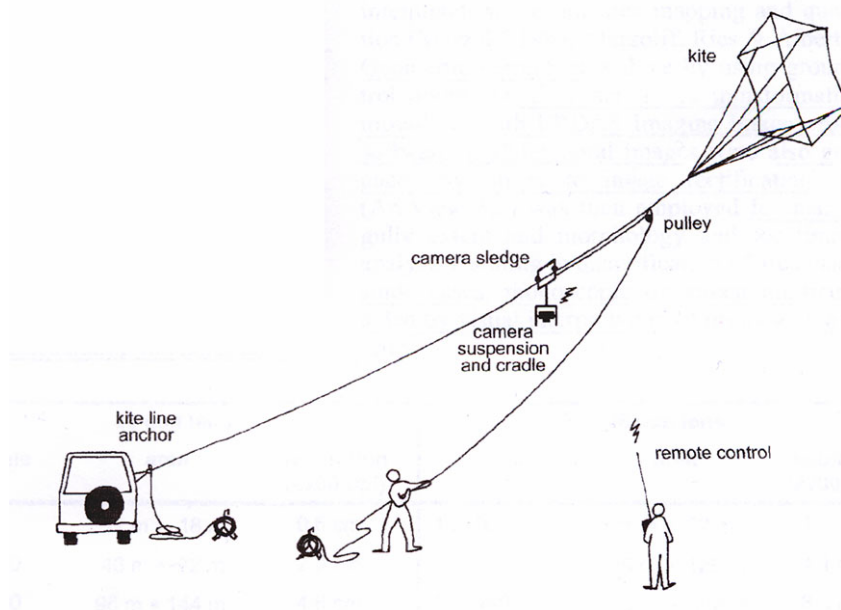


Fig. 2.4 Sketch of the kite aerial photography system used by Marzloff et al. (2002)

Because of decoupling vibrations and sudden movements of the kite and lines are absorbed and a self-leveling of the camera is possible. The two most frequently used types of camera suspensions are the pendulum and the cable and pulley suspension (Picavet platform) (Fig. 2.5 right). Boike and Yoshikawa (2003) used a simple T-shaped pendulum suspension made from a camera tripod to attach the camera directly to the kite line (Fig. 2.5 left). In that way they avoided the different handling of several tether lines.

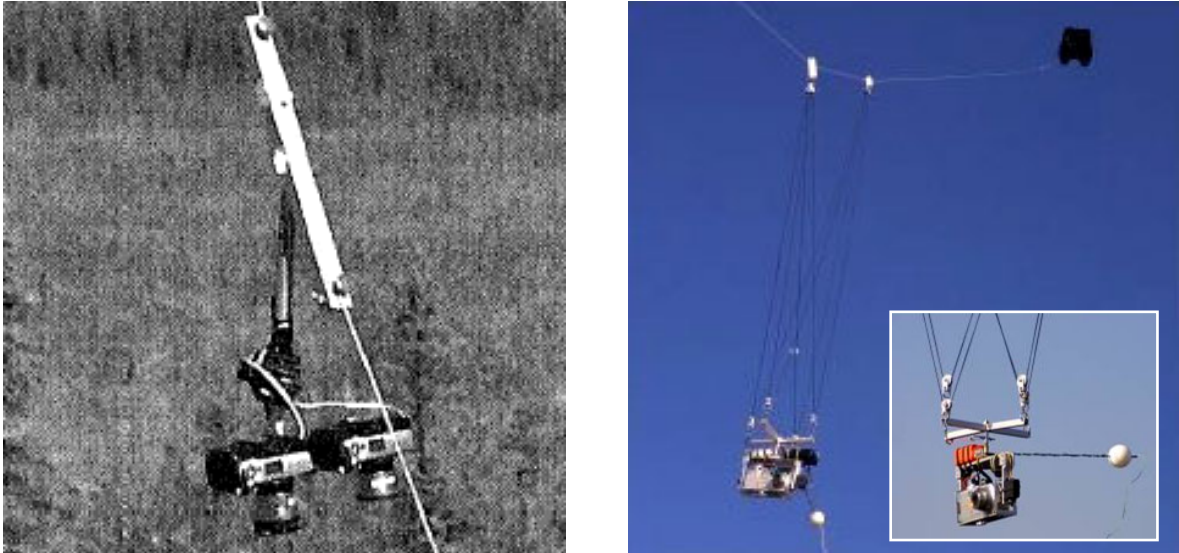


Fig. 2.5 Different types of camera suspensions; left: T-suspension (Boike and Yoshikawa 2003); right: Picavet suspension (Fuchs 2004)

Already in the early 1900s George Lawrence flew a 20 kg panoramic camera with the help of 7 and more large kites. Today, the typical payload of a kite is 0.5 to 2 kg (Boike and Yoshikawa 2003). Lightweight cameras and rigs keep the weight below 2 kg, and enable the use of smaller handhold kites. This again allows walking around and positioning the camera correctly (Charles C. Benton, written communication). Photos are typically taken from an altitude of 50 to 150 m above ground (Aber et al. 2001) being a function of line length, kite angle and wind velocity.

All in all, the kite aerial photography is a low cost alternative compared to aerial photography from manned platforms like airplanes or helicopters or from unmanned blimps (section 2.4). Kite systems are mostly easy to transport and photography can be carried out in windy regions where the balloon aerial photography is impossible to use.

2.4 AIRSHIP AERIAL PHOTOGRAPHY

Airships like balloons belong to the group of lighter-than-air crafts. In contrast to balloons that follow the direction of the wind an airship is usually powered and its heading is controlled by some means. Airships can be subdivided into four categories – the rigid, semi-rigid, non-rigid, and hot air airships (Airship and Blimp resources 2004). This section will only focus on non-rigid airships, also called blimps, and on hot air or thermal airships. From the technical point of view thermal airships belong to the non-rigid category but they

derived from the hot air balloons and are lifted by hot air in contrast to the gas filled non-rigid airships. In the following, hot air airships will be described as hot air blimps because that is the common description found in the literature. It will be distinguished between hot air and gas filled blimps. This section only describes unmanned blimp systems except the following history part.

The first flight in an own designed non-rigid airship was done by Alberto Santos-Dumont around the Eifel Tower in 1901 (Blimp History 2004). The first rigid airship LZ1 was produced by Ferdinand von Zeppelin in 1900 (Allstar 2004) and till 1917 Zeppelin's work had established Germany's lighter-than-air industry (Blimp History 2004). In America the non-rigid airships dominated. Goodyear Tire and Rubber - the most prominent company producing non-rigid airships - built its first balloon in 1912. Rigid and non-rigid airships were used during World War I and II by several military parties. Today mostly non-rigid airships are commercially used for sky advertising or smaller, tethered and remotely controlled blimps for providing television audiences with bird's-eye views of sports events (Rumerman 2004). But also scientists use manned and unmanned hot air or gas filled blimps for their investigations. In the following some projects with unmanned blimps will be presented.

Since spring 1995 two hot air blimp systems were used by the research group around Ries and Marzloff to evaluate processes leading to land degradation and desertification under intensified farming systems (EPRODESERT project). Large-scale aerial photography was necessary to study the relations between vegetation succession, geomorphodynamics and land use. The combination of an open hot-air system with the shape of a blimp is unusual

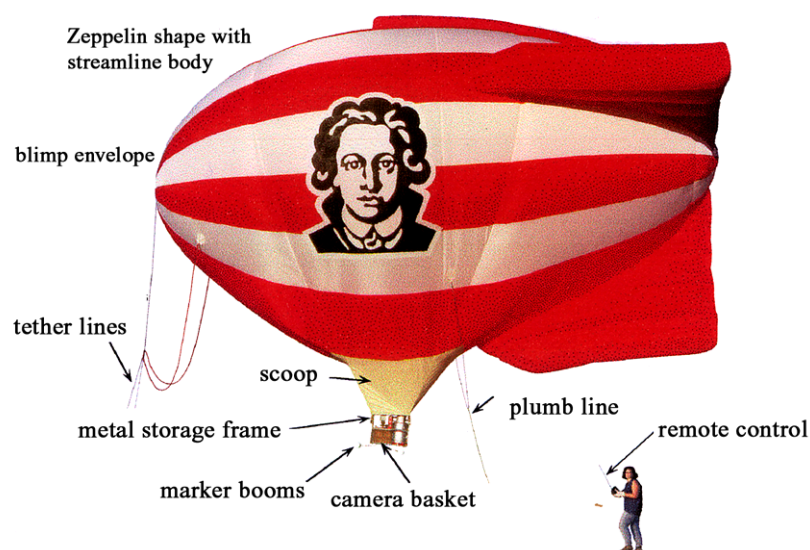


Fig. 2.6 Advanced hot air blimp system used by work group around Ries and Marzloff (2003)

but combining both systems yielded very good results that helped to understand and to document the development and dynamics of gully erosion systems. The first hot-air blimp system was a smaller one of 100 m³ volume, but its size proved to be at a critical lower limit (Ries and Marzloff 2003). Therefore a second, advanced system was employed with a volume of 220 m³.

More common helium filled blimps were used for locating dinosaurs' tracks at sites in the Rocky Mountains West and in Utah (Matthews et al. 2002a and b) and for geophysical measurements. Makino et al. (1991) monitored the geomagnetic field at low altitude in the Tanna Basin located in the northern part of Izu Peninsula and concluded that the comparison between blimp-borne and ground survey results indicated that a magnetic map could successfully be obtained from the blimp survey in remote and dangerous areas as for example volcanoes. That was done by Honkura et al. (1995) who investigated the Unzen Volcano. The first attempt in January 1992 was unsuccessful as the blimp burst on its way to the summit area of the volcano caused by the pressure difference between blimp base and summit area. The second time they reduced the payload by using no GPS but locating the blimp's situation from the earth. Therefore no precise aeromagnetic survey was possible but they got a magnetic structure of the volcano. Chase and Young (1990) used a blimp system to map shorelines and study the oceanographic forces creating and shaping these geologic features. In October 2003, Aber (2004e) conducted small aerial photography from a helium filled blimp system in North Dakota to investigate glacial landforms.

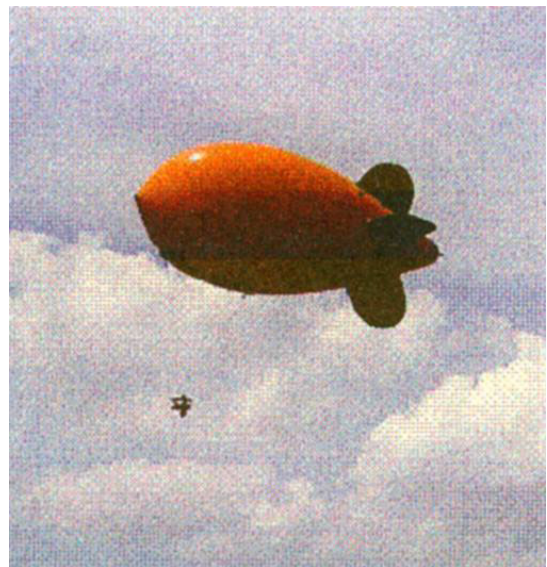


Fig. 2.7 Helium blimp used by Aber (2004d)

The basic equipment for the blimp aerial photography consists of the blimp envelope, the tether ropes, the rig for the camera and its suspension as well the camera. In addition a burner system producing hot air or helium is needed to lift the blimp.

The blimp's envelope must be robust and stable and if it is operated by hot air the material has to be fire-resistant around the burner system. Ries and Marzloff (2003) used a rip-stop nylon envelope that was not supported by a framework. The opening at the bottom was lengthened by a scoop of fire-resistant material surrounding the burner system from three

sides. The burner system consisted of four spiral burners that were powered by cheap and readily available liquid propane gas from an 8 L aluminum gas bottle. One gas bottle filling gave enough energy for about 50 to 60 minutes flying time (including inflation). As a rule, that time was sufficient to exposure two small format films (Marzloff and Ries 2000). The blimp's altitude was controlled by short intermittent blasts. It is to note that using a hot air blimp Ries and Marzloff (2003) described the inflating process as the most critical phase because wind of more than 4-7 mph will hinder the inflation. Working with helium filled blimps is less dangerous during the inflation and flight process because after the blimp is filled with helium it stays aloft until the helium slowly escapes by diffusion after several days (Aber 2004d). But regarding getting and transporting the helium there are the same problems as discussed for helium filled balloons (section 2.2).

For controlling and positioning the passive blimp from the ground tether ropes have to be attached. Ries and Marzloff (2003) used two special lightweight ropes of polyester coated dyneema (2.5 mm) attached at the blimp's nose and a third rope as plumb line marked in 5-m interval fixed at the blimp's bottom. Aber (2004d) used braided dacron with a breaking strength of 200 pounds (90 kg). Makino et al. (1991) didn't use tether ropes at all but propelled the blimp by two gasoline engines. Its flight direction 100 m above the ground was controlled by a ground operator with a radio control system. The maximum air speed was 70 km/h and in spite of little wind navigating the blimp in a special direction was trouble-free.

The carrying capacity of a blimp depends on the volume of hot air or gas the blimp contains. The helium lifting capacity of 1 g/L compared to the hot air lifting capacity of 0.2 g/L shows that helium lifts approximately five times more weight than hot air (Aber 2004d). That concludes that a hot air balloon has to be larger in volume to transport the equivalent payload as a helium balloon does. That results in a heavier blimp system that has to be transported to the study side. On the other hand helium isn't available everywhere and also has to be transported to the area of interest.

Comparing helium filled and hot air blimps Aber (2004d) concluded that considering cost and field operation, helium blimps are generally favored compared to hot-air blimps. With equivalent lifting capacity a helium blimp system is smaller, relatively inexpensive and easier to operate. Besides, helium blimps are commercially available while hot-air blimps have to be custom made which results in higher costs. If helium is not available a hot-air blimp is a practical lighter-than-air platform under low wind conditions.

It is to conclude that blimp systems are more stable in wind than balloons because of their aerodynamic shape. Blimps are vibration-free platforms for photographic survey in contrast to other large-scale remote sensing systems as model airplanes, helicopters or kites that might be impacted because of motor or wind vibrations (Ries and Marzloff 2003). The minimized camera motion reduces the number of blurred and tilted images compared to kite aerial photography (Aber 2004d). But with more than approximately 12 to 19 km/h wind speed the blimp navigation is not feasible any more (Ries and Marzloff 2003). Blimps are not suitable as well for investigating larger areas in a scale of square kilometers with overlapping images. In dependence on their weight they are more or less easy to transport by vehicle or by carrying bags.

2.5 MODEL AIRPLANE AND HELICOPTER

Unmanned, model aircraft and helicopter as remotely piloted vehicle (RPV) are well investigated and proven by the military (Warner et al. 1996). The first aerial photography from a non-military model aircraft was taken in 1939 (Harding 1989) and only since the mid 1970s reliable control equipment is commercially available. Today radio controlled airplanes are an inexpensive and resourceful technique (Thome and Thome 2000). The acquisition costs for rotary wing models (remotely controlled helicopters) are higher because of the integrated technique (Warner et al. 1996) but they are also available for commercial and scientific use.

Thome and Thome (2000) successfully used a high-wing model airplane prototype to take aerial photos remotely for testing the possibility of future habitat studies. Harding (1989) used a model airplane to take photos of reservoirs as quality surveys and also took photographs of sewage treatment. Successfully photographed Wessex Water sites convinced the company Wessex Water of adopting the system as an economical support for full size facilities. Nyquist (1994) tested a radio controlled airplane to detect waste trench boundaries from the color and character of the overlying grass, to update older aerial photos and to use repeated overflights of the same area to capture seasonal changes in vegetation and the effects of major storms.

Working with a remotely controlled model airplane or helicopter requires an aircraft model, a camera system and maybe film material, a construction that damps and absorbs the vibrations during the flight as well as a possibility to measure the altitude in some way

if necessary. Of course radio control equipment is essential to guide the aircraft. In addition the platforms are powered by gas and therefore needed to be supplied with that.

The robust aircraft should have a transportable size and enough payload capability. Stable flying qualities and a modified undercarriage for clearing lens angle are additional requests. Thome and Thome (2000) used a Knighthawk model airplane that operated for 13 minutes with one tank of gas and 4 kg (8.8 lbs.) payload. This model airplane was a medium to large high-wing trainer. They used a trainer because these types provide the highest stability and are easy to use. It is also possible to modify a model kit available at a hobby shop as it was done by Nyquist (1994) who used “Droop Snoops”, a modified “Senior Telemasters” (payload 1.8 kg / 4 lbs.). The modifications included an enlargement of the fuselage to mount the camera, a “Butterfly” wing and the added carbon fiber to reduce vibrations in the camera case. Wester-Ebbinghaus (1980) took a Schlüter model of the Bell 222 for the first model helicopter experiments, a training version without body to reduce costs and weight. The self-stabilized mini-helicopter of the Idaho National Environmental Engineering Laboratory (Robotics Division) is a Neural Robotics Incorporated Autocopter, with a lift capacity of approximately 25 pounds (11.3 kg) at sea level. It maintains position at whatever altitude is desired and the operator, without any helicopter piloting experience, can move the helicopter via joysticks on the transmitter. An innovative neural network control system maintains the flight stability. Furthermore the unit includes a dual backup system. An autorotation flight mode enables the helicopter to land powerless in case of engine failure. In addition a deployable parachute is integrated into the system.

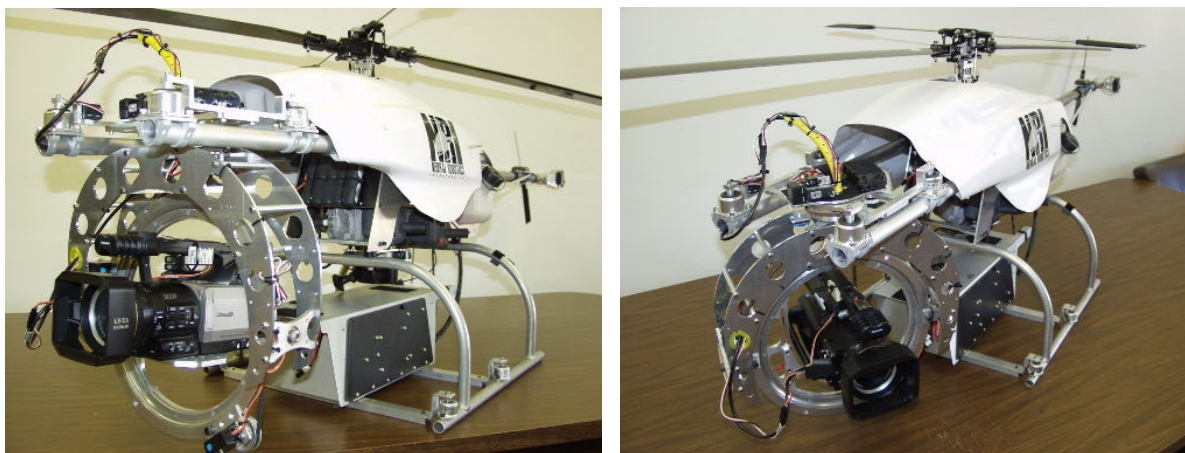


Fig. 2.8 Neural Robotics Inc. Autocopter from INEEL

That it is important to use robust models was proved by Wester-Ebbinghaus (1980) because of limited experience with the conventional mechanical equipment the helicopter was overloaded which was recognized after 8-10 hours of flying by abrasion of transmission gears.

To protect the camera system against vibrations and thus to prevent blurred images Harding (1989) housed the camera in custom made foam cradles. Wester-Ebbinghaus (1980) fixed the camera within a case of polystyrene walls to suppress the vibrations of the motor and rotary wing of the model helicopter used. High shutter speed is an additional possibility to reduce blurred images. A further problem that makes high shutter speed necessary is the flying speed of the model airplanes or helicopters. The faster they fly the higher the risk that the images are blurred. Therefore with a moderately slow speed at a low altitude a high shutter speed is necessary for high quality images. Nyquist's (1994) "Droop Snoop" was able to fly 15 to 20 mph and slower when turned into the wind. That means with a speed of 15 mph the plane covered about 0.26 (0.6 cm) inches in 1/1000th of a second and so the images were not blurred. Payload also influences the flying speed because carrying more weight the model airplane has to fly faster - about 5 mph for each additional pound. That results in less time over the target and poorer picture quality (Nyquist 1994).

To know the scale of the images taken it is necessary to know the altitude of the model aircraft. One possibility is to fix a GPS that takes coordinates and altitude in a preprogrammed interval or to use ground control points to be able to georeference the images later. Thome and Thome (2000) used a barometer based altimeter to calculate the altitude. Upon reaching a preprogrammed altitude the altimeter triggered a strobe light on the airplane. If the airplane deviated from that height the light ended flashing until the correct altitude was reached again. The optimal altitude for taking photos with a strobe signal is 30 to 160 m (98 to 524 ft), at heights up 180 to 210 m (590 to 600ft) visibility is poor and a spotter viewing the airplane through binoculars is necessary. If a radio transmitter wired to the altimeter transmits a signal at the desired altitude the strobe light would no longer be necessary.

Inexpensive, high-quality, fine-scale aerial photographs are the result of using model aircrafts as low flying platforms. Furthermore, Harding (1989) described the economic acquisition, operation and repair, the ability of low operating altitudes, the independence from full size airfield facilities and the immediate availability as the advantages of model

aircraft photography. As disadvantages he emphasized the limited ground coverage and the dependency on a practised and qualified operator. Thome and Thome (2000) mentioned the limitation of the necessary runway during takeoff but they point out that dirt roads are sufficient for this purpose. Nyquist (1994) solved that problem by taking a hand launched model airplane. Nevertheless, to land that one also a clearing is necessary. Further advantages are no problems with powerlines compared to low flying platforms controlled by tether lines and with disturbances of nearby residents especially in urban regions. In addition these systems are not significantly weather dependent and very quick for application. Generally, a crew of two people is necessary – an experienced pilot to fly the plane and a spotter to launch the plane and to instruct the pilot (Nyquist 1994).

2.6 SINGLE-ENGINE LIGHT AIRCRAFT

Speaking about single-engine aircrafts high-, middle and low-wings can be distinguished. Low- and middle-wing aircrafts present more problems for the oblique aerial photography because it requires steeper banks to get a clear view for the camera past the wings. The advantages of low-wing aircrafts are the better handling abilities in windy environment and a better upward visibility (Warner et al. 1996). For oblique photography through open side windows and for vertical aerial photography from externally mounted platforms high wing airplanes are more suitable. More professional equipments use camera holes in the airplane's fuselage (Warner et al. 1996).

An additional problem of the aerial photography from single-engine aircrafts is the necessity to fly tight turns slowly. Steep banks combined with slow airspeed are prone to stalls or spins. Regardless of whether using a high-wing or low-wing aircraft definitely two persons are needed for aerial photography from single engine aircrafts: the pilot concentrating on navigation and a co-pilot operating the camera.

Single-engine aircrafts are used in different ways. The NESPAL Precision Farming Team (NESPAL 2004) uses the cheap and simple technology of low-level aerial photography by a single-engine airplane to supervise growing crops. With the help of a camera mounted in the bowel of the aircraft true color and infrared aerial photographs of fields are taken. The maps of crop yields obtained at a reasonable cost enable the growers to assign resources, concentrate on crop growth problems and improve profitability of their farm operation. In California (USA) vineyards are monitored by using single-engine aircrafts to get a precise

snapshot of the vineyard's development (Tulsa World 2004). Anthony et al. (1995) mounted a video camcorder in a single-engine aircraft to investigate nesting density in black brant colonies on the Yukon Delta National Wildlife Refuge, Alaska during 1990 and 1992. They flew a Cessna 206 aircraft and fixed the Hi-8 camcorder over a 15-cm floor port near the aft bulkhead. The flown transects ranged from 1.2 to 2.5 km (0.7 to 1.5 miles) with a width of 10 m (30 ft) at an altitude of 140 to 155 m (460 to 508 ft). They concluded that aerial videography referenced with GPS is a flexible, precise and efficient method to estimate populations of nesting brant. Compared to conventional photography the much lower equipment and operating costs as well as the wide range of suitable light conditions are decisive advantages. Limiting criteria of this application pointed by Anthony et al. (1995) were that the investigated subject has to be stationary during the survey and easily distinguishable by colors.

All in all single-engine aircraft aerial photography enables to cover larger areas than unmanned aerial platforms. Additionally, the investigations are independent from the accessibility of the survey area. The (rental) costs for the aircraft are much higher and an experienced pilot has to fly the aircraft. A small terminal and fuel to operate the engine are prerequisites. Difficulties with blurred images can be avoided by slow flying and low exposure times.

2.7 CAMERA MODELS

For local, large-scale area mapping small format aerial photography is seen as a low-cost alternative to large-format photography (Mason et al. 1997). Today, it is possible to decide between using a digital or an analogue small format camera model (Single Lens Reflex or point and shot camera). Both offer small and robust cameras with light-weight plastic bodies and zoom lenses. Also automatic light control (shutter and aperture), film advance and automatic trigger of the photos (section 2.8) are important features of modern small format cameras. The advantages of digital cameras vis-à-vis film-photographic systems are among other things the direct computer-compatible output, the in-flight viewing of imagery, the dynamic range of digital cameras of about 12-bit (6- or 7-bit typical for films), and the higher sensitivity of the CCDs in the near-IR (Gupta 2003). Furthermore digital sensors have a better geometric stability (no film deformation) and better radiometric image quality (Mason et al. 1997). No film development or scanning is necessary and no chemical waste remains. Some digital cameras also offer the possibility

of filter attachment to separate specific spectral bandwidths (Boike and Yoshikawa 2003). One disadvantage is that digital images from low cost cameras have a lower resolution compared to analogues photogrammetric imagery (Mason et al. 1997). Thus a scanned conventional positive, negative or slide could have a better resolution taking a professional image scanner (up to 8000 dpi), but it is to point out that while scanning geometrical distortions of the image may occur (Luhmann 2000). Furthermore a second important influencing factor is the film resolution that is determined by the granularity (Warner et. al 1996). A film with fine grains has a higher spatial resolution than a film with coarser grains (Gupta 2003). Thus the end resolution of a scanned conventional positive, negative or slide is not just a result of the scanners but also of the films resolution.

However, the maximum resolution of the digital camera or of the film limits the altitude to pick the features in the required resolution. Of course, it is also possible to use video cameras. Larger cameras for medium-format aerial photography may be used for special purposes, as well as active scanners e.g. radar or laser scanning devices. Independent of using a digital or an analogue camera the overall contrast and brightness will decrease with increasing altitude due to atmospheric backscatter.

2.8 CAMERA CONTROL METHODS

There are different possibilities to operate the airborne camera from the ground. The cameras themselves offer several possibilities as the camera timer or the camera interval timer. The last one is recommended because it takes photos in a pre-set interval of seconds or minutes. The camera timer just takes one picture after the expired time. That means to launch and to position the low flying platform fast. A more comfortable possibility is the usage of radio controlled exposure. Radio controls are standard model-airplane components modified to activate servos on the rigs of low flying platforms (Aber et al. 2001). They enable to take pictures from any desired location in user-defined time intervals but need extra equipment and handling. Using a 4-channel system enables to rotate and tilt the camera and to activate the shutter when reaching the target area. But because of weight problems the system is often used without rotation and tilt system. When buying and using radio control instrument one should keep in mind that radio frequencies approved for remote control may differ from country to country.

Also mechanical shutter systems as rotating systems of pegs and reduction gears were developed to take pictures. User-installed timer and wires that run to the shutter release contact are other possibilities. Simultaneous photography by a double or triple camera rig is also possible by triggering the cameras simultaneously using DigiSnap (Boike and Yoshikawa 2003). Digital cameras often have the option for a remote control accessory; however, if it is based on IR (infrared) the distance is limited to a few meters. In contrast Bluetooth offers remote control depending on the type up to 100 m. Not yet a standard application but radio transferring the images online (e.g. by means of WLAN) offers new challenges as shots with visual control.

2.9 FEDERAL AVIATION REGULATIONS

Before operating any of the unmanned low flying platforms described before, one should be informed about aviation regulations of the corresponding country. In the United States, the Federal Aviation Regulations (<http://www.chem.hawaii.edu/uham/part101.html>) control the work with low flying platforms. In Germany it is the DFS Deutsche Flugsicherung (<http://www.dfs.de>). Any application in more than 500 ft (USA) or 100 m (Germany) above ground requires a permit from the respective Federal Aviation Agencies. Generally roads, bridges, trees, power lines or cables, radio towers and airports as well as water bodies should be avoided. For single-engine airplanes and echo class airplanes (manned) 500 ft is the minimum required by the most national aviation regulation authorities. For distinct areas (e.g. national parks, congested areas) 2000 ft above ground may be required.

3 MAPPING AREA YELLOWSTONE NATIONAL PARK

Being located halfway between the equator and the North Pole at the 45th parallel the Yellowstone National Park (9000 km²) belongs to the Northern and the Middle Rocky Mountains Provinces. Politically it belongs mainly to the state of Wyoming and partly to the states of Idaho and Montana. It was founded in 1872 as the world's first National Park and from the geological point of view it is probably the most famous "hotspot" site.

A broad, undulating, relatively flat plateau at about 2350 m (7700 ft) above sea level characterizes most of the park's topography. It was formed by diverse violent volcanic eruptions. Explosive blasts were followed by lava flows that filled the caldera structures. Furthermore, the landscape was smoothed by prehistoric glaciers. Today, Yellowstone National Park is surrounded by different mountain ranges. The eastern and the northern boundaries are formed by the Absarokas Mountains of volcanic origin. The Washburn Range being geologically related to the Absaroka Mountains is located in the north-central part of the park. The Beartooth Mountains border the Park to the northeast and the Grand Tetons to the south.

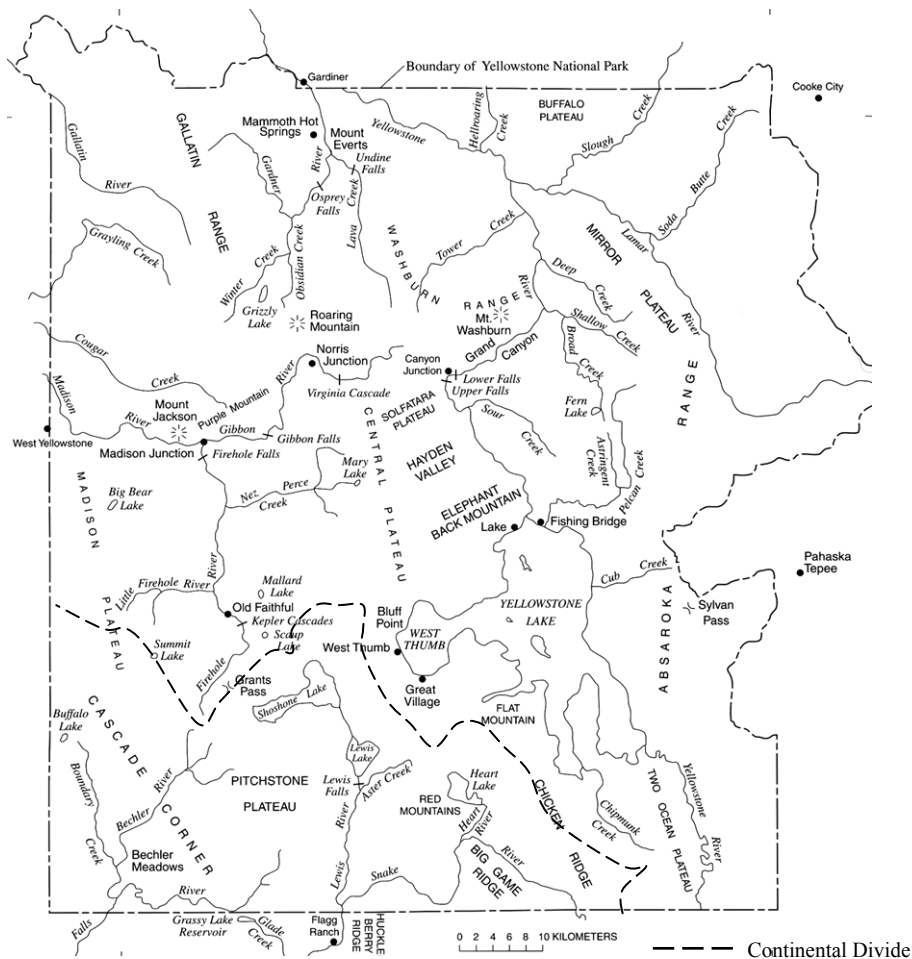


Fig. 3.1 Yellowstone National Park in detail (Christiansen 2001b)

The four great rivers Yellowstone, Madison, Green and Snake origin in the Yellowstone area and drain into the Pacific respective Atlantic Ocean. The Continental Divide runs through the southwestern part of the plateau (Fig. 3.1). Several large lakes are situated on the plateau – by far the largest one is the Yellowstone Lake in the southeast.

The vegetation of the area is characterized by near-desert vegetation to subalpine meadows and forests. Lodgepole pine covers 60 percent of the park and makes up 80 percent of the forests.

3.1 GEOLOGY

3.1.1 PRECAMBRIAN TO MESOZOIC

The oldest rocks that can be found in the park area are the 2.7 billion years old Precambrian metamorphic and plutonic basement rocks (Fig. 3.2; Fritz 2003). Most of the plutonic rocks are pink granites rich in potassium feldspar. The metamorphic rocks gneiss and schist are exposed in the Gallatin Range along the north-central edge of the park and in surrounding ranges such as the Beartooth Mountains and Madison Range (Kiver and Harris 1999). The Paleozoic and early Mesozoic age were comparatively quiet. Marine conditions predominated on the western edge of the eastward-moving North American Plate. Sedimentary rocks were deposited in shallow seas, swamps, rivers and lakes. In the early Mesozoic time the North American Plate began to move westward and collided with the

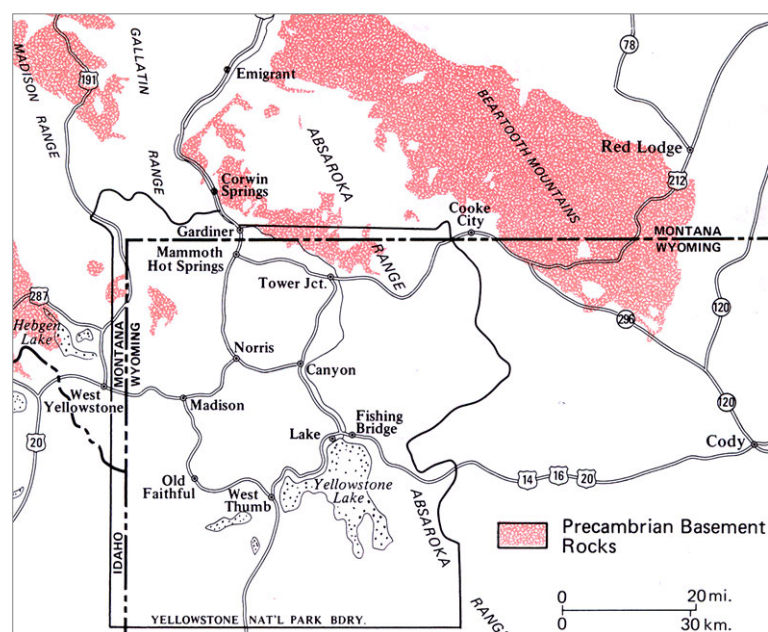


Fig. 3.2 Major exposures of Precambrian crystalline basement rock (Fritz 2003)

Pacific Ocean Plate and at least two smaller continents. The following Laramide Orogeny (100 and 50 million years ago) formed the wide-ranging anticlinal and overthrust structures of the Middle Rocky Mountains. The area was tilted and uplift continued till 50 million years ago. Today the remnants of the Paleozoic-Mesozoic time can be found in the Gallatin Range, along the northern edge of the park and in an area south of Heart Lake (Kiver and Harris 1999). All other places are covered or destroyed by the following Cenozoic volcanic events.

3.1.2 CENOZOIC VOLCANISM

Up to the Laramide Orogeny the geologic history of the Yellowstone area was similar to other Rocky Mountain areas. That changed with the beginning of volcanism following near the end of Laramide Orogeny about 40 to 50 Ma ago during the Eocene Epoch (Kiver and Harris 1999). Volcanoes started to erupt in today's central Idaho, southwestern Montana, Yellowstone and northwestern Wyoming. The Absaroka Volcanic Supergroup developed and andesite breccias, basalt lava flows and other volcanic deposits formed the Washburn and Absaroka Ranges. Magma intruded into the pre-Tertiary sedimentary rocks making up stocks, sills, dikes and laccoliths. The Absaroka volcanoes stopped erupting about 40 million years ago. Uplift as well as erosion dominated in the Park until volcanism started again about 2.5 million years ago in a region today called Yellowstone Plateau Volcanic Field (Fritz 2003).

The climaxes of three large volcanic eruptive cycles occurred in the Yellowstone area between two million and 600,000 years ago. Sporadic smaller eruptions continued until about 70,000 years ago. During one large eruptive cycle two caldera-phases can be distinguished. The pre-caldera-phase is characterized by lava rising to the surface, followed by a large climactic explosion. Because many cubic kilometers of material are ejected from a magma chamber, its roof collapses and a circular to elliptically shaped volcanic depression called caldera is formed. The post-caldera-phase is typified by periodically extruding great volumes of rhyolite that fill the caldera and leak over its edge. Besides the climax eruption each volcanic cycle includes smaller explosions and lava flows.

As mentioned above three eruptive cycles occurred in the Yellowstone area. Two million years ago the first climactic eruption produced more than 600 cubic miles of mostly rhyolitic magma (Fritz 2003). The precise dimension of the first caldera (Huckleberry Ridge) is not known (Kiver and Harris 1999). The second eruptive cycle was smaller and had its climax around 1.3 million years ago. The so-created Henry's Fork Caldera occurred several miles west from the first one in the Island Park of Idaho located west of the park boundary. Sixty-seven cubic miles of welded-ash were ejected and formed the Mesa Falls Tuff. After the end of the second cycle the next 500,000 years lava periodically extruded from the central part of Yellowstone Plateau Volcanic Field. The third eruptive cycle climaxed 600,000 years ago and created the youngest caldera, today known as the Yellowstone Caldera in the centre of the park area (Fig. 3.3). It overlaps with the Henry's Fork Caldera resulting from the second cycle. The Yellowstone Caldera is more than 47 miles long and 28 miles wide (Fritz 2003). Much of this caldera can still be noticed as a series of low hills around the central Plateau. The three eruptions were 2500, 280 and 1000 times larger than eruption of Mount St. Helens in Washington State 1980 (Smith and Siegel 2000).

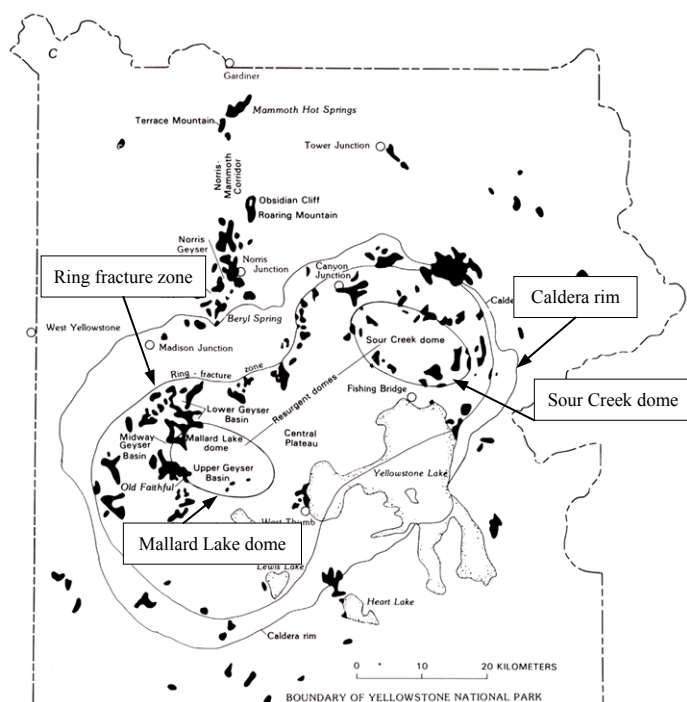


Fig. 3.3 Today's situation of the Yellowstone caldera, the domes and the ring fracture zone (White at al. 1988)

Among the irregular and few explosions from 600,000 up to about 70,000 years ago one formed a secondary caldera 150,000 years ago, today's West Thumb Basin. Between 80,000 and 70,000 years ago the youngest rhyolite lava flows (Pitchstone Plateau) and other flows extruded. Since this time no lava was produced.

During the explosive eruptions about 240 cubic miles³ of ash, pumice and blocks of rock were hurled into the air. The ash-flow deposits – some over 305 m (1000 ft) in depth – were trapped by hot rising gases and fused together forming the welded tuff formations that cover much of Yellowstone National Park today. The Lava Creek Tuff is the most predominant one. Regarding extruded lava flows rhyolitic ones dominated. They

controlled the dimensions of the caldera lake developed after the eruptions and formed the subsurface of the Madison, Central, Pitchstone, and Mirror plateaus. Only a few basalt flows are known today.

But what caused the volcanic events in the Yellowstone area? The ground at Yellowstone emits thirty to forty times more heat than the average of North America (Smith and Siegel 2000). It is second only to California considering the number of earthquakes (Smith and Siegel 2000). A partly molten plume in the upper mantle, only about 125 miles beneath earth's surface, is proved by geophysical investigations with the help of seismic tomography (Smith and Siegel 2000). Satellite radar interferometry showed that between Old Faithful, Fishing Bridge and Canyon two active areas of uplift and subsidence can be detected (Dzurisin et al. 1999). The theory favored today to explain these phenomena is the existence of a hotspot beneath the Yellowstone area.

The traditional idea of hotspots is that of continuous columns or plumes of molten rock that begin at the boundary between the earth's core and lower mantle. From there the molten material rises upward vertically through the entire mantle and crust.

The Yellowstone hotspot is more multifaceted. From the geophysical observations mentioned before it is known that the partly molten plume begins in the earth's upper mantle at about 125 miles beneath the surface. The seismic studies found no evidence of

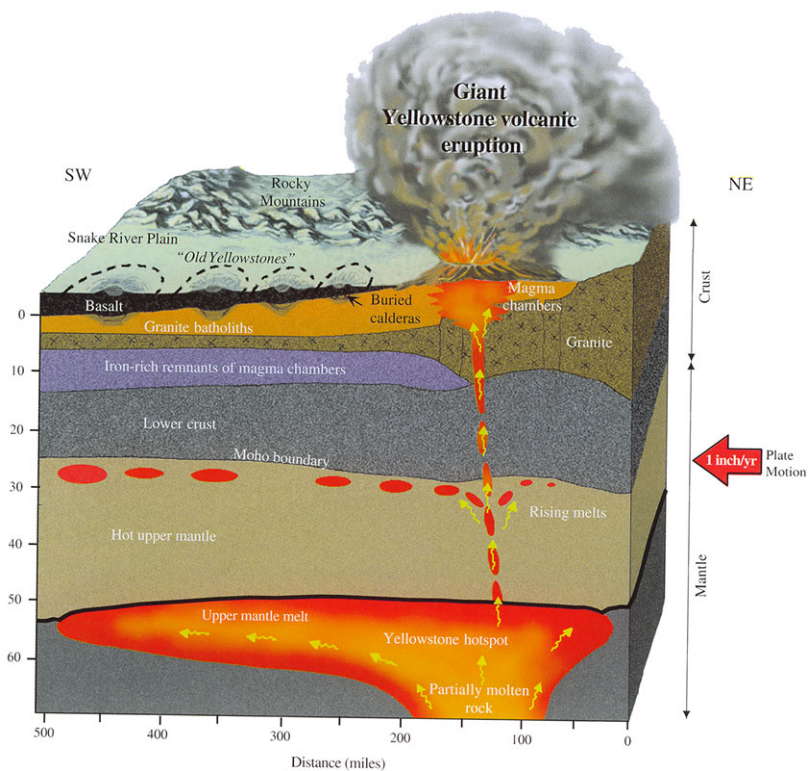


Fig. 3.4 Cross section of the Yellowstone hotspot (Smith and Siegel 2000)

molten or partly molten rock deeper than 125 miles. It seems that the heat rising from deeper within the earth partly melts rock that forms a plume. The nearly 50-miles-wide column of hot rock contains also some molten rock slowly flowing upward until it is stopped by the overlying North American Plate. There at the base of the plate and a depth of 50 miles the molten material forms an iron-rich basaltic magma pool with 300 miles width from side to side (Fig. 3.4). Blobs of molten material periodically rise through the rest of the upper mantle and into the earth's crust. There it heats the overlying crystal rock and creates a "magma chamber" with partly molten silica-rich crustal granite that is known as rhyolite when it erupts. The magma chamber begins about 5 miles beneath Yellowstone caldera and extends 8 miles deep. It may be as shallow as 3 miles in the northeastern caldera (Smith and Siegel 2000). Because the molten rhyolite is silica-rich, it is very viscous and thus the major eruptions of Yellowstone are very explosive.

As most other active hotspots the Yellowstone hotspot is located far from a plate boundary, but in contrast to most hotspots it is located beneath a continent instead of the seafloor. It is not only the largest hotspot under a continent but also among the largest of some thirty active hotspots on earth (Smith and Siegel 2000).

Because the North American Plate drifted southwestward over the Yellowstone hotspot away from the Middle Oceanic Ridge with about an inch per year an arc-shaped belt of mountains and earthquake epicenters borders both sides of the Snake River Plain lowlands. Additionally a chain of gradually younger calderas stretches along its way from the Idaho-

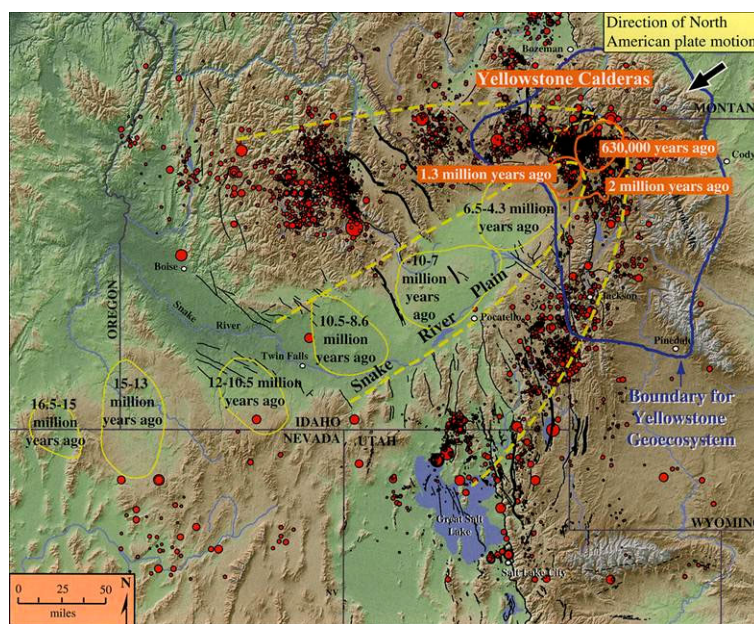


Fig. 3.5 Path of the Yellowstone hotspot (Smith and Siegel 2000)

Oregon-Nevada border 500 miles northeast up to Idaho's Snake River Plain and Yellowstone in Wyoming (Fig. 3.5). Since 2 million years the hotspot is located beneath the Yellowstone area.

Although greater volcanic events didn't appear in the last millenniums there are some indications for the existence of the hotspot and the movement of the plate even today. As mentioned above the Yellowstone area is rich in earthquakes triggered by the movement of molten rock and a continuous spreading. Furthermore, during 1923 and 1984 a rising of more than 3 feet was observed in central Yellowstone. After 1984, the caldera floor sank again. Thousands of small earthquakes appeared between 1985 and 1986. In 1995, the caldera floor had dropped by 8 inches. In 1995 and 1996 it began to rise again (Smith and Siegel 2000). This "breathing" is typical for calderas doing that for a long time without erupting.

3.1.3 GLACIATIONS

With the beginning of the Pleistocene and after the last volcanic eruption a cooling of the climate occurred and glaciers developed in the high mountains around the Yellowstone Plateau. The glacial events were partly triggered by volcanic eruptions. The "volcanic winters" started because particles blown into the atmosphere during an eruption lowered the intensity of the sun's radiation and thus enabled the cooling of the earth. Therefore the volcanic and glacial events overlapped.

Two main periods of glaciations shaped the surface of the Yellowstone area. The Bull Lake glacial events occurred about 200,000 – 130,000 years ago (Kiver and Harris 1999). The early Wisconsin glaciation started about 70,000 years ago. The most recent Pinedale glaciation took place about 30,000 – 13,000 years ago (Kiver and Harris 1999). Today, mountain glaciers are most common in the area (Fritz 2003).

During at least Bull Lake and early Pinedale time ice cap glaciers covered the Yellowstone Plateau. Outlet glaciers moved northward down the Yellowstone River Valley, westward through West Yellowstone in the Madison Valley, and southward across the Continental Divide into Snake River valley. The glacially scoured landforms give evidence for that time. Besides glacial outwash as well other glacial-derived sediments are deposited in thick layers all over the Yellowstone Plateau. Valleys were carved, smaller lakes were hollowed out and the Yellowstone and Jackson Lake were deepened.

3.2 HYDROGEOLOGY

About 70 percent of the world's active geysers and many hot springs are located along the Firehole River valley at the western side of the Yellowstone National Park (Kiver and Harris 1999). In total the Park contains about 10,000 hydrothermal features. From these 3 percent are geysers and the rest spouters, hot springs, mudpots as well as fumaroles. The spatial distribution of the geothermal features is mainly confined to the 600,000-year-old Yellowstone caldera and a zone of faults extending from the Norris Geyser Basin northward to the Mammoth Hotspring Terraces.

The thermal features are the surface manifestation of the increased heat flow occurring in the Park. In most regions of the earth's crust the temperature gradient averages about 1 °C (33.5 °F) per 33 m (108 ft). While drilling a test well at Norris Geyser Basin, one of the major hydrothermal basins of the Park, during the late 1920s a temperature of 205 °C (401°F) was observed at a depth of 80.8 m (265 ft). That means the ground temperature gradient is 50.5 °C (123°F) per 30.5 m (100 ft) – nearly fiftyfold higher than the average gradient (Schreier 1999).

Three components are necessary to get a hydrothermal feature – heat, water and a “plumbing” system (Fig. 3.6; Kiver and Harris 1999). In the Yellowstone area the heat is coming from the magma chamber heating the overlying salty water that again warms up the shallower groundwater (Smith and Siegel 2000). Rain and snow infiltrate into the

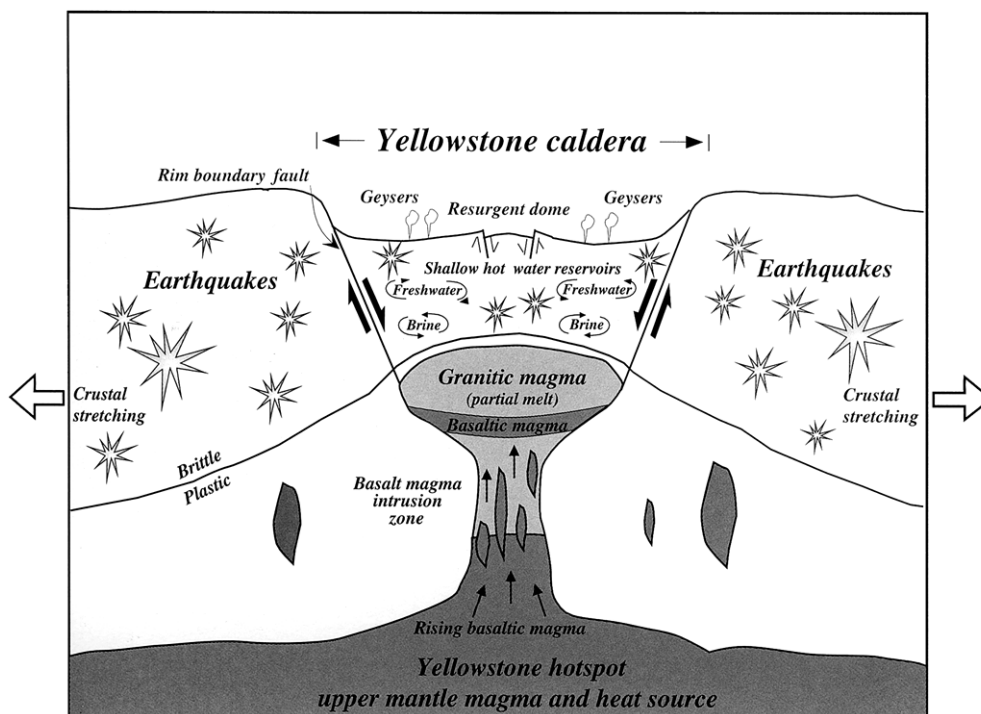


Fig. 3.6 Interaction between volcanism, earthquakes and thermal features (Smith and Siegel 2000)

groundwater system and provide the water source. Underlying fractures in the caldera rock enable heat transport by convection. Because hot water is less dense than cold water it rises to the surface along the fractures discharging usually in topographically lower areas between lava flow fronts.

As the acidic fluids flow through the rhyolite and other rocks minerals are dissolved. Rising upwards the water cools and minerals precipitate, for example silica dissolved from rhyolite, volcanic ash or tuff. If the silica is precipitated beneath the surface it cements the loose glacial sediments covering the Yellowstone Plateau and the rock becomes less permeable for water movement. This zone can typically be found in about 25 to 50 m (80 to 160 ft) depth (Kiver and Harris 1999). The up-heated groundwater trapped underneath gets overpressurized and escapes through cracks or where the gravel is still not cemented. Earthquakes can also break up clogged systems. Silica that is carried to the surface is deposited in rings and mounds around the vent as gray colored siliceous sinter, also called geyserite.

Another form of deposition appears at carbonate-depositing spring system Mammoth Hotspring Terraces where the underground doesn't consist of silica-rich volcanic sediments but is underlain by limestone deposits. The up-heated groundwater is rich in carbon dioxide rising from the magma chamber and dissolves large amounts of calcite while rising upward. When emerging at the surface carbon dioxide degasses from the water to the atmosphere and the ability to contain calcium in solution is reduced (Kiver and Harris 1999). Thus, the calcium carbonate is deposited and forms the remarkable Mammoth Hotspring Terraces.

Gases that degas at the surface include carbon dioxide, hydrogen sulfide, methane, hydrogen, oxygen, nitrogen, ammonia, argon, radon as well as other noble gases such as helium, neon, krypton, and xenon (Schreier 1999).

Diverse plant communities, algae and bacteria colonies live in and near the thermal waters. Water chemistry and temperature determine where which species live in a run-off channel of



Fig. 3.7 Mix of colors – resulting from algae, bacteria as well minerals deposition

a discharging feature (Fig. 3.7). Near its source a run-off channel is nearly clear or white. Only a few strangely heat-adapted archaea bacteria can live in boiling water about 100 °C (hyperthermophiles). At temperatures above 60 to 62 °C (140 to 144 °F) also only prokaryotes as bacteria and archaea are able to live (Brock 1994). Furthermore the non-photosynthetic bacteria exist under higher temperature conditions than the photosynthetic bacteria. Eucaryotic microorganisms as algae are unable to adapt to higher temperatures than about 60 to 62 °C (140 to 144 °F). But besides the temperature also the water chemistry limits the biosphere for algae and bacteria – for example photosynthetic prokaryotes as cyanobacteria are not present in acid waters. In contrast the main alga of hot (up to 56 °C) acid water is *Cyanidium caldarium* (Brock 1994). In colder acidic water thick long strands of a brown filamentous alga (*Zygogonium*) are observable (Schreier 1999).

Also mineral precipitations can influence the color of a hydrothermal feature and its surrounding area. Iron hydroxides and oxides appear as pink to red and orange precipitations, sulfur minerals as yellow deposits.

3.2.1 HYDROTHERMAL FEATURES

Most of the hydrothermal features occurring in the Yellowstone Park are **hot springs** formed when the up-heated water rises in open conduits without constrictions and appear at the surface as a pool with or without an overflowing discharge.

Water from hydrothermal springs can be classified in four groups: alkali chloride, acid sulfate, acid sulfate-chloride and bicarbonate (Schreier 1999). Especially the acidic conditions result in a barren landscape without vegetation. For plants, algae and bacteria it is difficult to live in such conditions. Acidic water also changes the form of sinter deposits.

Silica is deposited in small, sharp spines instead of thick layers that are more common under alkaline conditions (Schreier 1999).

Lots of the hot pools have water colors ranging from deep blue to emerald green (Fig. 3.8). The blue hue is caused by



Fig. 3.8 Grand Prismatic Spring – Yellowstone’s most famous and colorful hot spring

fine particles of silica or clay absorbing the whole spectrum of the visible sunlight except for the blue rays reflected by the water. Because the intensity of light and the amount of suspended particles in the water change from day to day also the color intensity differs over time. A blue thermal pool with yellow sulfur or yellow bacteria appears emerald-colored (Schreier 1999).

While the discharge of hot springs is constant and non-violent **geysers** erupt in intervals. These eruptions are triggered by narrow restrictions in the plumbing system. More than 200 geysers exist in the Yellowstone National Park and most of them erupt infrequently and unpredictable (Fig. 3.9; Kiver and Harris 1999). Besides the many small sputter and splash ones that nearly reach 3 m (10 ft) in height, only six grand geysers exist that erupt higher than 30 m (100 ft) (Schreier 1999). The geyser basins are located in the western part of the park – from the Upper Geyser Basin in the south with Old



Fig. 3.9 Upper Geyser Basin - Lion Geyser; cone type

Faithful as the most famous geyser, to the Norris Geyser Basin in the north. A geyser eruption is triggered by a series of reactions. An important fact that influences the eruptions is the increasing boiling temperature with increasing water column and thus higher pressure. The surface water at Yellowstone's high elevation of 2350 m (about 7700 ft) boils at 93 °C (198 °F). For every 1 m (3 ft) of water column the boiling point is about 2 °C (3.4 °F) higher (Rinehart 1976). If the geyser's tube is filled with water the lower parts of the water column near to the surface begin to boil and steam bubbles are generated. Surges of steam move to the surface and the preliminary splashing reduces the pressure on deeper parts of the water column. The boiling temperature decreases and again steam is produced by the gas bubbles. During the following explosion gas, a water column or a mix of both expand in the tube and finally erupt. It is necessary that a geyser has a nearly vertical underground tube that is linked with side chambers of porous rock where water is stored. Furthermore a constriction near the surface in the plumbing system must exist.

How often and how strong a geyser erupts depends on the energy spent and the necessary recovery time. Earthquakes can cause geysers to increase as well to decrease or even cease in activity. Geysers vary in duration and volume of discharge that is determined by the

opening or vent surrounding a geyser. The cone-type (Fig. 3.9) and the fountain-type formations are the two predominant types of mineral depositing forms occurring around a geyser's vent (Schreier 1999).

In contrast to a geyser a **spouter** continuously ejects water in a column (Kiver and Harris 1999).

If little water is available only steam and gas will discharge at the surface. These features are called **fumaroles** (steam vents) with the typical hissing and roaring sounds. Roaring Mountain gets its name from that noise. Characteristic are also encrustations of minerals dissolved from the subsoil.

Mud pots occur where some more water exists as well as hydrogen sulfide gas that produces sulfuric acid. The acid dissolves the surrounding rock into its components of silica particles and clay. These precipitates mixed with the little amount of water result in a thick pasty mixture of water, fine clay, and silica. Mud pots have no discharge.

3.2 NORRIS GEYSER BASIN



Fig. 3.10 Norris Geyser Basin

Named after an early Yellowstone Superintendent the Norris Geyser Basin is the hottest and most unstable geyser basin in the Yellowstone National Park (Schreier 1999). It is located in the northwest of the Park and includes the mapping area Ragged Hills in its northwest. Since the early 1990's Ragged Hills attracted attention by an increasing thermal activity, and thus by the development of many new hydrothermal features.

The Norris Geyser Basin is in different sorts of respect very interesting and a kind of “superlative” hydrothermal basin. Among the major geyser basins of the park it is the one with the longest thermal activity history and the variations of this activity occur more often and powerfully than in other Yellowstone Park areas. Besides the highest diversity of hydrothermal features of the Park area, also the highest erupting geyser, Steamboat, and the fumarole with the highest surface temperature, Back Growler, are situated there. The

water contents the highest silica concentrations of all thermal waters of the Park (White et al. 1988). Those phenomena enable a wide diversity of chemical types of water, precipitates, and altered rocks.

3.2.1 GEOLOGY

The basin is situated just 4 km outside the northwestern rim of the Yellowstone Caldera. It is integrated in a multifaceted subsidence structure reaching from the caldera's margin to the Mammoth Hotsprings described as Norris-Mammoth Corridor by White et al. (1988). The basin is known for intense swarms of small earthquakes. Besides also large quakes can occur as for example the second largest recorded earthquake in Yellowstone's history that was observed near Norris Junction in March 1975 with a magnitude of 6.1 (Smith and Siegel 2000). Several north trending faults defining the Norris-Mammoth Corridor and north-east trending faults related to the Hebgen Lake system cause those seismic events. Faults with noticeable displacement are not documented within the Norris Basin. The weak zones of faults, volcanic vents and the caldera boundary enable the easier rising up of the heat and thus support the geothermal activity.

As far as observable the basin was only influenced by the third eruption 600,000 years ago. The Lava Creek Tuff is the dominant bedrock outcropping in the area. Older rocks are not exposed. The Lava Creek Tuff consists of the older member A and the younger member B (Fig. 3.11). The lower member A doesn't crop out at the surface of the basin in contrast to the upper member B consisting of gray, brown or pinkish-gray ash-flow tuff that is devitrified throughout and is generally densely welded except for a partially welded vapor-phase zone near its base (White et al. 1988). Member A normally mantled by glacial and other deposits lies beneath all of Norris Geyser Basin.

Furthermore important to the Norris Basin are the Gibbon River Flow (~90,000 years B.P.) and the Norris Dome Flow (160,000 years B.P.). The

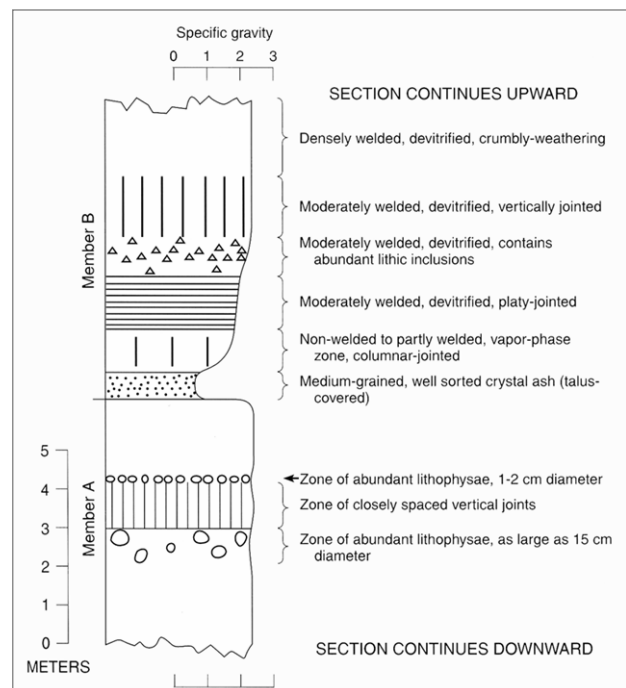


Fig. 3.11 Lava Creek Tuff members A and B (Christiansen 2001b)

rhyolitic activity began between 320,000 and 400,000 years ago with the extrusion of the Willow Park and the Cougar Creek domes followed by the extrusion of several further domes and flows from 180,000 to 80,000 years ago. The mentioned Gibbon River Flow is the youngest dated flow in the Norris area and played an important role during the early Pinedale glaciation. Because the northern end of the Gibbon River Flow confined the Norris Basin in the south (Christiansen 1975) the southward flowing Pinedale glacier was stopped. Therefore many kame deposits resulted from the early Pinedale glaciation stage (White et al. 1988). The glacial ages are generally difficult to date resulting in the problem to explain the hydrothermal history of the park exactly.

Chalcedony-cemented sandstone (hydrothermal quartzite), consisting of clastic quartz hydrothermally cemented by chalcedony and adularia (hydrothermal K-feldspar), is the oldest preserved thermal record. Older deposits of siliceous hot-spring sinter were completely removed by glacial abrasion probably by early Pinedale glaciers (White et al. 1988). Unusually rounded chalcedonic sinter pebbles locally included in the hydrothermal quartzite even point to an older (Bull Lake) interglacial hydrothermal event. Because hydrothermal activity went on through the early Pinedale glaciation and since the Gibbon Flow blocked the moving of the glacier the rapidly melting of the ice ended in dumped debris ice load forming kame deposits on the ice margins. As also the meltwater was hindered to flow off, kames and fractured ice were saturated with hot water to elevations of at least 2375 m (7800 ft) resulting in the moderate cementation of the kames with amorphous opal (White et al. 1988). When the dam of the lava flow was broken off, the water level in the upstream basins dropped down close to today's level causing a discharge of hot springs on the basins floors and along the kame margins. The late Pinedale kames are generally not cemented. After the end of the glaciations the Norris Geyser Basin's thermal activity developed fast to conditions comparable to today's.

As mentioned above the mapping area Ragged Hills is situated in the northwest of the Norris Geyser Basin. The dominating sediments of the mapping area are undifferentiated alluvial and lacustrine deposits (Fig. 3.12 - yellow). The thickness of those sediments including some normal stream, lacustrine and lenticular thermal deposits is not known. To the south-southeast the area is bordered by the brown and grey cemented kame deposits of the older Pinedale glaciation (Fig. 3.12 - red). Those sediments with a thickness up to 40 m are chaotically bedded because of the fast hydrothermal melting of the ice and the slumping of sediments. To the northwest unsorted and unstratified till with a thickness generally 0.5 to 1 m can be found besides the deposits mentioned before (Fig. 3.12 - grey).

This till consists of angular to rounded cobbles and gravel in fine-grained matrix. Besides these dominating sediments also sinter deposits of white, grey, yellow, and brown amorphous opaline can be found (Fig. 3.12 - light blue) as well younger deposits of the Pinedale glaciation (Fig. 3.12 - dark green) consisting of sand and gravel locally cemented by amorphous hot spring silica. The debris mainly came from the Lava Creek Tuff and lithoidal and vitric flows of rhyolite (thickness < 0.5 to > 5 m).

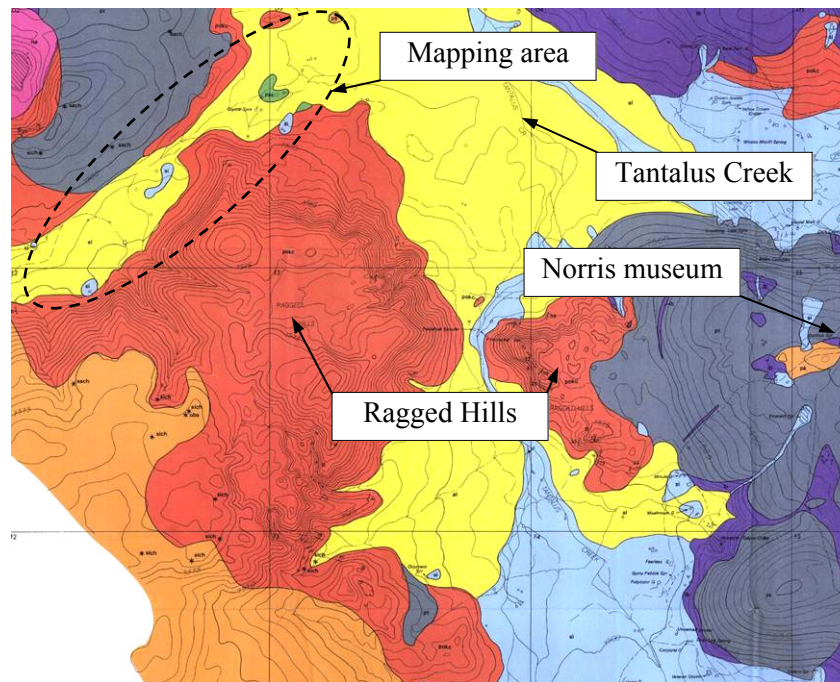


Fig. 3.12 Situation and geology of the mapping area Ragged Hills in the Norris Geyser Basin (Geologic map – Christiansen 2001)

3.2.2 HYDROGEOLOGY

The geysers and most hot springs of the Norris Geyser Basin change once a year in their behavior and chemical water composition. This annual disturbance is not known for other park areas and seems to be seasonally controlled, occurring most commonly in August and September (White et al. 1988). The very high water temperatures of the main aquifer (at least 270°C) enable the highest silica concentrations (at least 600 ppm at such temperatures) known in the park (White et al. 1988). When thermal waters rise and cool down gradually deposition of silica minerals begins near and below 200°C and clogs the plumbing system. The overpressure increases beneath this self-sealing zone until it is great enough for an abrupt fracturing along weak points such as fractures. Geysers and springs get muddy and turbid, high discharges of hot water and steam are observable and geysers

can erupt after months of quiet or their eruption interval can change (Smith and Siegel 2000). During the snow and water rich seasons the high water table helps to keep the hydrostatic pressure high enough to compensate the overpressure (Smith and Siegel 2000). During drier months the water table drops and the local hydrostatic pressure is reduced resulting in an eruption through which the mineral deposits in the underground get broken by the power of the pressure (Smith and Siegel 2000). Furthermore, the dilution by cold and low-silica surface water is low and thus silica concentrations and depositional rates are the highest in times of low water supply.

White et al. (1988) distinguished 4 water types in the Norris Basin:

- (1) Nearly neutral waters high in chloride and silica
- (2) Dilute recharging meteoric waters
- (3) Acid chloride-sulfate (or sulfate-chloride) waters
- (4) Acid-sulfate waters

The main water type (1) is nearly neutral in pH (6 to 8) and high in chloride and silica. Furthermore it is associated with very high subsurface temperatures. The water color ranges from clear blue to opalescent blue resulting from light-scattering by the colloidal silica. Sulfate concentrations fluctuate remarkably but nevertheless sulfate is mostly the second abundant anion only after chloride. The high water temperature and the chemical characteristics as well the absence of tritium suggest that this water type is supplied from deep thermal sources.

The second dominant water type is composed of cold to warm dilute meteoric waters resulting from rain and snow (2). This type can be distinguished into type 2a and 2b. Being nearly neutral in pH type 2a is understood as the major source of local mixing and dilution of the basin's chloride waters. It discharges especially at the basin's margins in springs of moderate temperature. Water type 2b is moderate in temperature, with low pH values and its discharge ranges from low to considerable. It occurs on the lower slopes of the Norris Dome.

The acid waters of the third type are rich in chloride and sulfate. There are different explanations regarding the formation of that water type. Either a mixing of deep chloride-rich water of the type 1 and shallow acid meteoric water of the type 2b may occur near the surface or recirculating surface-acidified water exists that mixes with the chloride-rich waters.

Waters of the last water type (4) are characterized by low chloride concentrations, low discharges and are commonly located on slightly higher ground. The chemistry of these waters is caused by the subsurface boiling of chloride-rich waters of type 1 and 3 and the rising of steam and H₂S separated from the chloride water. While the steam partly condenses, the H₂S is oxidized inorganically or by bacteria. This water type is normally near boiling and it is often related with other types of water.

The present thermal activity in the Norris Geyser Basin could be explained by three different hydrogeological models (White et al. 1988). The first one presumes that local sources of magma, heat and convection exist under or near Norris Geyser Basin, but this model did not find any significant support by the scientific community. The second model assumes all thermal areas of the park including Norris Basin belong to one Yellowstone System, perhaps confined strictly to the caldera. Because of diverse problems this model seems unlikely (White et al. 1988) The third model proposes several places of magma, heat and convection along the Norris Mammoth Corridor – maybe with main foci near the Gibbon River flow and the Roaring Mountain-Obsidian Cliff flow. This model with lots of variants is the most complex and attractive of the three. But a “best” solution isn’t found yet.

These hydrogeological models gave an idea where the heat could come from driving the hydrothermal basin. But the annual disturbances at the Norris thermal features and the association of different water types in that area have to be explained furthermore.

First the whole Norris Mammoth Corridor has to be considered. The Fig. 3.13 shows a cross section of the corridor and the idea of White et al. (1988) how the water is moving in the underground and why different water types appear in individual places of that area. White et al. (1988) assume from different references that a temperature of 340°C exists near the base of or below the Lava Creek Tuff near Roaring Mountain. When the up-heated groundwater flows southward, gases such as carbondioxide and H₂S concentrate in vapor bubbles without reacting with the surrounding rock. As far as possible these gas bubbles use fractures and other hollows to escape to the surface. Chloride is excluded from that steam phase. At or near the surface H₂S reacts with atmospheric oxygen to sulfate that again is dissolved in condensing steam and local meteoric water to sulfuric acid. These acid waters cause a zone of bleaching southward towards the Norris Geyser Basin. The residual groundwater, rich in chloride, cools in the subsurface to about 270°C. The resulting neutral water high in chloride and silica dominates the deep aquifer underlying the Norris Geyser Basin.

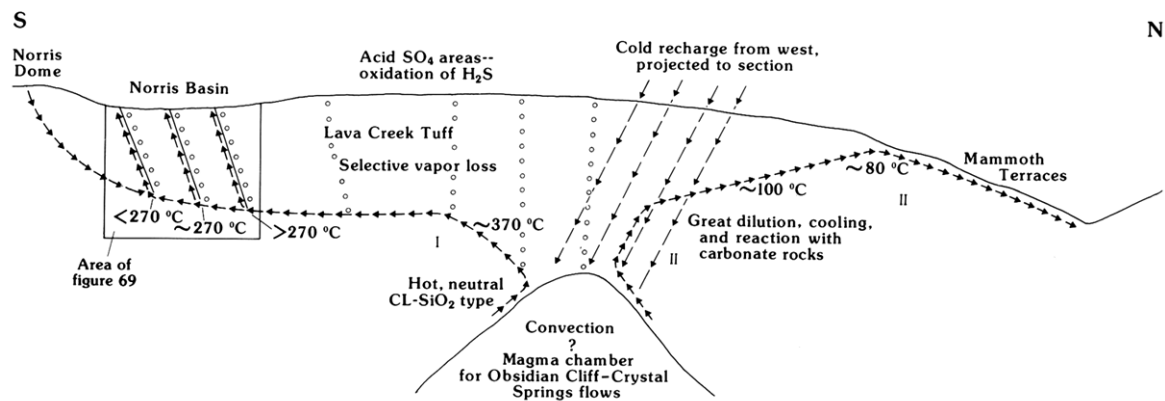


Fig. 3.13 Cross section of the Norris Mammoth Corridor (White et al. 1988)

The Fig. 3.14 illustrates a cross section of the Norris Geyser Basin with a tentative model that tries to explain the distribution of the water types, their constituent ratio and why the sudden changes in chemistry and behavior of the features occur. Three belts can be distinguished where water is rising up. The central north-striking belt runs through the Back and the Porcelain Basin involving all water types. Most dominant are high discharges of the nearly neutral water with the highest chloride and silica concentrations. This water type 1 is absent in the belts bordering the Norris Geyser Basin in the west and the east. These belts are dominated by the acid chloride-sulfate water types that are only moderate in salinity and seldom affected by the widespread annual disturbances in contrast to the central belt. Furthermore, the neutral chloride rich waters of the central belt normally flow out at altitudes a little higher than the basin's floor. In contrast the acid chloride-silica hydrothermal features usually discharge in the low water regions of the basin.

That description includes the major problem of the Norris Geyser Basin regarding its water chemistry: the water types are nearly randomly associated in the central belt and the neutral waters, highest in salinity and silica but lowest in sulfate, dominating in the central belt are not found in the marginal belts.

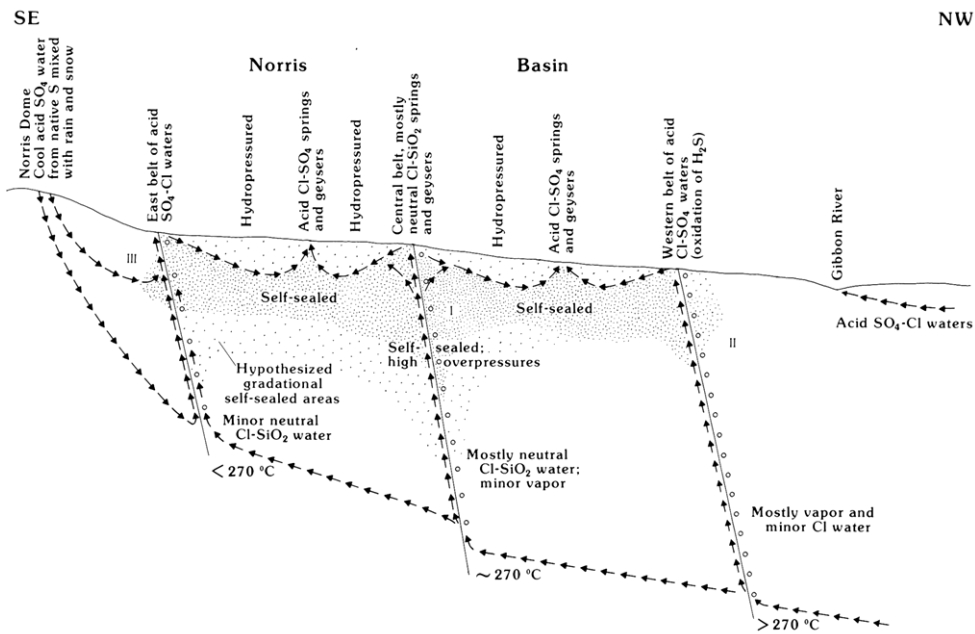


Fig. 3.14 Cross section model of the Norris Geyser Basin trying to explain distribution and development of the major water types (White et al. 1988)

As illustrated the Norris Geyser Basin is a thermal area with a long thermal history and with many peculiarities not found in other thermal regions of the Yellowstone National Park. The mapping area Ragged Hills as a part of the Norris Geyser Basin is situated between the central and the western belt. As mentioned before this area attracted attention by an increasing thermal activity since the beginning of the 1990s. Detailed maps of the thermal inventory did not exist owed to the problem of mapping the rapidly changing features by time-consuming traditional ground survey methods. The next chapter describes how the individual hydrothermal features with different sizes from the centimeter to the meter range were mapped in the field and from the air by low flying platforms in a time effective way.

4 METHODS APPLIED

4.1 DESIGN OF EQUIPMENT

Two different approaches were used for taking high resolution aerial photographs. Pictures were obtained by a helium balloon from 80 m (262 ft) and from a single engine airplane from about 610 m (2000 ft) altitude. The constructions to mount the camera at the balloon respective at the airplane were designed and built in Freiberg at the mechanical workshops of the faculty of geosciences geotechnique and mining.

4.1.1 THE AIRPLANE

Fig. 4.1 shows the construction to mount the digital camera (Canon P5) to the Cessna 172.

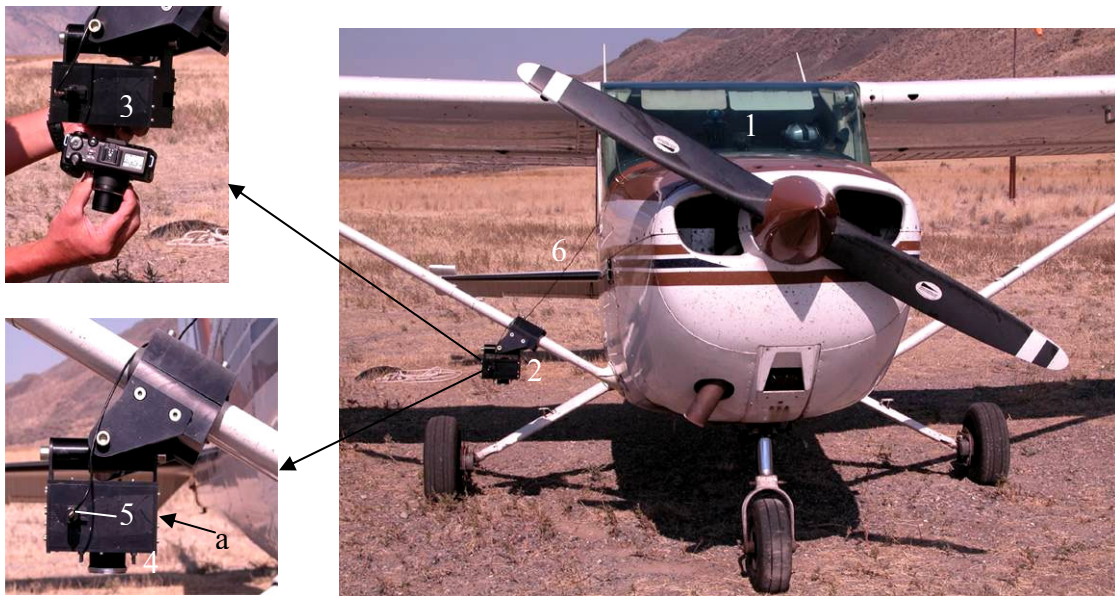


Fig. 4.1 Construction to mount the camera to the Cessna 172

1. The airplane was a Cessna 172 single engine high wing airplane.
2. The cardan construction carrying the camera was fixed at the airplane's right wing strut
3. The box that hold the camera (9.0 cm high, 14.6 cm wide, 8.3 cm deep).
4. Lens of the box oriented to the ground by means of the cardan construction (\varnothing 4.6 cm).
5. The outlet for USB-cable and pneumatic shutter directly connected to the camera's shutter. Infrared triggering was possible through the glass window (a – not visible at the picture) (5.3 x 5.9 cm), but not used.
6. The pneumatic shutter string led from the camera to the interior of the airplane, where it was operated by the co-pilot.

4.1.2 THE BALLOON

The camera carrying construction for the helium filled latex balloon is shown in Fig. 4.2.

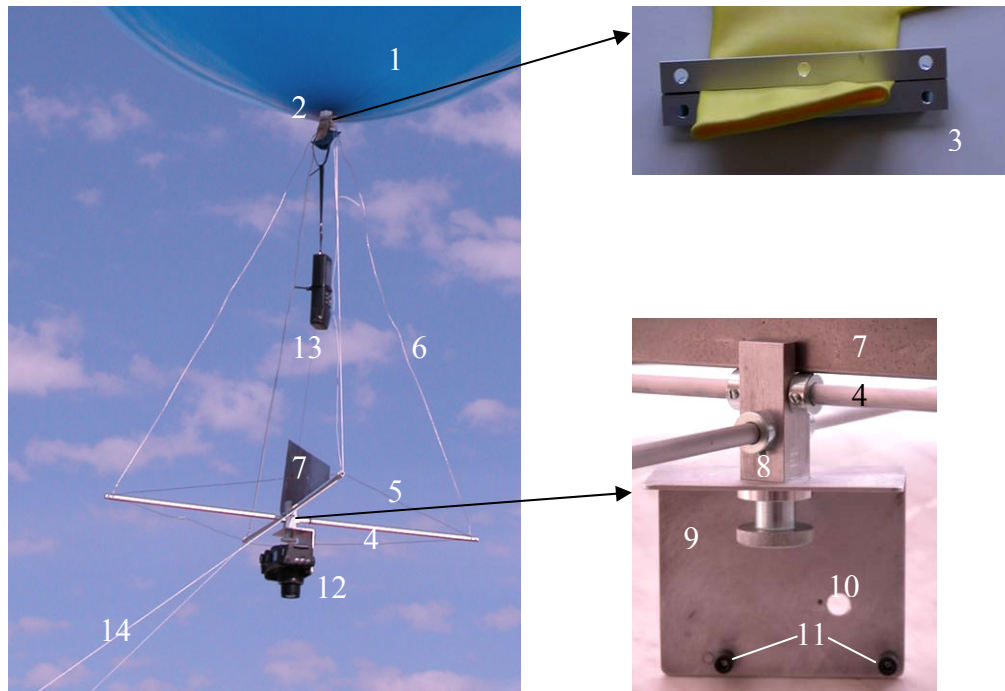


Fig. 4.2 Construction to mount the camera to the latex balloon filled with helium

1. The latex balloon was able to carry 1.5 kg. Because the camera weighted 0.46 kg and the construction including two 80 m lines approximately 0.5 kg, the difference of 0.54 kg between the maximum possible and the actual load provided sufficient lift. Filled with helium the balloon had a diameter of around 1.50 meter and a perimeter of circa 4.50 meter. Two balloons including plastic clips (2) were bought at www.lollipop-ballon.de.
2. The white plastic clip closed the balloon gas tight.
3. Two small metal angles with holes for fixing the tether lines and the framework were placed by two screws at the lower end of the balloon below the plastic clip (2). They served to connect the framework and the tether lines to the balloon and as an additional gas tight seal.
4. Two hollow aluminum sticks of 0.75 meter length attached in a 90 degree angle to the middle axis (8) formed the main part of the framework.
5. Two 1 mm thick, intertwined wires spun around the four ends of the aluminium sticks (4) and helped to stabilize the main carrying construction.

6. Four 1 mm thick, intertwined wires attached the camera carrying framework to the balloon (3).
7. The wind metal plate helped to orient the construction into the wind.
8. The middle axis connected the metal plate supporting the camera to the aluminum sticks framework (4).
9. One screw fixed the metal plate supporting the camera to the aluminum sticks (4).
10. Hole to fix the camera with a tripod screw at the metal plate.
11. Two small rubber stoppers supported the camera weight.
12. The digital camera “Canon Power Shot G5” (5.0 M pixel, 4x optical zoom, focal length 7.2 – 28.8 mm, 35 – 140 mm equivalent to 35 mm film) took the pictures from the air (section 4.2.2.1).
13. The GPS “GARMIN-12” was a handheld, robust instrument with a waterproof casing. The 12-canal-GPS-receiver was able to use up to 12 satellites for the position calculations. The coordinates of the balloon’s location were updated every second and saved in a 30 second interval (Fig. 4.8). It measured with an accuracy of 15 meter (Garmin 2004).
14. Two persons controlled the balloon from the ground with help of two 1 mm thick nylon kite tether lines.

4.2 FIELD WORK

4.2.1 GROUND CONTROL POINTS

To create a georeferenced, rectified overview from the taken aerial photos, sufficient ground control points with known coordinates were needed. The necessary density of check points depended mainly on the balloon’s altitude above ground, the small format camera and the camera’s focus. As Fig. 4.3 shows, a raster of 28 x 28 m was required for a proposed balloon altitude of about 80 m (262 ft) above ground, the 35 mm focus of the small format camera and an optimum number of 6 reference points per picture. However, because of uncontrolled rotations of the airborne platform this number wasn’t realistic. The grid was laid out with marked stones with a distance of 28 meter between the points measured by steps. For surveying the ground control points coordinates a differential Global Positioning System and a reflectorless working total station were used. Both were provided by the GIS department of the National Park Service in Mammoth.

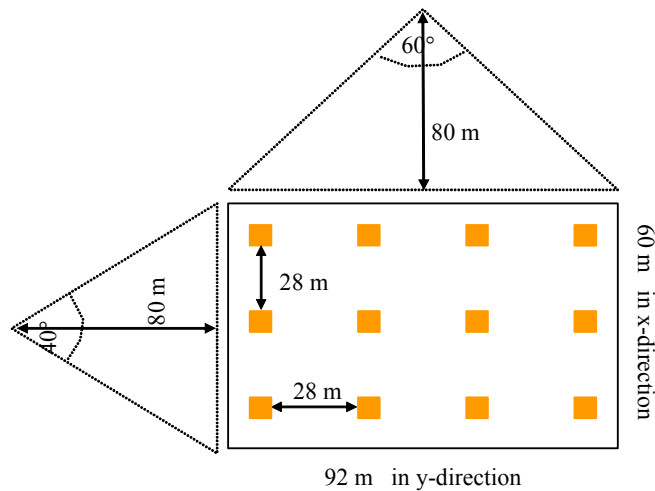


Fig. 4.3 Calculation of the distance between ground control points

Navigation Satellite Timing And Ranging - Global Positioning System (NAVSTAR-GPS) is a satellite-based positioning system developed by the United States Department of Defense since the mid 1970's. In the year 1995 the Global Positioning System (GPS), as it is called today, achieved its full operational capability. Twenty-four operational satellites orbit the earth every 12 hours at an altitude of 20200 km. They send signals to the earth that are acquired by the GPS receiver. At least four satellite signals are needed to calculate a three dimensional position from the satellites positions that are determined from the mathematically calculated distance between the satellite and the GPS receiver. One limitation of the Global Positioning System is the necessary relatively clear "line of sight" between the GPS antenna and the satellites. Any obstacles can weaken the transmitted signal. The multipath interference is another problem that is caused by the GPS signal bouncing off close objects. At all influencing errors can be distinguished in satellite-, spreading- and receiving mistakes (Bauer 2003). Errors caused by the non-correction of the satellite clocks mistakes (differences to 1 m) and fluctuations of the satellite courses (differences to 1 m) are two more examples for that (de Lange 2002).

Since the random timing errors in satellite signals (Selective Availability) introduced by the Dept. of Defense of the USA to limit the efficiency for civilian users were removed with May 2nd 2000, the GPS receivers achieve accuracies of about 10 m when using the Standard Positioning Service that based on the Clear/Access (C/A) code (Bauer 2003). The protected Precise code (P-Code) of the Precise Positioning Service provides better precisions but can only be decoded by military or authorized civilian users. To get better precisions when using the Standard Positioning Service a differential correction of the data

is necessary. Therefore differential GPS was developed in the late 1980's and early 1990's. Two receivers that are relatively close together and experience similar atmospheric errors are needed for that. One represents the base or reference station from which the precise location is known. It calculates the difference between the know location coordinates and the actually measured ones. The difference is applied to the GPS data recorded by the second GPS receiver, the roving receiver that is used in the field.

To correct the locations measured by a Differential GPS two main methods exist – the real time differential correction in the field and the postprocessing correction. The real time correction is done by transmitting the correction signals directly to the roving receiver in the field. The postprocessing correction follows the field measurements and requires for special office software.

Initially, the differential **GPS Pathfinder Pro XR** was used to measure the coordinates of the control points for a first position overview. The system consists of a field computer, a rucksack with the batteries, the receiver and an antenna. The instrument offers real-time differential GPS and postprocessing options. It integrates a 12-channel GPS and a real-time beacon. Optional real time correction with the Wide Area Augmentation System (WAAS) and European Geostationary Navigation Overlay System (EGNOS) would be possible. Additionally it has RTMC (Radio Technical Commission for Maritime Services) input and output. It uses the patented EVEREST™ multipath rejection technology to eliminate multipath signals in reflective locations (Trimble 2004).

All ground control point coordinates were measured by the differential GPS for 150 seconds each (Fig. 4.4). Thus the average of 150 differentially corrected reachings was used. With the help of the software “GPS Pathfinder”, version 2.90 the determined coordinates were downloaded from the field to the office computer and offline corrected. The correction factors for this postprocessing calculation were taken from the reference station in Bozeman. When adjusting the data the software automatically detected inexact coordinates to correct them. The survey grid was plotted and some control points, especially in the



Fig. 4.4 Working with the DGPS

southwestern part, were shifted in the field to obtain a better adaptation to a regular raster. The marked stones were replaced by crosshairs of 1 x 1 m red-white plastic stripes that were removed after the field work (Fig. 4.7a).

Because the differential GPS has a deviation of 2 to 5 m (de Lange 2002), the positions of the marked stones were surveyed additional by a **LEICA TCR 307 reflectorless total station** (Fig. 4.5) to get even more exact coordinates of the control points. Steve Miller from the GIS department of the Park operated the theodolite in the field. In the following selected technical parameters of the theodolite are given:

- Angle measurement: 7", 2 mgon
- Distance measurement: 3000 m with reflector
- Measuring-time: 1 sec with reflector
- Integrated programs: Setout; Surveying; Free Station; Area; Tie-distance
- Recording: Internal 4000 data records
- Magnification: 30 x
- Plummet: Laser accuracy + 0.8 mm at 1.5 m

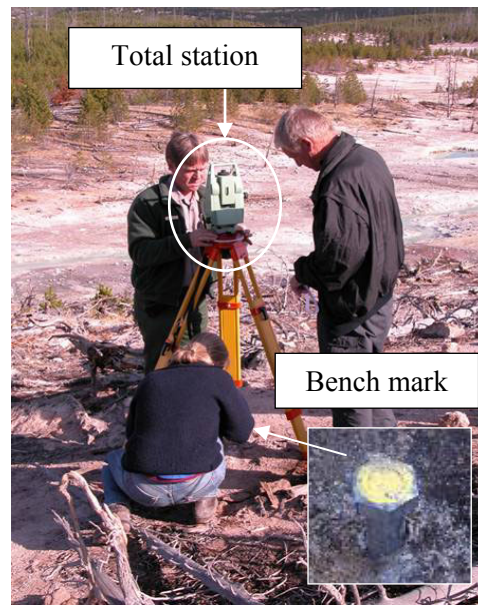


Fig. 4.5 LEICA TCR 307

Before starting the measuring process the calibration of the theodolite had to be done in the following order:

1. The theodolite consisting of the tripod and the total station had to be leveled out horizontally and vertically with help of the laser plummet and the dual axis compensator.
2. The total station was turned around 90° and checked again regarding the leveling.
3. The instruments height was measured above the bench-mark (Fig. 4.5).
4. The last step was to set the station and to start the new job by entering the coordinates and heights of the theodolite's location and of the check point.

Surveying grid was done from two bench marks - one fix point and one check point – that were marked permanently in the ground by 2 cm hexagonal stainless steel nails. The coordinates of the fix points were determined by differential GPS Pathfinder Pro XR averaging for 15 minutes. A total deviation of 0.2 meter from the correct position in the world coordinate system was assumed for the fix point. From the fix point the coordinates of 81 of the total of 102 ground control points were visible and thus accessible (Fig. 4.7b).

The determination of the remaining 21 points was inhibited by trees and other natural obstacles. For measuring a control point the reflector had to be leveled out by a spirit level (Fig. 4.7a). As soon the reflector was aligned vertically the relative coordinates of the control point were determined through a laser beam from the total station to the single bar reflector. From that its true coordinates were calculated.

The check point was determined before and after determining the 81 ground control points to check the external conditions changing through the time (atmosphere). It was off by 0.00426 meter easting, 0.00494 meter northing and minus 0.0338 meter elevation. So it can be assumed that the measuring conditions were stable during the survey process.



Fig. 4.7a Working with the reflector

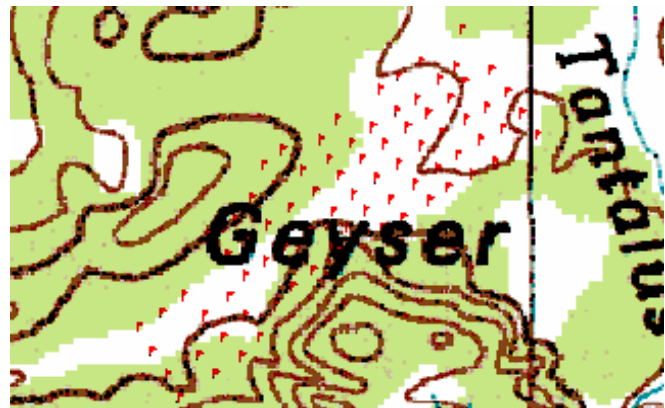


Fig. 4.7b Location of the 81 ground control points

4.2.2 AERIAL SURVEY

4.2.2.1 SURVEY FROM THE BALLOON

To get the balloon airborne it had to be filled with a gas that is lighter than air. Therefore the noble gas helium was used. There was no risk during working with that balloon gas because it is non-toxic, environmentally friendly, not inflammable, stable and inert towards all other chemicals. By international norms it belongs to the group of the non-hazardous material (Weilerwelding 2004).

To fill the balloons two gas bottles with helium were bought in Bozeman, each contained circa 2 m³ helium. The bottles weighted about 12 kg and were transported in a backpack to the sampling site. One bottle was needed to fill one balloon. For filling the balloon in the

field its opening of about 6 cm diameter was slipped over the valve of only 1.5 cm diameter keeping it tight by hand. While inflating the balloon an increasing pressure built up at that manually tightened connection. After having filled up the balloon completely it was closed by the plastic clip (2 in Fig. 4.2). The next step was to attach the construction for mounting the camera and then the camera itself to the balloon. Additional to the camera the GPS (13 in Fig. 4.2) was fixed to the framework. Because of the diffuse loss of helium the operation time was according to manufacture's brochure approximately two to three days dependent on the weather and storage.

The first time the balloon was launched on September 27th 2003, from 11.00 am to 1.00 pm. Weather conditions were sunny to slightly cloudy with low winds from variable directions. After starting the "pre-set time" program that took one picture per minute with an auto timer the balloon was lifted up. Taking the photos in a short interval succeeded in the necessary overlap that enables the mosaicking of the images later. Two persons controlled the balloon from the ground by two tether lines. During the first track problems had to be managed with uneven uplifting and with the nylon lines that got entangled in with some trees. After getting the balloon back to the ground it was realized that the memory card of the camera quit working in flight and no pictures were obtained. After changing the memory card the balloon was launched again for a test in The Gap area. After the camera took pictures without any problem, the balloon was launched two more times the same day. One track was conducted over the eastern and the other over the western part of Ragged Hills. A total of 65 pictures were taken. The camera adjustments were auto focus, no zoom and an exposure time of 1/1000. A fail function of the GPS firmware made it impossible to download the coordinate data that were taken every 30 seconds. The balloon was damaged at the ground later this day.

Four days later at the 1st of October the second balloon was launched two times between 10.00 to 12.00 am. Weather was sunny to slightly cloudy again but no winds disturbed the flight. During these trips a total of 112 photos were taken from those parts of the mapping area that were missed before. This time

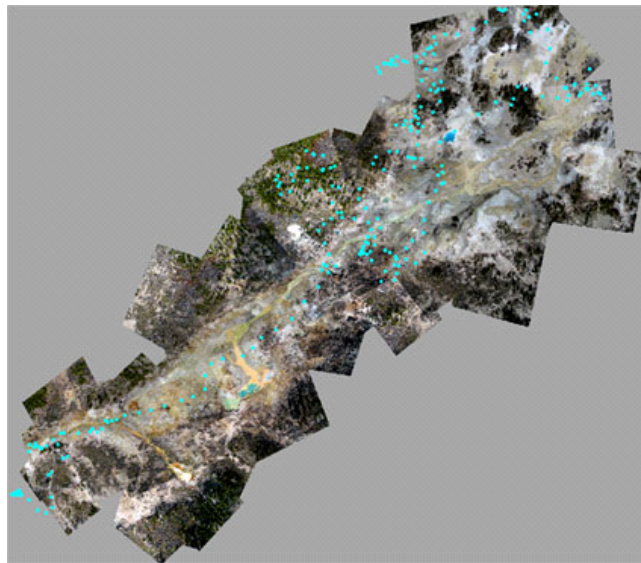


Fig. 4.8 Example for balloon track

the tracking registered by the GPS (same brand and type, but different firmware) was saved as mps.file. Camera adjustments differed a bit from the first time: exposure time 1/2000, no zoom and manual focus (infinite) were chosen. Because of calm wind conditions the flying altitude was more stable this time. However, at the end of the second track the balloon was destroyed when gusty winds pushed it down to the ground; camera, GPS and framework were not damaged.

4.2.2.2 SURVEY FROM THE CESSNA

Two different methods were practiced to control the camera from the inside of the airplane. The first one was to control the camera completely by laptop via a USB cable. This method was tested at the 28th of September 2003 without giving the expected results. One problem was the insufficient contrast of the LCD making it hard to identify single structures. But the major problem was the time delay in triggering a shot when overflying the target area.

The second possibility was to use a pneumatic shutter that was connected directly to the camera. With that the “power shot” program (11 pictures in consequence, 2 per second) of the camera was started when the target area was reached. While flying over the area the releaser had to be pushed down continuously. That means the co-pilot had to hold the rubber ball of the pneumatic shutter pressed during the whole time.

Both methods required a precise determination of the flying route before starting the flight. Coordinates of the area of interest were taken from the map and entered in the GPS as go-to-points. These points consisted of the „starting point“ to line up the airplane horizontal, the „shooting point“ where the “power shot” program was started and the first photo was taken and the “end

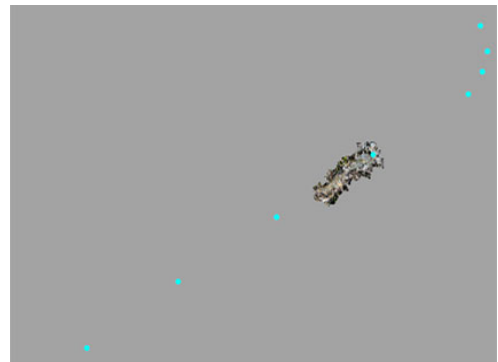


Fig. 4.9 Flying route with the airplane point”. Finally the “turning point” followed where the airplane left the course over the area of interest. As a matter of fact a precision approach technique was established based on the GPS go-to-function with the pilot in command responsible for precise altitude (from barometer) and proper wind correction. While taking the pictures flying speed was 104 km/h (65 mph) with 20° flaps retracted.

All flights were conducted at 610 m (2000 ft), the minimum safe altitude required over National Parks in the United States.

Tab. 4.1 Dates, over flights, camera adjustments for aerial images taken with the pneumatic shutter

| Date | Number of over flights | Camera adjustments | | | Number of photos |
|----------|------------------------|--------------------|--------|------|------------------|
| | | Exposure | Focus | Zoom | |
| 09/30/03 | 4 | 1/1000 | manual | 4 x | 40 |
| 09/30/03 | 1 | 1/2000 | manual | 4 x | 10 |
| 10/02/03 | 2 | 1/2000 | manual | 4 x | 28 |

4.2.3 GROUND SURVEY

4.2.3.1 MAPPING

The ground survey was done in the beginning of October. Each hydrothermal structure was mapped with the help of a special, self designed parameter catalogue. It included the following parameters:

- Identification number, date, time, weather
- Location: GPS coordinates (GARMIN-12), nearest ground control point numbers, possibly sketch, photo documentation
- General characteristics (hot spring, mud pot, geyser, fumarole)
- Number of individual features for structures mapped as group
- Water color, turbidity, precipitation, and shape of each hydrothermal feature
- Drainage (yes or no, shape and direction)
- Gas activity and number and position of degassing points
- Water chemistry – on site parameters (of the bigger features)
- Special observations

The decision to characterize the features after those parameters built up on the experiences from the preceding field work and on the observations by what the features could be differentiated. The Tab. 4.2 shows the turbidity and gas activity classifications. They only allow a qualitative comparison and no quantitative evaluation.

Additional to the mapping of the features, also the surrounding area was characterized and photos were taken generally with a red-white plastic stripe as scale. One white or red bar of the stripe was about 20 cm long. A total number of about 100 features were mapped.

Tab. 4.2 Classification clouding and gas activity

| Gas activity | Turbidity |
|------------------|----------------------|
| 1 – no degassing | 1 - clear |
| 2 - little | 2 - little |
| 3 - moderate | 3 - moderate |
| 4 - strong | 4 – opaque to strong |
| 5 - geyser | |

4.2.3.2 WATER CHEMISTRY - SAMPLING

Taking water samples was not only important for characterizing an individual feature. It also enabled to compare different water types and to draw conclusions regarding their formation conditions. Changes in the water chemistry were often caused by modifications in the environment and vice versa. Therefore it was important not only to register changes of hydrothermal features in size and geometry but also in the water chemistry.

In Ragged Hills 19 hot springs were sampled by B. Planer-Friedrich for her PhD thesis (Planer-Friedrich 2004). Besides on site parameters, total Fe, Fe (II), S^{2-} , and SiO_2 were determined with a field photometer and Arsenic species As (III), As (V), mono- and dimethylated As were separated by solid phase extraction.

**Fig. 4.10** Measuring on site parameters in feature

The **on site parameters** such as pH, conductivity, water temperature, redox potential and dissolved oxygen gave a first hint regarding the water composition. They were determined by submerging the probes directly into the thermal feature. Values were read from the display of the WTW MultiLine P4. Water temperature was determined both with the SenTix 97/T pH electrode and

and the TetraCon 325 conductivity cell and generally the mean value of both reachings was taken. The determination of the redox potential and the dissolved oxygen was not possible directly when the sampling site's water temperature was higher than $50^{\circ}C$ because the probes (CellOx 325 and redox Pt 4805/S7) quitted working then. Sporadically both values were measured in a container after cooling the water below $50^{\circ}C$. But mostly the redox

potential and dissolved oxygen were not measured for sampling sites with temperatures higher than 50°C. The redox potential was measured with a Ag/AgCl electrode and was corrected for standard hydrogen potential and temperature.

With the HACH **photometer** DR/890 applying the FerroVer, 1,10-Phenanthroline, silicomolybdate, and methyleneblue method total Fe, Fe²⁺, SiO₂, and S²⁻ were determined. These species had to be analyzed on site because with decreasing water temperature and increasing storage time they might be oxidized and their respective hydroxides would precipitate so that their original concentration might have changed. For sampling 10 to 25 mL water from the sampling site a 20 mL PE syringe rinsed 5 times prior to sampling was used. After filtering the sample through a 200 nm cellulose acetate filter (Membrex) it was analyzed right away with one of the mentioned methods. To determine Fe³⁺ the difference between total Fe and Fe²⁺ was taken.

Additionally dissolved **arsenic species** were determined. To separate on site As (III), As (V), mono-methylated arsenic acid (MMAA) and dimethylated arsenic acid (DMAA) commercial cation and anion resin columns were used. The strong resin based cation-exchanger (particle size of 45-150 µm, exchange capacity of 1.9 meq/mL) was acquired from Alltech, the silica based anion exchanger (particle size of 50 µm, total capacity of 0.14 meq/g) from Supelco. The exchanger material (500 mg) is packed between one mm

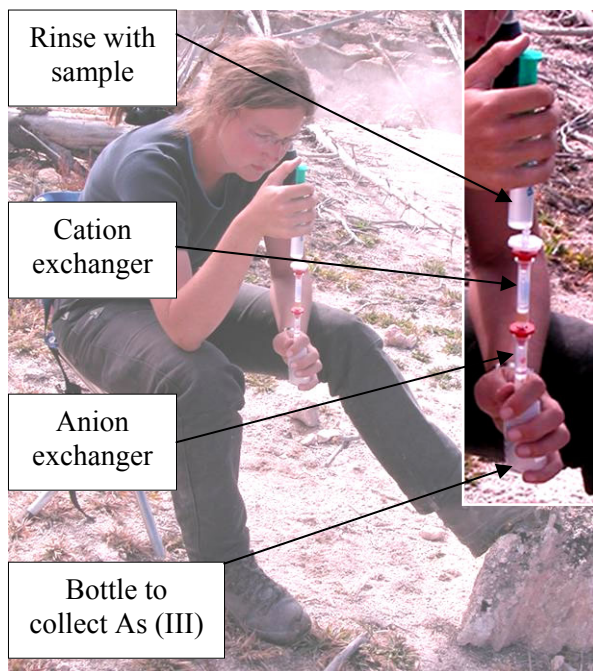


Fig. 4.11 Planer-Friedrich separating arsenic species in the field

thick, porous disks in 4 mL cartridges. After 20 mL of sample were taken from the site with a pre-rinsed PE syringe the water sample was filtered through a 200 nm cellulose acetate filter (Membrex). Then it was passed through the ion exchangers with a flow rate of around 0.5 to 1 mL/min. As (III) was collected at the end in a 50 mL PE bottle. The exchanger cartridges were separated, wrapped in aluminum foil and stored in the refrigerator at about 6°C together with the PE bottles until analysis in the laboratory at the most 4 weeks later (Planer-Friedrich 2004).

Additionally **samples** were taken for later analysis in the laboratory:

- 200 mL unfiltered in a PE bottle (for IC)
- 100 mL unfiltered in a glass bottle (for TOC/TIC)
- 50 mL filtered through a 200 nm cellulose acetate filter (Membrex) in a PE bottle and stabilized with 1 mL concentrated HNO₃ suprapur (for ICP-MS, ICP-AES, and AAS)

The bottles for IC and TOC/TIC were rinsed 5 times with unfiltered sample water, the bottles for ICP-MS, ICP-AES, and AAS with filtered sample water before filling them up.

For **laboratory** analyses see Planer-Friedrich (2004) and the digital atlas of Ragged Hills (section 5.1). The Appendix No. 9.1 summarizes the measurements methods and the elements analyzed. The results from 19 hot springs sampled by the U.S.G.S. from 1999 to 2003 were also included in the digital atlas (Ball et. al 2002, McCleskey et. al 2004, hydrochemistry data 2003 unpublished).

4.2.4 THERMAL PHOTOGRAPHY

Still today only high-altitude aerial thermography is available for the Park area. The resolution of such images is usually inadequate to detect changes over time especially from smaller thermal features. New techniques are necessary for acquiring high-resolution thermal imagery that could be applied for monitoring an altered thermal activity that may precede visible surface changes.

Cooperation with Dr. Mitchell Plummer and Dr. Earl Mattson from the Idaho National Engineering and Environmental Laboratory (INEEL) Geoscience Research Group made it possible to take thermal images of the Ragged Hills area from the ground and from the air. They used the thermal camera FLIR Systems Thermovision 320 for their work:

- Detector Type: 320 x 240 uncooled microbolometer
- Wavelength: 7.5-13 μm (long wave)
- Thermal sensitivity: 0.1 C° at 30 °C
- Optics: 24° x 18°
- Focus range: 0.5m to infinity (standard lens)
- Measurement range: -20 to 500 °C (standard)
- Extended ranges available to 2500 °C
- Operating range: -15°C to 45° C

The resolution of the camera is a function of the distance from the target, the focal angle of the lens ($24^\circ \times 18^\circ$) and the number of pixels on the microbolometer array (320×240). Therefore the x-dimension of a single pixel is:

$$(\text{Distance from target}) * 1/320 * 2 * [\tan (24 \text{ degrees})]$$

and the y-dimension is:

$$(\text{Distance from target}) * 1/240 * 2 * [\tan (18 \text{ degrees})],$$

(Plummer 2004, written communication).

Each pixel in an image is recorded as a temperature value. The temperatures recorded in the camera are based on a number of assumptions and parameter values that are input to the analysis software. These parameters include values like the distance to the source, the emission of the target (which varies with material) and atmospheric conditions like atmospheric humidity, air temperature, etc. The software to collect the images from the camera and to analyze them was ThermaCam Researcher Pro. V 2.7. It is a Windows-based infrared software package that provides detailed, precision analysis and measurement tools for capturing, recording, and studying extremely high speed thermal events (FLIR Systems 2004).

First some pictures of hot springs were taken from ground. Therefore a tripod was used where the thermal camera was installed. The photos were released from the laptop. Parallel pictures were taken by a digital camera to assign the thermal images later.

Following the thermal ground survey a thermal aerial overview was planned. The camera weighted around 3900 g plus the large 12 V battery to run the camera. So it was impossible to carry it by the balloon. Additionally there was no way to control the camera from the

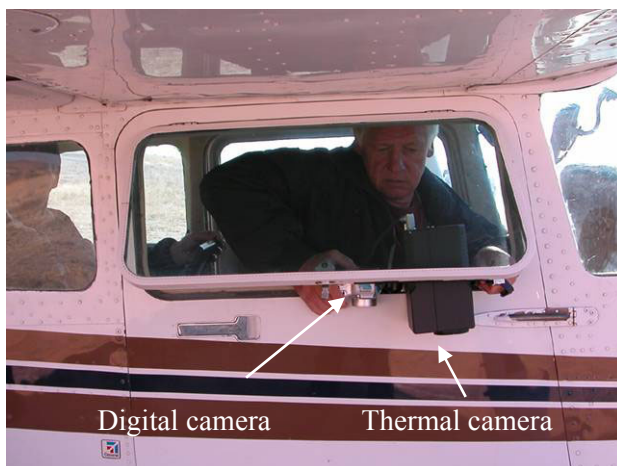


Fig. 4.12 Getting thermal pictures from the Cessna

ground. For ground operations it was connected to a laptop from which the photo was released. Those problems didn't give the chance to make some high resolution aerial thermal pictures from the balloon as it was done with the digital camera for the area of Ragged Hills. The only possibility to get some impressions of the mapping area's thermography was to over fly the area

with the airplane. To get the pictures from the airplane a digital camera (Fuji Fine Pix, 2.1M pixel, 6x optical zoom) and the thermal camera were mounted parallel on one axis. The co-pilot held that construction out of the window – as horizontal to the ground as possible (Fig. 4.12). The person sitting behind the co-pilot determined the time the picture was taken by looking at the laptops screen that was connected to the thermal camera and showed the active picture section. When getting the command the co-pilot manually released the digital camera at the same time the other person released the thermal camera from the laptop. The digital photo served as comparison to the thermal photo making it much easier to mosaic the thermal photos later on.

To georeference the thermal pictures some ground control points were marked before the flight. One meter squares of aluminum foil were laid out below some of the red-white stripes (Fig. 4.13). The foil has a much lower heat emission than natural ground, and thus should provide enough contrast in radiance to be visible in the thermal images. However, because the resolution of the pictures (from calculation: 0.8 m, digital atlas: 1.3 m) wasn't high enough the control points were not identifiable. Consequently the thermal overview images had to be georeferenced with the help of the mosaicked overview from the balloons images. Because only a rough adaptation was possible the coordinates of the thermal overview are of low precision.



Fig. 4.13 Cross with aluminum foil

A calibration of the thermal images to distinct temperatures was not possible while calibration data were not available. Nevertheless, the primary interest was to get an impression of the relative thermal activity and temperature distribution of the area Ragged Hills.

This part of the work aided the collection of first experiences with high resolution thermal photography and it showed in which direction further investigations have to go: To look for a low flying platform that is strong enough to carry the thermal camera should be the aim for future projects. Then it is possible to get high resolution images as the overview of Ragged Hills.

4.3 DIGITAL ATLAS

4.3.1 GEOGRAPHICAL INFORMATION SYSTEMS

During the last two decades GIS technology has developed very fast and today its application is often a matter of course. The collection of different environmental-geological data and their steady updating require an organized management and permanent processing. Different objectives require the summary of different subjects in one map. Therefore the digital map created by GIS replaces the conventional paper map more and more.

The difference between a standard Information System and a Geographical Information System is the given location of the object by a set of geographic coordinates. The georeferenced spatial data, the geobjects, consist of the individual geometry and the corresponding attribute information (de Lange 2002). The data structures (geometry) can be of two types: vector and raster data.

Vector data show the geobjects by their exact position with regard to a coordinate system. The objects are determined by their digitalized border. Dependent on the geometrical form the element is modeled as point, line or polygon and described by corresponding pairs of coordinates. Within the vector data model one can distinguish between models with and without topology. The topology of the features is the mutual relation between various spatial elements (Gupta 2003) and specifically defined. It is based on the fact that every structure has its own position. The topology vector model is very well suitable for problems addressing neighborhood relationships.

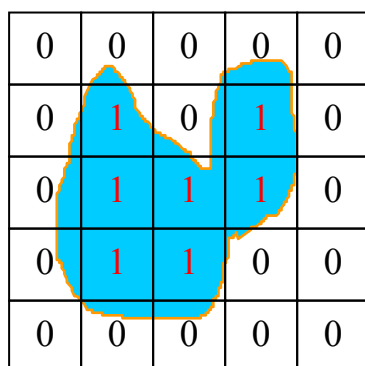


Fig. 4.14 Lake model (blue) in raster (1 = lake, 0 = land) and vector structure (orange)

The raster data have a regular cellular organization and the position of an object is given by terms of row and column positions. The border of the geobject is not given exactly as an own object but consists of pixels. Therefore the disadvantage of that data structure is the loss of accurate information about position, size and form of the features because the resolution of a raster model is limited by the pixel size. The pros are the uncomplicated handling and its suitability for image processing, GIS operations and showing areas and solid objects.

The data attributed to a vector or a raster object can be distinguished in spatial, time and thematically information. These data are stored as tables in data files and can be of two types: the categorical and continuous data. The categorical data are measured in nominal and ordinal scales, the continuous in interval and ratio scales.

Altogether the different tools of a GIS permit the data acquisition, storage, pre-processing, management, manipulation, analysis and data output of georeferenced geobjects and spatial information.

In this work two different softwares were used; the TNTmips version 6.8 (Copyright (C) 1988-2004 MicroImages, Inc.; www.microimages.com) among other things usable for geographic information analysis (GIS), advanced image processing, CAD, cartography, electronic atlas preparation and the Geomatica Version 9.1 (PCI Geomatics; www.pcigeomatics.com), a software for remote sensing, photogrammetry, GIS and carthography.

4.3.2 TNTMIPS

4.3.2.1 CREATING THE OVERVIEW MAP

To generate the digital atlas it was first necessary to import the aerial photos (jpg-files) taken with the balloon as raster objects into the program TNTmips. Then, every image with a minimum of three ground control points was georeferenced. That was only relevant for a few pictures in the western part of the mapping area. On average five to seven crosses were available in each image.

When all aerial photos were georeferenced the next step was to mosaick the images to one overview map. The best fitting images were selected and added one by one because in that way the best adaptation between the images could be achieved. Furthermore it was necessary to position the images manually as the offsets between the images often were too big if the mosaic process was done just automatically by the given control points. The manual mode implemented in TNTmips uses a bundle of adjustment algorithms to compute a least-squares best fit for the set control points and additional tie points. Tie points identify the corresponding locations in a pair of overlapping images and help to increase the adaptation between the images.

The mosaic process required adjustments in various menus. Tab. 4.3 shows the different panels and their functions.

Tab. 4.3 The mosaic process menus and their functions

| Panel | Function |
|--------------|--|
| Input | Inserted images are listed here |
| Output | Manages the geographic extents of the output image |
| Parameters | Defining the mosaicking and display options |
| Contrast | Offers different contrast matching options |
| Trend | Helps to reduce or remove brightness trends |

In the panels further options could be set. In the menus “Trend” and “Contrast” the default settings were not changed. In the menu “Output” just the “Null Value” was changed from none to set without determining a value to prevent the black colored null cells around the mosaic. In the panel “Parameters” the following options were tested in various combinations. The settings printed in *italic* were used for the mosaic process in the end.

PARAMETERS - Warping Model

- **Bilinear:** rectangles mapped onto non-planar quadrilaterals; preserves horizontal or vertical lines of the source image and the equal spacing of points along these lines; diagonal lines drawn onto quadratic curves
- **Affine:** corresponds to orthographic or parallel plane projection from a source XY-plane onto a target XY-plane; preserves parallel lines and equally-spaced points
- **Conformal:** restricted version of the affine model
- *Plane Projective:* transforms coordinates between any pair of source and target planes, including nonparallel ones; uses a perspective projection; commonly used for non-vertical aerial images of relatively flat terrain; includes all transformations of the affine model

PARAMETERS - Resampling Methods

- **Nearest Neighbor:** center of output cell equals center of cell in input raster; four closest cells in input object determined; unmodified value from the closest input cell assigned to the output cell; feature edges can be offset by distance up to half of the input cell size
- **Bilinear Interpolation:** new cell's value average of the four closest input cell values with weighted factors regarding their distance to the cell; results often similar to Cubic Convolution, but not as sharp and smoother than Nearest Neighbor
- **Cubic Convolution:** new cell value computed from a 4x4 block of surrounding input cells; generally smoother outputs

PARAMETERS - Overlap Methods

All of the following techniques except for "Last raster" compute the overlap cell values by comparing or mathematically combining the corresponding cell values of the input images.

- **Feathering:** the weighted average varies with distance from the image boundaries
- **Average:** assigns the mean of the analogous input cells
- **Maximum:** uses the maximum value
- **Minimum:** uses the minimum value
- **Chessboard:** input cell values from overlapping rasters are steadily alternated in two dimensions
- **Random Mixing:** weighted average of matching input cells used
- **Last raster:** uppermost raster in each overlap area is used for computing the output image

After the mosaic process was completed the whole overview was checked for parts where the mosaic didn't fit very well. In two cases the border between the images cut right through the main drainage respectively a hydrothermal feature. Therefore a complete part from a non georeferenced image was cut out and mosaicked to the overview map by tie points. Fig. 4.15 gives an example for that.

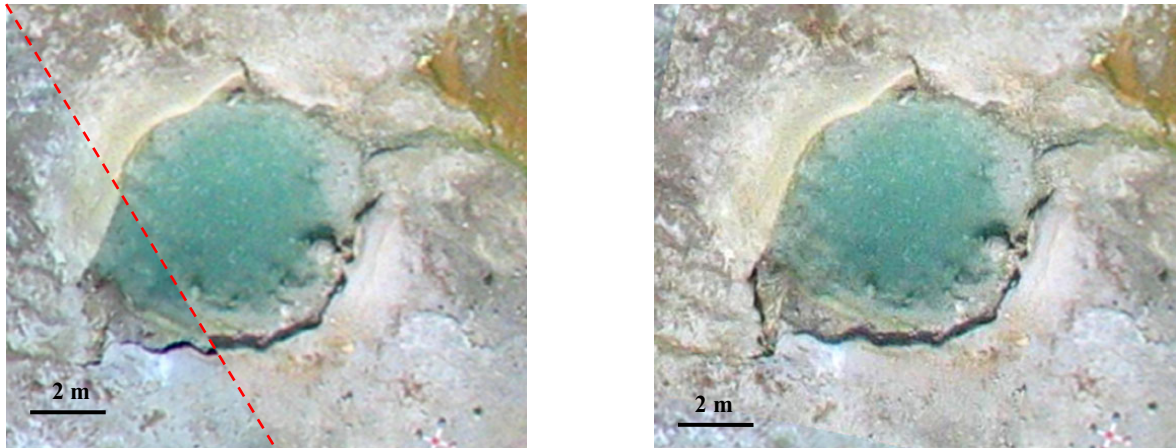


Fig. 4.15 Left – border of two images cuts through the feature; right – the whole feature was replaced by a part from a non georeferenced image

When the mosaic process was finished the whole image was georeferenced and rectified again with a total of 81 ground control points because their original coordinates were changed by the manual positioning. Then the resampling process was started to remove or reduce simple geometric distortions from the aerial pictures. For that the automatic resampling process compares ground control points with known coordinates in a standard geographic reference system to the locations predicted by the selected geometric transformation model. The results are used to determine numerical coefficients for coordinate transformation equations. For the automatic resampling process it is important that enough ground control points are exactly located and uniformly distributed across the image, which was the case (Fig. 4.7)

Similar to the mosaic process also the automatic resampling process required adjustments in different menus. Tab. 4.4 names them and describes their functions.

Tab. 4.4 The automatic resampling menus and their functions

| Menu | Function |
|----------|---|
| Model | Different transformation models selectable |
| Resample | Methods for interpolation of cell values for the output raster |
| Scale | Chosen method determines the scale of the output raster |
| Orient | For orienting the output raster relative to the output projection |
| Extents | Sets the geographic extents of the output raster |

The following adjustments were tried for the automatic resampling process. The final choice for the resampling process is printed in italic.

MODEL

- *Plane Projective:* refer to “Mosaic – Parameters – Warping Model”
- *From Georeference:* takes the transformation model that is saved in each object’s georeference subobject
- *Piecewise affine:* performs a Delaunay triangulation using the set of GCPs; for each triangle affine transformation calculated; benefit: all GCPs positioned in the exact georeferenced place

RESAMPLE

- *Cubic Convolution:* refer to “Mosaic – Parameters – Resampling Methods”

SCALE

- *by cell size:* allows to specify the size of the output cells (meter) by making entries in the text fields on size (meters); nothing was written down here, the input cell size was applied

ORIENT

- *to projection:* this selection orients the output raster to the map projection specified by the georeference control point subobject associated with the input raster

EXTENTS

- *entire input:* specifies the aerial extent of the output raster as that corresponding to the entire area extent of the input raster

The end version of the mosaicked overview has a spatial resolution of 0.025 m (calculated by the TNT mips tool “Georeference”). Features of 0.1 to 0.2 m size are clearly to identify.

The generation of orthophotos with TNTmips was a further aim of that work. But the process did not work, presumable because the estimations of the interior orientation (Camera Parameters, Principle Point) were not exact enough. Canon was contacted but not able to communicate the technical data. Therefore the GIS software Geomatica with the menu “Ortho Engine” was taken (section 4.3.3) for that process.

4.3.2.2 DIGITIZING THE GEOOBJECTS AND IMPORTING DATA

When the mosaic was done it was extracted to get uniform borders of the area. During this process the default settings were maintained.

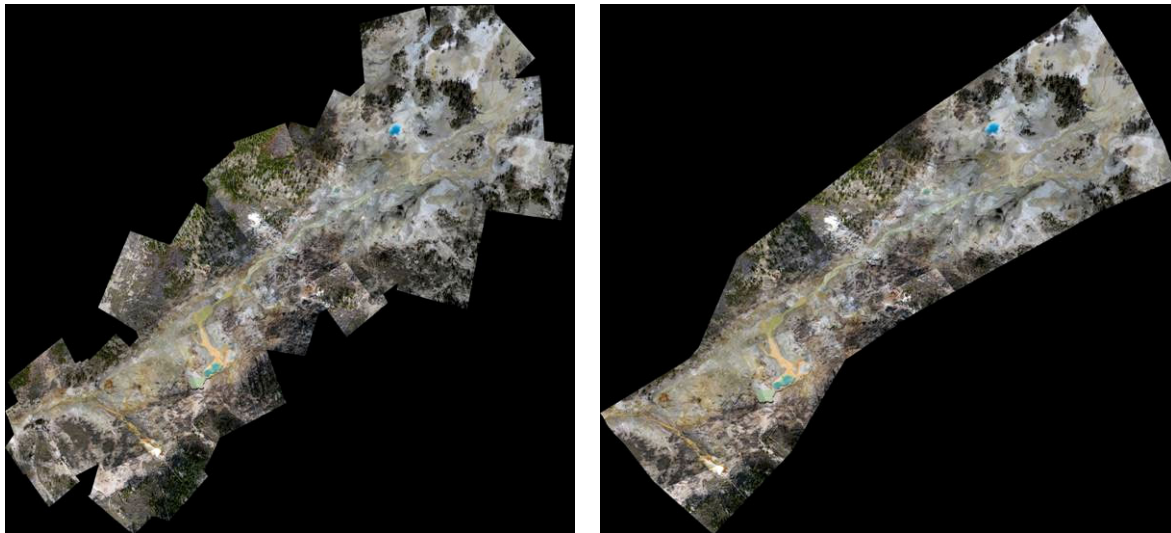


Fig. 4.16 Before (left) and after (right) the extracting process

Then all geobjects (hot springs, discharges, wet zones, fumarole areas and mud pots) were digitized from the mosaic overview and a vector layer was created (section 5.1.2.2.2). After that the different databases were imported and their data displayed in different layers with special subjects.

4.3.2.3 CREATING THE DIGITAL ATLAS

The digital atlas consists of two atlas layouts. The overview layout gives a general idea about the situation of the mapping area Ragged Hills in the Yellowstone National Park and shows the geology, hydrology and other characteristics of the whole park area (section 5.1.2.2.1). The second layout focuses on the detailed description of Ragged Hills (section 5.1.2.2.2). The mosaicked overview is complemented by aerial pictures from 1986 and

1993, a thermal overview and a geological map as well as by the representation of hydrochemical data and the mapping notes from October 2003. Additionally two pdf-files are linked to the atlas' home page – the diploma thesis and the help chapter.

The two layouts were created by opening “Display spatial data” and then “New display layout”. There, several thematic groups were defined, the respective layers were added and the new layout was saved. While creating the detailed layout one additional step was to hyperlink the photos of the hydrothermal features, fumarole areas and wet zones with the polygons of layer “General characteristics”, group “Feature”. With the help of the “Hyper Index Linker” the photos were linked to the layer as external files. Finally the start page was designed, imported as raster object and saved as atlas file (atl.). Again with the help of the “Hyper Index Linker” the atlas layouts and text files were linked to the titles in the start page. By the “Hyper Index Navigator” it is possible to activate the different levels, switch between the layouts, and return to the home level.



Fig. 4.17 Start page of the digital atlas of Ragged Hill

4.3.3 GEOMATICA

As Fig. 4.18 shows the work with the GIS software Geomatica “Ortho Engine” started with the definition of a new project and the selection of a math model. Following the adjustments for the “Options”, the “Output Projection” and dependent on the chosen mathematical model the “Camera Calibration” had to be done. Then the non-georeferenced aerial photos were imported by the option “Data input”. With the menu “Collect GCPs manually” the coordinates of the crosses were selected in all images (Step 2 of Fig. 4.18). The possibility to import the corresponding GCP coordinates from a text file simplified the work. In contrast to the simple math model “Rational Functions” it was possible to use tie points for fine adapting the images when using the rigorous math model “Aerial Photograph”. Having ended this work the math models were computed and afterwards the orthorectification or geometric correction took place (Step 3 of Fig. 4.18). The last step was to mosaic the computed orthophotos.

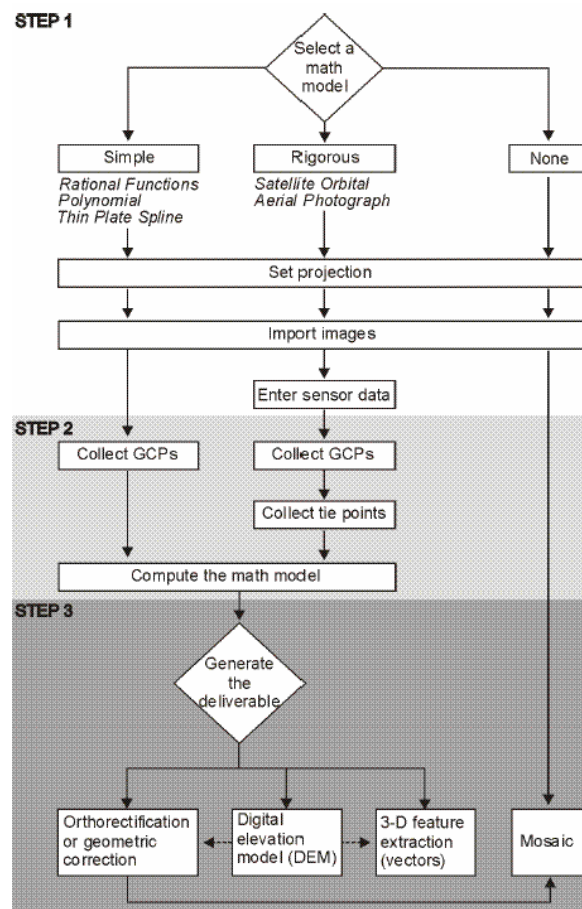


Fig. 4.18 Basic workflow of “OrthoEngine” (PCI Geomatics Enterprises Inc. 2003)

Two different mathematical models were tried for generating orthophotos. First the rigorous math model “Aerial Photography” was used with the following settings:

- **Options:** Compute from GCPs
- **Output Projection:** UTM, Zone 12, Row T, NAD 83, GRS 1980
- **Camera Calibrations:**
 - Focal Length:* 37.5 mm¹
 - Chip Information:* width 2.45 mm and height 4.572 mm
 - Y-scale factor:* 1.00
 - Radial Lens Distortion:* 0.00
 - Decentering Distortion:* 0.00
 - Other Parameters:* Photo scale 1:200

This precise mathematical model, based on the geometry of a frame camera, can compensate the effects of topography and warping inherent to the camera. Because the necessary camera calibration standards were missing for the “Canon Power Shot G5” it was only possible to estimate the values needed. Nevertheless the model wasn’t able to generate orthophotos, presumable the estimations of the camera calibrations weren’t exact enough. The second rigorous math model “Satellite Orbital Modeling” wasn’t tried because in this case the balloon would be supposed as satellite. That presumption deviated too much from the reality.

The simple mathematical modeling method “Rational Functions” worked without camera calibration. The new project was just defined by the

- **Math Modeling Method:** Rational Functions
- **Options:** Compute from GCPs
- **Output Projection:** UTM, Zone 12, Row T, NAD 83, GRS 1980

¹ The focal length was approximately calculated by the ideal formula $m_b = h/c$ (m_b : scale, h : height, c : focal length; Luhmann 2000).

This method calculates a correlation between the pixels and their ground locations and can be more exact than the Polynomial Model that doesn't include the elevation or the Thin Plate Spline Math Model that is more inaccurate. The mathematical model is computed separately for each image and it uses the ratio of polynomial functions to compute the image row and column. The polynomials are described by using a set of coefficients which were in that case calculated automatically by OrthoEngine. Three of them were used in this case, ten are recommended for producing generally the best results.

In the window "Ortho Generation" the default settings were not changed and all georeferenced images run through the "Ortho Process" when using the "Rational Functions" math model. While using the "Aerial photography" method the program wasn't able to do the geometric correction before.

After that some orthophotos were mosaicked manually. However the offsets between the pictures were too big and for a better adaptation the usage of additional tie points would have been necessary. But tie points can't be used in the "Rational Functions" method. Therefore the work was terminated at this point. The adaptation between the images would not get better than with TNTmips.

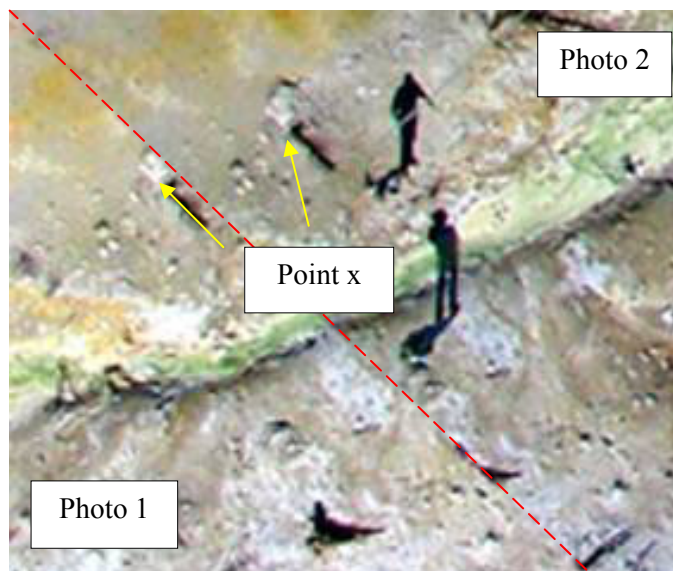


Fig. 4.19 Part of the mosaic created with the math model „Rational Functions“

5 RESULTS AND DISCUSSION

5.1 DIGITAL ATLAS²

The atlas represents the area Ragged Hills from different points of view. The subdivision into four sections helps to find the required information:

1. Overview Yellowstone National Park
2. Study area Ragged Hills
3. Diploma thesis (pdf-file)
4. Help (pdf-file)

The overview layout (1) gives a general idea about the location of the Ragged Hills area in the Yellowstone National Park and includes the geological and hydrological settings, a digital elevation model (DEM), the major roads, and the topography map of the whole park area. The second layout “Study area Ragged Hills” (2) contains detailed information about the Ragged Hills area with different vector and raster objects on hydrochemistry, geology, the geothermal situation, the development of the features through time and their distribution. Additional data such as the mapping notes about the hydrothermal features from October 2003 and hydrochemistry data from different sampling campaigns are included in tables linked to the vector objects.

The digital atlas documents the development of the hydrothermal features as of September 2003 as a basis for future observations. It combines different subjects and enables a comparison between individual layers for various objectives.

The atlas of Ragged Hills was created with the GIS software “TNT mips” version 6.8 (Copyright (C) 1988-2004 MicroImages, Inc.; www.microimages.com). With the public domain software “TNT atlas for x” the atlas can be browsed at any computer without having installed the full licensed version of “TNT mips”.

² Mapping part of the diploma thesis

5.1.1 WORKING WITH THE ATLAS

5.1.1.1 NAVIGATION



Fig. 5.1 Start page of the digital atlas Ragged Hills with the main tool bar

After opening the atlas it is recommended to choose the “TNT atlas for x” with the “X Desktop”. Using the “Windows desktop” some diagram colors won’t be displayed correctly. To navigate through the atlas the following tools exist (Fig. 5.1):

 **Hyper Index Navigator:** Activate this icon, click on the underlined text of the section titles and the corresponding pdf-file or atlas layout will open. This tool is also helpful in the section “Study area Ragged Hills”, group “Features” where photos are linked to the individual feature polygons or in the overview layout, where legends are linked to the geological map.

 **Back to previous level:** Directs to the level used before.

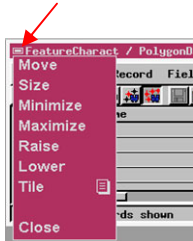
 **Back to home level:** Opens the start page of the digital atlas.

 **Show Hyper Index Navigator:** This icon opens the Hyper Index Navigator that offers different options to navigate the atlas. Besides the links to the start- or previous level, the arrows direct to the start page sections. Cursor over indicates the associated section.



5.1.1.2 IMPORTANT TOOLS

In the following, the most important tools for effectively working with the layers and their database are explained. For further questions use the help index in TNT atlas.



Click on the small rectangle in the upper left corner to open the main menu for changing the window size, order, and position. The options “raise” and “lower” only appear when there are overlapping windows.



Select: Use this icon to select features and structures of vector objects. If a table is linked to the selected structure it will open (section 5.1.2.1).



GeoToolbox: Gives different possibilities to measure lengths, areas and so on. For example in the layout “Study area Ragged Hills”, group “Survey control points”, the difference between the ground control points coordinate measured with the DGPS and the theodolite may be examined.



Zoom Box: Zooms in any section of the layer.



View-in-view: Turns the top layer transparent and the selected layer below can be seen. When activating this icon pink checks appear next to the black ones. The required layer can be selected by activating the pink checks (section 5.1.2.2.1, Aerial photos). Right mouse-click activates the reverse display.



GeoLock: Automatically connects the position and scale between multiple View windows. Scroll and zoom actions in one window are simultaneously applied to the linked views. It is possible to turn off the geolocking in selected views to adjust viewpoint and zoom independently.



Pan View: Shifts the view over a chosen distance in a defined direction by drawing a line in the view to define the pan operation.

5.1.2 THE GROUPS AND LAYERS

5.1.2.1 GETTING STARTED

The atlas layouts are subdivided into several thematical groups that are further separated in different layers. The default overview shows only the basic groups and layers. For combining different layers click on the grey rectangle to the left of each group to display it. The group opens and it is possible to select different layers. Displaying the layer also opens the corresponding legend. If this is not the case clicking on the plus sign to the left of the layer title opens the legend view.



Fig. 5.2 The black checks mark the displayed layers; the black box determines the active group/layer

Tables with further information are connected to the vector layers. Activate the  “Select” icon and chose one feature in the view. The corresponding table opens automatically and the selected structure is marked by a red point in the table. If not, the corresponding table can be opened in the “TNT layer manager”. Vice versa, selecting a record in the table marks the corresponding feature in the layer in pink (select the record by clicking on the grey rectangle left of the record  and then click on “Select elements” ).

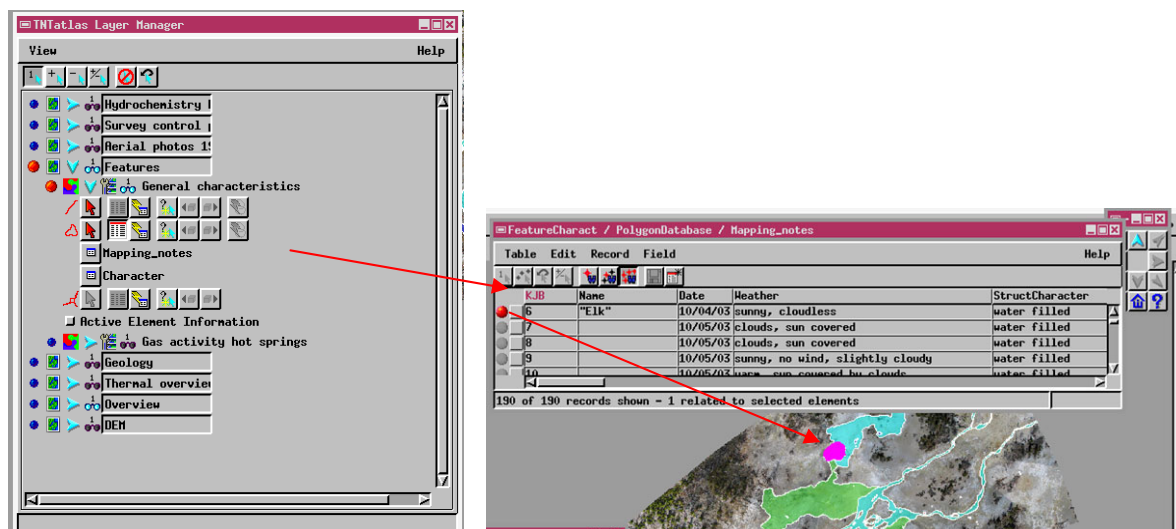


Fig. 5.3 Left: TNTAtlas Layer Manager, right: linked tables and selected feature

When working with the tables it might be advisable to switch between the “Tabular view” and “Single record view” that are offered by the menu “Table”. Especially when a record contains numerous data the “Single record view” is recommended for a better overview. For comparing different data, the “Tabular view” is suitable.

5.1.2.2 INDIVIDUAL LAYERS

If not stated otherwise, all layers were georeferenced based on the Universal Transmator System, Zone 12 North, spheroid GRS 80, datum 83.

5.1.2.2.1 GROUPS OF THE OVERVIEW LAYOUT

- **Situation Ragged Hills:** The vector object layer informs about the approximate situation of the study area Ragged Hills in the Yellowstone National Park.
- **Boundary YNP:** The vector object layer contains the boundary line (Spatial Analysis Center, Yellowstone National Park 1995).
- **Hydrology:** The two vector object layers include the rivers (National Park Service Water Resources Division 2001) and the major lakes (Spatial Analysis Center, Yellowstone National Park 2000) of the park.
- **Major roads YNP:** The vector object layer illustrates the course of the Park’s major roads (Spatial Analysis Center, Yellowstone National Park 1997).
- **Overview Ragged Hills:** The raster object layer (section 4.3.2.1) is based on the aerial photos taken from the balloon. Reference points marked as crosses on the ground and their corresponding coordinates from the theodolite measurements were taken for georeferencing the balloon images. After the images were mosaicked³, the aerial overview was resampled⁴ and the mosaic of about 40 pictures was extracted to a semi regular rectangular shape with smoothed borders⁵.

³ **Mosaic process:** manual positioning by tie points, *Parameters* – plane projective, cubic convolution, last raster, *Output* - null value from none to set, nothing else changed at the default settings

⁴ **Resample process:** *Model* – piecewise affine, *Resample* – cubic convolution, *Scale* - by cell size, *Orient* – to projection, *Extents* - entire input, *Output extents* - default settings, *Output Projection* – UTM, *Output cell size (m)* – default settings, *Null Value* - user defined 0.00

⁵ **Extract process:** default settings

- **DEM:** The raster object layer (Spatial Analysis Center, Yellowstone National Park 1998) with a ground resolution of 10 m was extracted to the extensions of the Yellowstone National Park as in the vector object “Boundary”. The elevation in feet is shown by the mouse over function. The layer has to be active (black box around, refer to Fig. 5.2) to apply this function.
- **Topography map YNP:** The raster object layer consists of several topography maps combined in one object (WGIAC 2004).
- **Aerial photos:** The two raster object layers consist of two aerial photos from 1986 and two from 1993 (Technical Information Center 2004). The images were first mosaicked⁶ and then georeferenced from the objects “Overview Ragged Hills”, “Major roads YNP” and for the aerial photos 1993 additionally referring to the photos from 1986. Therefore the coordinates from these aerial photos are not exact but only very rough estimates.

Hint: Using the “View in view” tool  and drawing a rectangle with the cursor opens a “window” through which the layer below can be seen. The user has to select the desired combination of layers by activating or inactivating individual layers. As the example in Fig. 5.4 shows, the black check determines the layer above (*Overview Ragged Hills*) and the pink check the layer that is visible through the window below (*Aerial photos 1993*) and therefore to see through the “window”.

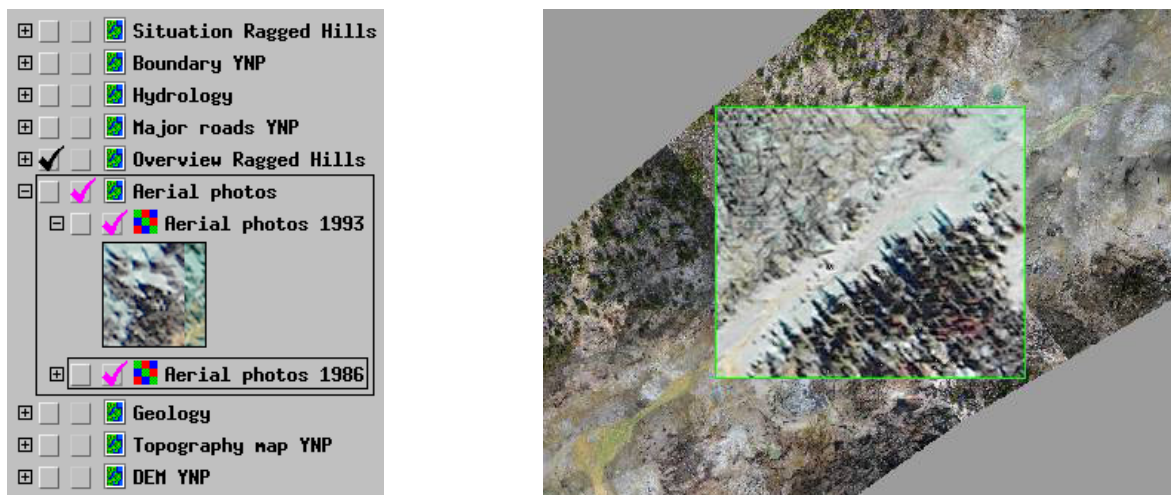


Fig. 5.4 Using the View in view tool enables to watch layers that lie on top of each other

⁶ **Mosaic process:** manual positioning by tie points, *Parameters* – plane projective, cubic convolution, last raster, *Output* - null value from none to set, nothing else changed at the default settings

Geology: The raster object layer (Christiansen 2001a) was georeferenced and extracted to the extensions of the Yellowstone National Park as in the vector object “Boundary”. The coordinates are not exact because of the rough adaptation. For a legend refer to the individual geological units in the appendix (Appendix No. 9.2 and Appendix No. 9.3). The two vector object layers (Henry Heasler, National Park Service, written communication) include information about the shape of the dome and the caldera in the Park area.

Hint: Using the Hyper Index Navigator tool  and clicking anywhere in the layer opens the legend part A and B of the geological map (imaging-files).

5.1.2.2.2 GROUPS OF THE DETAILED LAYOUT

- **Survey control points:** The two vector object layers illustrate the ground control point coordinates measured by theodolite (red flags) and differential GPS (green flags) (section 4.2.1).
- **Aerial photos from 1986 and 1993** (section 5.1.2.2.1): The mosaicked aerial photos were extracted to the extension of the raster object “Overview Ragged Hills”.
- **Geology:** The vector object layer is based on a scanned and imported geological map (White et al. 1988). The map was georeferenced from the vector object “Major roads of YNP” and the coordinates are therefore not precise. The area of Ragged Hills was digitalized and the legend for the geological units obtained from the original map. The legend data are saved in a table linked to the vector object.
- **Features:** The two vector object layers show the general characteristics of the features and the gas activity of the hot springs (section 4.2.3.1). A table including the mapping notes from October 2003 is linked to the features.

Hint: Photos are linked to the individual feature polygons. Activate the Hyper Index Navigator  and click on the polygons to open the corresponding image (jpeg-files).

- **Overview map Ragged Hills:** The raster object layer is already described in section 5.1.2.2.1.

- **Thermal overview:** The raster object layer (photos taken by Mattson, E. and Plummer, M., Idaho National Engineering and Environmental Laboratory, Geoscience research group, 2003) consists of images mosaicked to one overview⁷. The overview is georeferenced from the aerial mosaic from 2003 and the coordinates are therefore not precise.
- **DEM** (section 5.1.2.2.1): The raster object layer is extracted and resampled from 10x10 m to 1x1 m⁸.
- **Hydrochemistry U.S.G.S. – part A** (pH, EC, iron species, arsenic species): Twenty vector object layers represent the chemical data part A (Ball et. al 2002, McCleskey et al. 2004, hydrochemistry data 2003 unpublished). All sampling data given in the table are in mg/L units if nothing else is stated.
- **Hydrochemistry U.S.G.S. – part B:** Seven vector object layers represent the predominant elements chloride, potassium, lithium, sodium, sulfate, silica and fluorine (Ball et. al 2002, McCleskey et al. 2004, hydrochemistry data 2003 unpublished). All sampling data given in the table are in mg/L units if nothing else is stated.
- **Hydrochemistry BPF – part A** (pH, EC, iron species, arsenic species): Seventeen vector object layers represent the chemical data part A (Planer-Friedrich 2004). All sampling data given in the table are in mg/L units if nothing else is stated.
- **Hydrochemistry BPF – part B** (predominant elements): Seven vector object layers represent the chemical data part B (Planer-Friedrich 2004). The predominant elements chloride, potassium, lithium, sodium, sulfate, silica and fluorine taken from PHREEQC modeling with the database WATEQ4F. All sampling data that are given in the table are in mg/L units if nothing else is stated.

Hints and explanations: refer to following page

⁷ **Mosaic process:** manual positioning by tie points, *Parameters* – plane projective, cubic convolution, last raster, *Output* - null value from none to set, default settings for remaining adjustments

⁸ **Resample process:** Model - from georeference, Resample – cubic convolution, Scale - by cell size, Orient - north at top, Extents - entire input, Output extents - default settings, Output projection – UTM, Output cell size (m) - line 1.00, column 1.00, Null value - user defined 0.00

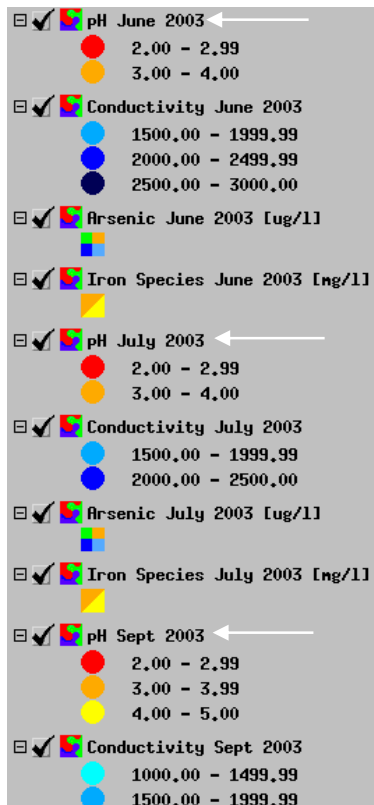


Fig. 5.5 Hydrochemistry legend

The legend of the group “Hydrochemistry BPF – part A” shows 17 layers of hydrochemistry data (Planer-Friedrich 2004). The on-site parameters and the arsenic as well the iron species layers are separated according to their sampling dates (e.g. pH June 2003, pH July 2003, pH September 2003; see white arrows in Fig. 5.5). For pH and conductivity circles in different colors represent different concentration as explained in the legend.

The group “Hydrochemistry BPF – part B” illustrates the predominant elements in one layer as 3D bar graphs (Fig. 5.9; Planer-Friedrich 2004). The colors of the bar graphs are shown in the legend. The units of all elements are given in the legend in brackets.

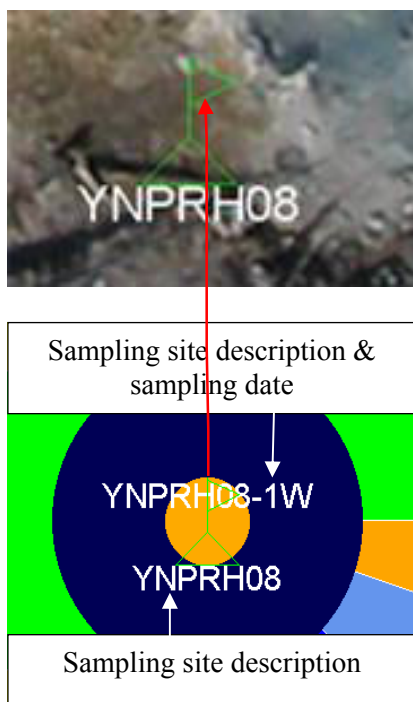


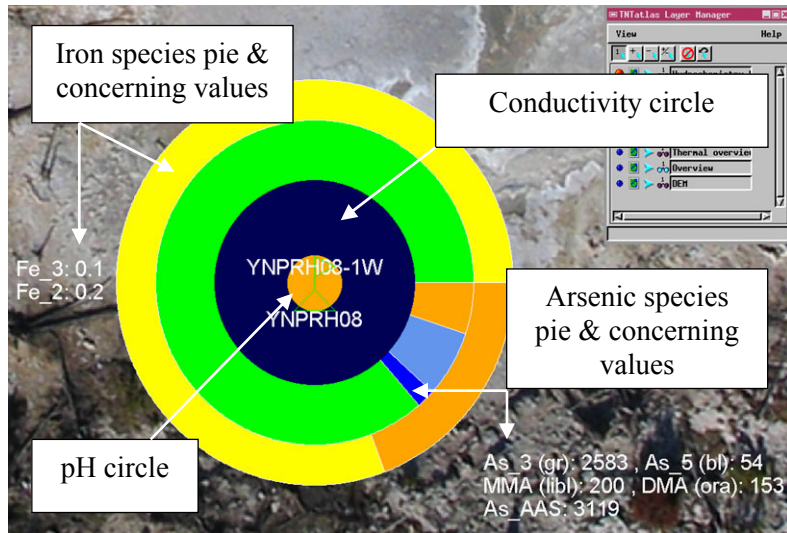
Fig. 5.6 Sampling site description

At each sampling site the site code is displayed. It is connected with the layer “sampling point” (small green flag) that shows the exact sampling site location. The example of Fig. 5.6 “YNPRH08” stands for “Yellowstone National Park Ragged Hills sampling site number eight”.

Additionally a site sampling code might be displayed. It is attached to the pH-layers and includes the sampling time. “YNPRH08-1W” means “Yellowstone National Park Ragged Hills sampling site number eight – June 2003”.

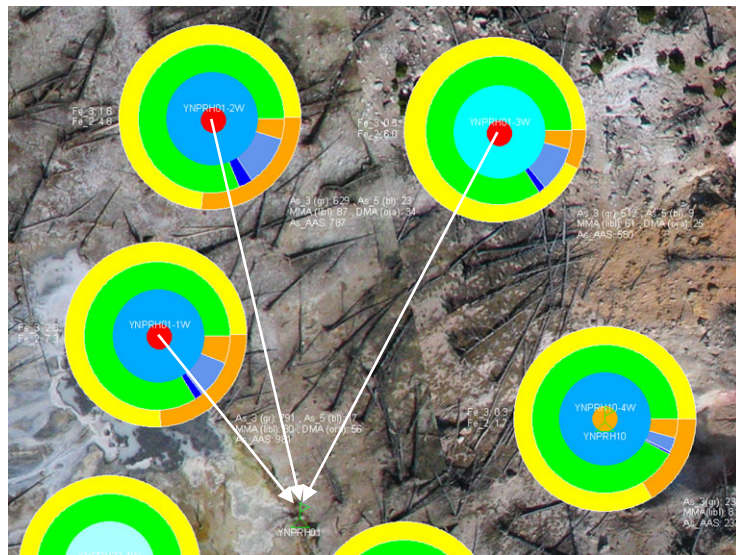
The following definitions for the sampling dates of exist (Planer-Friedrich 2004):

1W - June 03, 2W - July 03, 3W - Sept 03, 4W - Oct 03.



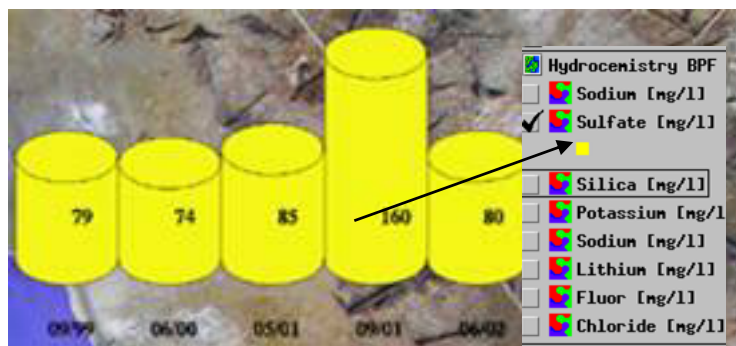
The hydrochemical pie chart shows a combination of the on-site parameters pH and conductivity as well as the share of arsenic species and iron species. Additionally, the concentration for the iron and arsenic species are printed next to the pie chart. The corresponding units can be seen in the legend.

Fig. 5.7 Explanation of the hydrochemical pie charts



When sites were sampled two or three times it was necessary to rearrange the pie charts to show the hydrochemical results of all sampling campaigns in one layer. The small green flag marks the sampling location (missing in the rearranged pie charts). The sampling site description connected with the pH layer enables to assign the pie charts to the corresponding sampling site.

Fig. 5.8 Connection between sampling site and pie charts



Predominant elements are displayed in 3D bar graphs. To see them the pie charts should not be displayed. The bar graphs are arranged along an x-axis for the different sampling times that are printed below the axis. The concentrations are given in the corresponding bar, and its units are written in the legend.

Fig. 5.9 Illustration of the elements shown by 3D bar graphs

5.2 METHODS EVALUATION

The following sections evaluate the field and computer work regarding time and expenses based on the experiences from this project. The timetables are estimated not including familiarization with programs or equipment nor major breaks or delays. Of course the time estimates also depend on the surrounding conditions such as the weather, functioning of the equipment and personal experience of the people employed. Therefore the following evaluations should only be seen as clues for other projects to give an idea about the time it takes to carry out the several working steps and to help preparing similar projects.

This section is subdivided into the ground survey work that evaluates the establishment of the survey grid and the measurements of coordinates by differential GPS and theodolite. It is followed by the aerial survey chapter that calculates the aerial photography survey by balloon and airplane. The digital processing of the digital atlas is described at the end.

5.2.1 GROUND SURVEY

The ground survey began with collecting stones for laying out the preliminary raster of ground control points. Because there was enough material around, it didn't take too much time to collect the necessary 102 stones. More time it took to mark the stones as research equipment by blue, inscribed plastic stripes. Marking was necessary because the work took place in a National Park (Fig. 5.10). While one respective two persons were looking for stones and marking them another one distributed them in an interval of 28 m.



Fig. 5.10 Marked stone

Because it took too much time to measure the distance exactly by ruler the distance between the stones was estimated by the step width of one and the same person to get a regular raster. Collecting and marking the stones as well as distributing 102 ground control points took two persons two days. The following differential GPS measurements were done by one person in 9 hours, including problems of GPS signal reception, walking between the ground control points and troubles re-locating some of the marked points in the undergrowth. The differential correction and evaluation of the measured coordinates took about 4 hours. After the last modification of the raster that was done by two persons

in about an hour (10 points had to be relocated to obtain a more regular raster), the stones were replaced by the crosses consisting of two red-white plastic stripes. Cutting the 1 m stripes from continuous tape took two persons about 3 hours. Two persons worked 10 hours to place each time two of the 1 m long plastic stripes right-angled to each other, fix the four ends by stones and the middle of the cross by a small screw. The cross-head screw helped besides fixing the cross also to put the one feed reflector in place during the theodolite measurements later (Fig. 4.7). After the final survey grid was established survey work with the theodolite began. A minimum of two better three people was necessary for that work. One person had to operate the total station and one person the reflector. Because of the difficulty to level the one feed reflector and give simultaneously a signal to the total station's operating person to start the measurement, it was better to operate the reflector by two people. In this way one leveled the reflector and the other one gave the signal that the measurements could start by lifting his arm. In addition the second person replaced natural obstacles that hindered the measurements. Because of data processing problems the theodolite measurements were done two times. The first time it took three persons 5 hours, the second time two persons 7 hours. The second time a way was found to give a signal while leveling the reflector by moving the finger in a special direction. That movement didn't disturb the leveling process and the person working at the total station saw it through the theodolite's viewfinder and started the measurement. The given working time additional depended on outer conditions as with strong wind leveling the reflector was difficult and natural obstacles as trees or also grass also hindered the total station to shoot the reflector.

The detailed ground mapping of about 100 feature groups that mostly consisted of several single features took 8 days for two persons.

The water sampling was done in irregular intervals during the other work. It took two hours to sample one feature with two persons including all determinations as described in "Methods applied".

The Tab. 5.1 summarizes the timetable, equipment and expenses for the ground survey work described above.

Tab. 5.1 Timetable, equipment and expense⁹ for ground survey work

| Work | Equipment | Expenses | Man days |
|--|---|--|----------|
| Collection, marking and distribution of 102 stones | Stones; ca. 5 m blue plastic stripe of 1.5 cm width; waterproof pen | Blue plastic stripe: 4 € (5 \$) | 4 |
| Differential GPS measurements | Differential GPS | ~ 4000 € (4800 \$) | 1-2 |
| Replacing 102 stones by crosses | 200 m red-white plastic stripe of 0.08 m width, 4 stones and one cross-head screw per cross | Red-white plastic stripe for 8 € (10 \$), 100 screws for 1.60 € (2 \$) | 2-3 |
| Theodolite measurements | Total station, tripod, reflector | ~ 9000 € (10800 \$) | 2 |
| Mapping of about 100 feature groups | Book, pen, rule, compass, camera | Compass 300 € (360 \$); camera ~ 300 € (360 \$) | 16 |
| Water sampling of 19 feature | Probes for pH, EC, redox potential, oxygen and field computer | ~ 1666 € (2000 \$) | 10 |
| | Photometer, chemicals | 1000 – 2000 € (1200 - 2400 \$) | |
| | sampling bottles | 100 mL bottle ca. 1 € (1.20 \$) | |
| | Anion, cation exchangers | 54 SAX 163.53 € (196.20 \$); 50 SCX 120 € (144.00 \$) | |
| | Syringes; container | 10 syringes about 3 € (3.60 \$) | |

5.2.2 AERIAL SURVEY

The balloon survey took two times 2 hours to get a total of 180 images of the 530 m x 250 m area that were sufficient to create the overview mosaic. Two days were necessary because the balloon aerial photography was only feasible during the calm hours of the day. Early in the morning too much steam raised up from the hot springs because of the temperature differences between the cold air and the hot springs. Taking pictures at that time no features would have been seen at the shots. Therefore the time around midday was chosen for the balloon survey. To inflate the balloon three persons were necessary, to operate it two.

⁹ 1 € = 1.2 US Dollar

To take images from the airplane two people were necessary. The pilot operated the airplane while the co-pilot worked the camera system. After having found the best method to release the camera (section 4.2.2.2), the mapping area was overflown several times. Unfortunately, the images taken were not usable for creating the digital atlas as during the first flights the images were blurred. After the exposure time was reduced to 1/2000 clear images were obtained. But the pictures from the following flights didn't show the target area as it was difficult to fly the exact route over the mapping area. In addition flying at 610 m (2000 ft) with 4 x optical zoom (comparable with 152 m/500 ft height) enabled an average image resolution of 0.06 m. That is sufficient but not comparable to that of the balloon's images (0.03 m). To get better resolutions it is necessary to fly at lower heights as for example at 152 m (500 ft). That is prohibited in National Parks in the USA. At least an 8 M pixel camera or a 6 x 6 camera should be used for better resolutions.

It is to conclude that this technique still has to be optimized. Taking aerial images with the thermal camera two persons were necessary additional to the pilot: One person for exposing the camera construction outside the window, a second for operating the thermal camera by a laptop (Fig. 4.12).

The photos from the balloon and from the single-engine airplane were taken by the "Canon Power Shot G5". The price for this digital camera was 799,- € (958 \$) (Canon 2004). To determine the tracking of the balloon and the flying route of the Cessna the GPS "Garmin-12" was used that costs around 200 € (240 \$).

The constructions to mount the camera at the balloon respective at the airplane were designed and built in Freiberg at the mechanical workshops of the faculty of geosciences, geotechnique and mining as already mentioned before. Building the balloon construction took 28 hours, the Cessna construction took 72 hours.

The Tab. 5.2 and Tab. 5.3 give estimations for the balloon's respective airplane's aerial photography equipment expenses. For more detailed description of the equipment assembly and structure refer to "Methods applied" page 47.

Tab. 5.2 Calculated expenses for the aerial photography equipment with the balloon

| Equipment | Expense |
|--|--------------------------------|
| Latex balloon with 4.5 m perimeter | 16.35 € (19.62 \$) per balloon |
| Plastic clips | 1.25 € (1.50 \$) per clip |
| Tether lines | 8,- € (9.60 \$) |
| Wire, aluminum sheets and sticks, screws | 20,-€ (24 \$) |

Tab. 5.3 Calculated expense¹⁰ for the aerial photography equipment with the Cessna 172

| Equipment | Expense |
|--|--|
| Cessna 172, rented | approx. 56 €/h (70 \$/h); (58 \$/h for Cessna 152 that would also be sufficient) |
| Aluminum plates for the whole construction | 132,-€ (158.40 \$) |
| Oval drill hole of the cardan construction | 406,-€ (487.20 \$) |
| Screws | 30,-€ (36 \$) |
| Pneumatic shutter | 10,-€ (12 \$) |
| UV filter | 29,- € (34.80 \$) |

It is to conclude that the balloon's construction is cheaper and easier to build than the airplane's that requires a higher expenditure in money and time.

5.2.3 DIGITAL ATLAS

The following timetable is calculated for one person who is already familiar with the GIS software used (Copyright (C) 1988-2004 MicroImages, Inc.; www.microimages.com). An Acer Travel Mate 660 (processor 1400 MHz, 1.40 GHz memory and 480 MB Ram) was used for that work.

The evaluation of 180 balloon aerial images and the following georeferencing of 90 images took 2 weeks. Georeferencing nearly all images enabled to choose the fit with the highest quality for the mosaic process. Only images with too few ground control points and double pictures were sorted out. That part of the work was with 2 weeks very time intensive because the coordinates of every control point had to be entered manually. Afterwards the mosaic process was started. As the best fitting images were added one by one and the fine adaptation was done manually that work took again 6 days. Additional the computer processing time increased with every new adapted image. Computer processing problems and thus necessary repetitions are not included in the time estimation. The rectification of the mosaic – resampling and extracting processes – took a maximum of two hours provided that the combination of adjustments is known. After finishing the mosaic overview the digitizing of all features took one day. Then all necessary data were processed and imported as tables. It took three weeks to enter the field notices into the computer and thus to process the table “Mapping notes”. The arrangement of the water

¹⁰ 1 € = 1.2 US Dollar

chemistry tables of Planer-Friedrich and the U.S.G.S. took 1 week. Afterwards the layers were arranged. The raster layers didn't take too much time because in most cases they only had to be georeferenced, mosaicked and extracted. The arrangement of the vector layers were more time intensive because as in the layer "Features characteristics" or in the hydrochemistry layers the data entered were illustrated by bar graphs or pie charts and scripts had to be written for that. Furthermore the records of the table "Mapping notes" had to be linked one by one to the corresponding polygon features in the layer "Features characteristics". The arrangement of all layers took three weeks. The hydrochemistry groups of Planer-Friedrich and the U.S.G.S. with 10 days and the group "Features" with 4 days were most work intensive. Linking the total of 181 ground photos (jpegs) to the features polygons in the layer "Features characteristics" as external jpg.files took one day. Arranging the atlas consisting of the two layouts and the start page was done in one day.

Tab. 5.4 Timetable for processing the digital atlas by a person experienced with GIS software

| Work | Work in detail | Man days |
|-----------------------------|--|-----------------|
| Georeferencing the images | -- | 14 |
| Mosaicking the images | -- | 6 |
| Rectification of the mosaic | Resampling and extracting | 1 |
| Digitizing the features | -- | 1 |
| Data processing | Combining the field notices in one table, arranging the chemistry data of Planer-Friedrich and the U.S.G.S. | 28 |
| Designing the layers | Georeferencing, extracting and mosaicking the raster layers; linking tables, writing scripts and illustrating the data for the vector layers | 21 |
| Linking the images | -- | 1 |
| Arrange the atlas | Combining groups and layers to the two layouts, drawing the start page, linking the layouts and pdf-files | 1 |

5.3 INTERPRETATION OF MAPPING RESULTS

“Change has always characterized the thermal features located in the Norris Geyser Basin.” (Lewis, 1964)

Data from different sampling campaigns and diverse references were used for the following report about the changes that appeared in the Ragged Hills area since the early 1990s. Those alterations are results from an increasing geothermal activity and heating of the area’s subsoil. The section is subdivided into the description of morphological changes of geothermal features and the evaluation of the hydrochemistry data. Regarding the morphological changes just a visual evaluation from the aerial photographs was possible as for using automatic classification processes the area was too small.

5.3.1 MORPHOLOGICAL CHANGES

The topography of the mapping area is characterized by a flat terrain with low elevations in the southwestern part of the region. The area can be differentiated in two characteristic districts. The northeast is a wide, flat plain (Ø 2283 m asl) drained by one main and

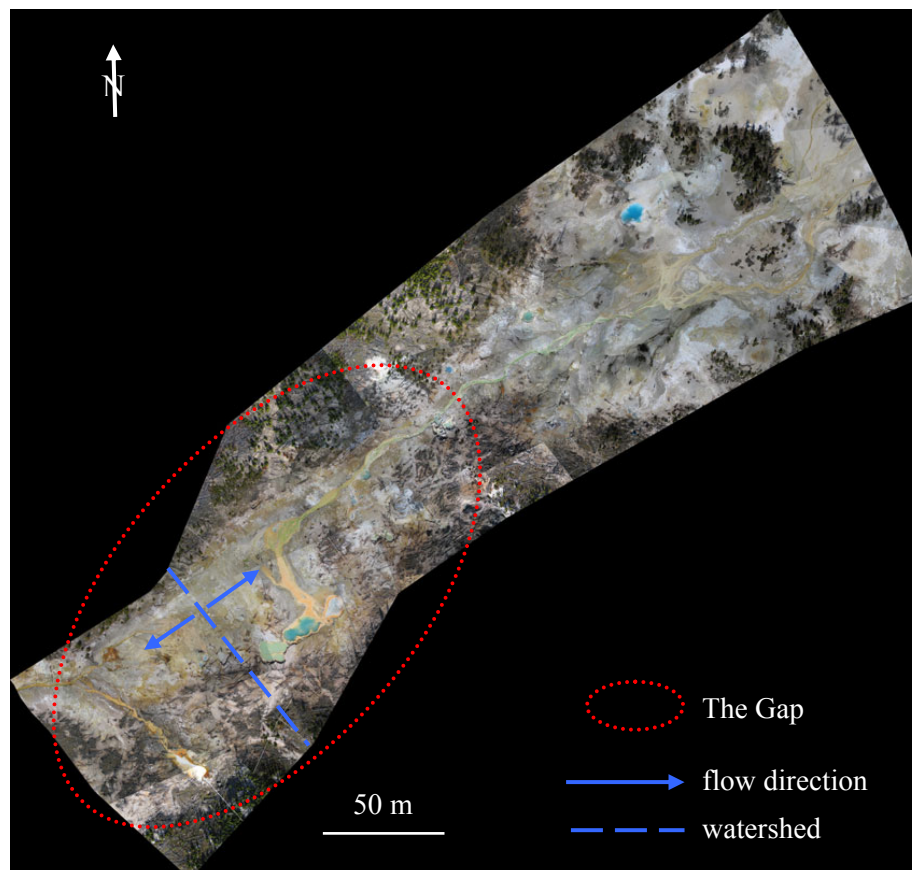


Fig. 5.11 Overview Ragged Hills

several smaller discharges. The southwestern region is also flat (\varnothing 2286 m asl), but more comparable to a long stretched valley bordered by the hills mentioned before, a smaller one in the northwest (2295 m asl) and a higher one in the southeast (2310 m asl). Because of its shape this region is named The Gap. The watershed in the southwest of The Gap area is also the highest point of the mapping area (2288 asl). The water flowing to the southwest discharges into the Gibbon River, the discharges running to the northeast pass the flat northeastern plain and drain into Tantalus Creek. Hydrothermal features feed these discharges and strongly characterize the landscape today.



Fig. 5.12 Norris Geyser Basin looking northeast, right in the foreground Ragged Hills, October 1967 (White et al. 1988)

That this was not always the case is proved by the aerial photos from 1967 (Fig. 5.12) and 1986 (Appendix No. 9.4). In contrast to today's situation hot springs or other hydrothermal features were rare at that time. The aerial photos illustrate an area with small, hardly visible drainages and green trees at the hills that prove vital vegetation and thus no upheated subsoil as typical for other geothermally active regions in the Park. In the aerial photo of 1986 some hardly identifiable hot springs may have already existing – one at the place of the today's "Persnickety Geyser" (marked in blue Appendix No. 9.4). About 60 m northeast of this first structure, a second feature can be distinguished (marked in green Appendix No. 9.4). A third one might be supposed at the southwestern end of the Ragged Hills area, where a small barren place can be found in a group of trees (marked in red Appendix No. 9.4).

The only hot spring that is mentioned in the Annual Reports of the Norris Geyser Basin from that time is Crystal Spring. It is not visible at the aerial photographs but it is the oldest hot spring described from that area. It is already mentioned in the U.S.G.S. map of Norris Basin from 1967. The Annual Reports refer to that hot spring although there were some uncertainties about its existence in the late 1970s. Crystal Spring remained hidden along the base of the Ragged Hills and a cursory search in early summer 1977 found no feature big enough to bear a name (Pittenger 1977). Similar statements can be read in the

That this was not always the case is proved by the aerial photos from 1967 (Fig. 5.12) and 1986 (Appendix No. 9.4). In contrast to today's situation hot springs or other hydrothermal features were rare at that time. The aerial photos illustrate an area with small, hardly visible drainages and green trees at the hills that prove vital vege-

Annual Reports of 1978 and 1979. Only in 1980, Hirschmann again mentioned the hot spring in the Norris Annual Report and its location was identified definitely by Lee Whittlesey in summer 1983 (Rocco 1984). The Tab. 5.5 compares the characteristics of Crystal Spring measured in 1973 and 2003. Significant changes are not noticeable. That could prove the statement that the northeastern plain shows less hydrothermal activity than The Gap area (see below).

Tab. 5.5 Characteristics of Crystal Spring in 1973 (Hutchinson 1973) and in 2003 (own data)

| Time | Length (m) | Width (m) | Depth (m) | Temp. (°C) | pH | Water |
|---------------|-------------------|------------------|------------------|-------------------|-----------|-------------------|
| 1973 | 6.4 | 2.75 | 0.6 | 86 | 3-4 | clear, colorless |
| 06/09 2003 | 8.00 | 2.4 | 0.3 to 0.5 | 83.40/71.30 | 5.7/3.1 | cloudy, colorless |

A comparison of the aerial photos of 1967 and 1986 to the aerial overview from 1993 demonstrates first changes again hardly identifiable, also because of the poor resolution of the aerial photographs. At the northwestern border of the area the trees were damaged by a fire, probably the big fire from 1988. On the other side the trees changed less, only in the southwestern corner they died off. Presumably a hot spring developed there; the discharge is clearly visible (marked in red, Appendix No. 9.4). In October 2003, “Milky Way II” was located in that place. Also the other two features marked in green and blue have grown and are visible at the aerial photo of 1993. The discharges appear to be more distinctive. Those observations would prove the statement that hydrothermal activity increased in the Ragged Hills area up from the early 1990s. That was also established by the statement in the U.S.G.S. Open File Report 1999/2000 (Ball et al. 2002) that with beginning 1995 the Ragged Hills area erupted with intense hydrothermal activity, with three small springs appearing in a 20- by 50-m area –today’s “Persnickety Geyser”; “Titanic Spring” and “Lifeboat”.

Comparing the aerial overview from 1993 with that of October 2003 changes regarding vegetation are obviously noticeable. Most of the trees steadily died off since about 1995-96 because of the gradual upheating of the area’s subsoil since 1993-94 (Nordstrom 2004, written communication). A relation between the increasing geothermal activity in Ragged Hills and seismic activity can be assumed because earthquake activity increased significantly in 1999 at the same time as hydrothermal activity (Ball et al. 2002). As already mentioned in October 2003 the area was rich in hot springs and fumaroles. Also

mud pots and a few geysers were established. Especially in The Gap area lots of new hydrothermal features have developed – more than in the plain in the northeast. Whittlesey (1995) described The Gap as the area of most intense hot spring and geyser activity that is known in the Ragged Hills area. In October 2003, the major structures of the Ragged Hills area were the three merged features “Lifeboat”, “Persnickety Geyser” and “Titanic Spring”, “Dynamo”, “Elk”, “Rainbow Growler”, “Kaolin spring” with “Milky Way” and “Milky Way II” as well as the geyser “Steam engine” that isn’t shown on the map but will be described at the end of this section. Furthermore there were around 100 unnamed hot springs from a few centimeters up to several meters in size. The hill in the southeast attracted in special attention by its instability. Especially along the slope from “Rainbow Growler” to “Persnickety Geyser” it was steep and very instable. Walking along that slope had to be done very carefully because the ground slipped away below one’s feet. Besides along this slope the ground was steaming. The area’s discharges had also increased and a clearly visible main drainage system had developed with an estimated discharge of 0.5 L/s to the southwest and 2 L/s to the northeast. Along the main drainage in the direction to Tantalus Creek there were lots of green algae called *Cyanidium caldarium* that can live in acid conditions up to a maximum of 56° Celsius. In the smaller drainages distributed along the flat plain in the northeastern part of the mapping area there were huge amounts of dark purple to dark brown algae known as *Zygonium*. They only seem to live under acid conditions with a temperature maximum of 35°C.

In the following, the changes of some hot springs respectively groups of hot springs and geysers will be described from 1999 to 2003. It is recommended to fold out the corresponding overview of the photos in the appendix.

“Titanic Spring”, “Persnickety Geyser” and “Lifeboat” (overview page 123)

N 4952739.52, E 522639.16 / N 4952750.34, E 522655.33 / N 4952727.37, E 522623.65

The hot springs "Titanic Spring" and “Lifeboat” did not exist before 1995-96 (Nordstrom 2004, written communication). “Persnickety Geyser” appears to be the oldest structure as it is visible at the aerial photography from 1993. The overview of the photographs (page 123) illustrates the growth, development and merging of the three features from 1999 to 2000 and 2003. As it is to observe the features changed in shape, size and water color. Above all “Persnickety Geyser” grew from 1999 to 2003 and changed its shape from nearly circular to oval. In October 2003 it had an extent of 12 m length and 10 m width. Its colorless water

didn't change in its clarity and also it kept the orange shelf at its edges. Regarding its activity "Persnickety Geyser" has changed from a sub-boiling to a violently surging spring, to a small geyser in 2001, and boiling has ceased in the nearest feature to the southwest, "Titanic Spring" (Ball et al. 2002). Comparing the photographs, "Titanic Spring" didn't seem to have altered its size and shape distinctively, but the water color changed from a muddy grey to intensive blue with the same orange shelf at its edges as "Persnickety Geyser". "Lifeboat" got a bit bigger but didn't modify its shape conspicuously. Its water color changed from milky gray to light green with the same orange shelf as the other two features. The gentle surging mentioned in the U.S.G.S. Open File Report 99/00 (Ball et al. 2002) was observed again in October 2003 when grey muddy bubbles rose up in large time intervals. Considering the merging of the three structures, first "Persnickety Geyser" and "Titanic" were connected from 1999 to 2000. An unnamed, smaller hot spring situated between these two features was integrated in that connection. "Lifeboat" visibly joined in 2001 (Ball et al. 2002). Furthermore it is to remark that the discharge, mainly coming from "Titanic", was grey, clay-muddy in 1999. That already has changed in 2000 to light red and in 2003 to intensive orange depending on the precipitated minerals in the drainage stream.

"Milky Way" and "Kaolin Spring" (overview page 127)

N 4952802.13, E 522699.08 / N 4952791.41, E 522712.62

"Kaolin spring" arose as implosion in 2001 and its discharge flooded "Milky Way" that already existed before with white clayey, silica material (Nordstrom 2004, written communication). As it is to be seen at the photography from 2000 "Milky Way" was a flat hot spring with white colored water. In 2003 that had changed to a mix of white to grey water partly covered by black foam consisting of carbonized particles. These particles result from woody material carbonized by heat and sulfuric acid carbonize woody material. In 2003, lots of degassing points were observed southwest of "Milky Way".

“Elk” (overview page 127)

N 4952951.67, E 522810.58

Today, “Elk” is a 15 x 12 m large hot spring with intensive blue water. As it is to observe at the first photo that wasn’t the case in 1999. “Elk” erupted in the early 1999’s and was geysering up to 20 to 40 cm height (Nordstrom 2004, written communication). The muddy water had a black-white color. Already in 2000 there was no geyser activity any more; the water had the typical blue color. Between 2000 and 2003 no distinctive changes took place.

“Rainbow Growler” (overview page 129)

N 4952802.13, E 522725.02

In 1999, “Rainbow Growler” was a much smaller depression structure than today. It was dry and no steam rose up. It did not get enough water to sample until 2001/02 but got active then (Nordstrom 2004, written communication).

“Dynamo”

N 4952843.37 / E 522711.09

If “Dynamo” already existed in 1998, it was much smaller than today and it grew a lot within the last 4 years (Nordstrom 2004, written communication). Today, it consists of several hot springs with gas activities ranging from little to strong.

In the evening of the 31st of October 2003 a change in activity could be observed, when the hot spring adjacent to the main drainage was geysering (Fig. 5.13). Next day there was no geyser activity any more and the discharge was of a clayey muddy grey.



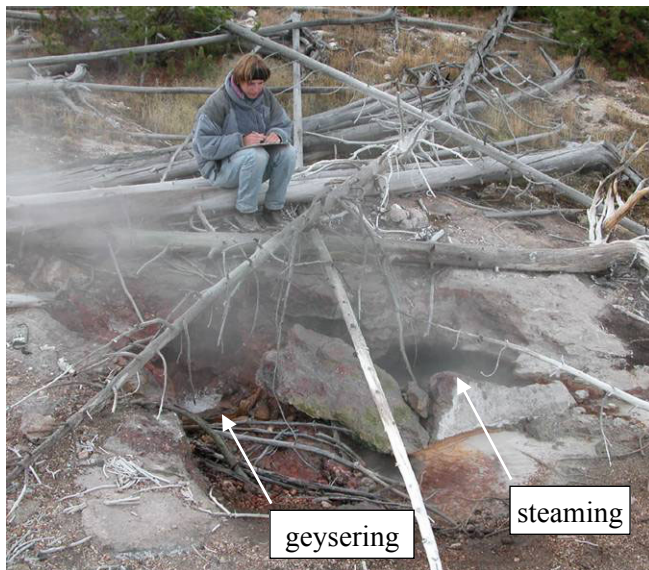
Fig. 5.13 Hot spring of “Dynamo” - left: moderate gas activity, right: geysering

“Steam Engine”

N 4952644.53 / E 522441.75

Because this hydrothermal feature couldn't be integrated into the digital atlas of Ragged Hills due to a lack of sufficient overlapping aerial photographs, a short characterization will be given in the following. The lack of data about the geyser prevents the description of changes in the last few years.

The geyser "Steam Engine" is a collapse structure with an extension of 3.3 x 2 m. Steam was rising up from several holes and in the southwest water hurled out from a strong geysering outlet. A discharge was meandering to the northwest into the main drainage



system. Mostly white to light grey, clayey loamy material was deposited and mainly in the area of the discharge russet coatings covered the ground. On-site parameter measurements resulted in the following informations: pH: 4.28, T: 87.2 °C and EC: 1.89 mS/cm. In the surrounding area several degassing points were audible. Lots of dead trees characterized the neighborhood around the geyser.

Fig. 5.14 „Steam Engine“

5.3.2 INTERPRETATION OF HYDROCHEMISTRY DATA

With increasing geothermal activity and therefore a growing number of hydrothermal features Ragged Hills got interesting for several research groups. Besides microbiological investigations above all water chemistry is studied among different topics. The work group of the geochemist Nordstrom from the United States Geological Survey (U.S.G.S.) carried out sampling campaigns in Ragged Hills since 1999. The corresponding water analyses are documented in the U.S.G.S. Open File Reports (Ball et al. 2002, McCleskey et al. 2004, hydrochemistry data 2003 unpublished). Planer-Friedrich from the TU Bergakademie Freiberg in Germany investigates the area of Ragged Hills since 2002 for her PhD thesis (Planer-Friedrich 2004). The water chemistry data collected by the U.S.G.S. from 1999 to 2003 and by Planer-Friedrich from 2002 to 2003 will be interpreted in the following sections.

5.3.2.1 WATER TYPES

To classify the different water types appearing in the Ragged Hills area the chemistry data of Planer Friedrich (2004) and the U.S.G.S. (Ball et al. 2002, McCleskey et al. 2004, hydrochemistry data 2003 unpublished) were combined. Only parameters that were determined in both studies were considered for the hierarchical cluster analysis. The calculation was done with the statistic program SPSS, standard version 11.0 (Copyright (C) SPSS Inc., 1989-2001; www.spss.com) and cluster methods “Average Linkage” and “Ward’s Method” with the measuring interval “Squared Euclidean Distance” were chosen. All data were transformed to ranges between 0 and 1. Groups of 2, 3 and 4 clusters were calculated to get an impression of the different grouping possibilities. Afterwards the calculated clusters were checked regarding their significant difference with the help of the “K-Independent Samples Test”. Most variables were significantly different between the clusters on a significance level of 0.01. Only nitrate for all calculated cluster groups, conductivity for the groups of 3 and 4 clusters computed by the “Ward’s Method” and iron III for the group of 3 clusters estimated by the “Average Linkage Method” exceeded the significance level.

After having checked the significance level each cluster group was analyzed regarding its medium elemental concentrations to determine the main elements classifying the water type. All anions or cations with medium concentrations higher than 18 meq% were taken into consideration. The following three types were computed by all cluster analyses and the assignment of cases to individual clusters was always similar (see below):

- **Type I** $\text{SiO}_2 - \text{Cl} - \text{SO}_4^{2-}$
- **Type II** $\text{Cl} - \text{SiO}_2 - \text{Na}$
(Silica is only slightly higher in concentration than sodium.)
- **Type III** $\text{Cl} - \text{Na} - \text{SiO}_2$
(Sodium is higher than or similar in concentration to silica.)

Furthermore, the water types can be distinguished by the on-site parameters: the pH value is lowest (2.6) for type I, followed by type III (3.1) and type II (3.6). Also, the conductivity of water type I is the lowest. Water type III has with around 40°C a significant lower water temperature than the types I and II with a temperature level of about 70°C. That explains the lower silica concentration of type III because the lower the temperature the less silica is soluble. The waters with higher chloride concentrations (type II and III) are also higher

concentrated in the other halogens fluorine and bromine. This case also is illustrated by the positive bivariate correlation (significance level 0.01, “Kendall’s tau_b”, “Spearman’s rho”). Moreover, the alkaline metals potassium and lithium also correlate with high or low concentrations of sodium (Fig. 5.15). The aluminum concentrations of water type II and III are about half of the concentration of type I. Vice versa the element boron is about three times higher concentrated in type II and III than in type I. Arsenite and total arsenic show the lowest concentrations in type I and the highest in type II, followed by the type III waters. The highest Fe (II) and Fe (III) concentrations can be found in water type I with the lowest pH-value (Fig. 5.16).

Correlation alkaline metals

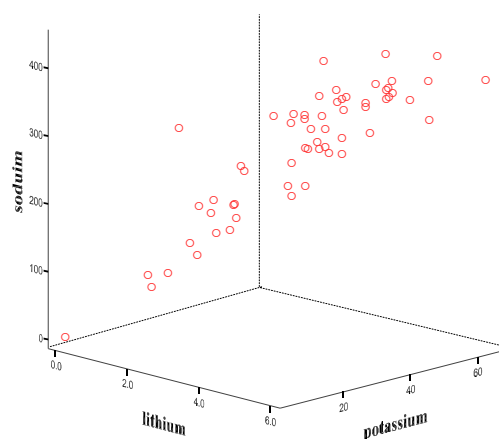
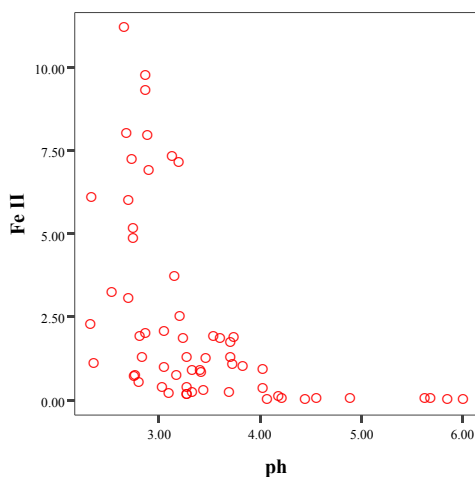


Fig. 5.15 Correlation alkaline metals (significance level 0.01)

Correlation pH and FeII



Correlation pH and Fe III

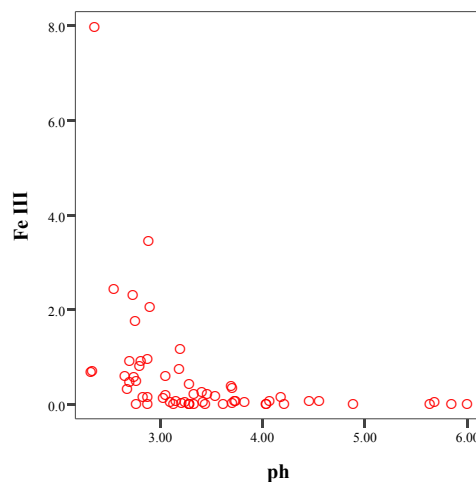


Fig. 5.16 Correlation between iron species and pH-value

Tab. 5.6 Described characteristics of the calculated water types (*low, **middle, ***high)

| Water type | pH | EC (µS/cm) | T (°C) | SiO ₂ | Cl, Br, F | K, Na, Li | Al | B | As | Fe |
|------------|-----|------------|--------|------------------|-----------|-----------|-----|-----|-----|-----|
| Type I | * | * | *** | ** | * | * | *** | * | * | *** |
| Type II | *** | *** | ** | *** | *** | *** | * | ** | *** | * |
| Type III | ** | ** | * | * | ** | ** | ** | *** | ** | ** |

Range silica, sulfate, chloride and sodium

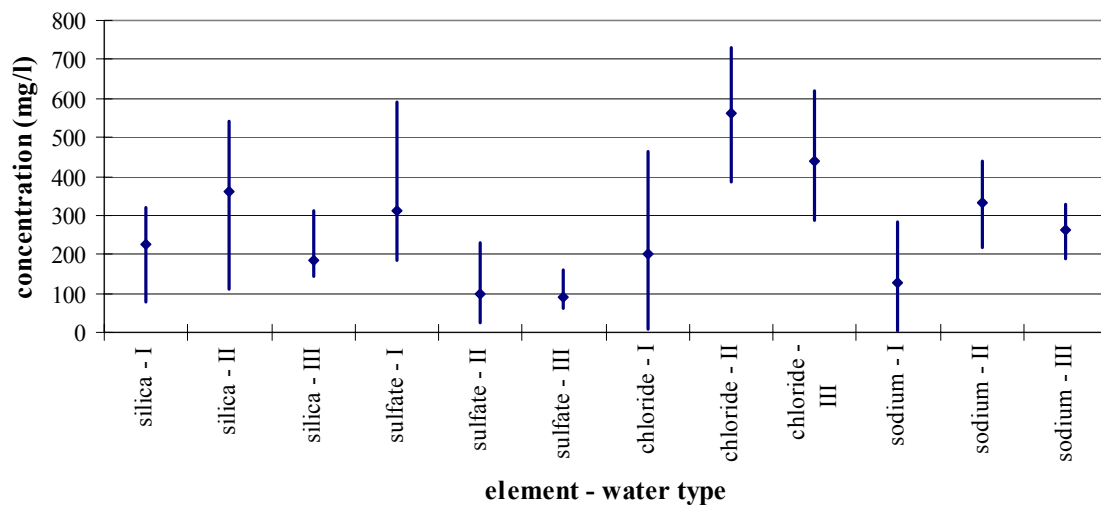


Fig. 5.17 Range (min, max, mean) of the silica, sulfate, chloride and sodium concentrations of the different water types (results of the clusters calculated after Ward's Linkage)

Regarding the spatial pattern of the classified water types the Ragged Hills area is mainly dominated by water type II. The water type I only occurs at the hot springs “Milky Way” and “Kaolin Spring”. The water type III with more sodium than silica is limited to the area around “Orpiment Puddle”. Only YNPRH05 (sampling site Planer-Friedrich) situated near “Orpiment Puddle” belongs to the water type III with sodium concentrations similar silica concentrations as well as “Persnickety Geyser”, YNPRH25 (sampling site Planer-Friedrich, 75 m southwest of “Persnickety Geyser”), “Titanic Spring” and “Milky Way-01WA134” (sampling site U.S.G.S.). Because later samples of the sites “Titanic Spring”, “Persnickety Geyser” and “Milky Way-01WA134” also were clustered in the water type II with slightly more silica concentrations than sodium it is to presume that the concentrations of silica and sodium are fluctuating over the years. “Orpiment Puddle” sampled from 1999 to 2003 however is stable in type III with more sodium than silica.

5.3.2.2 THERMOGRAPHY AND GAS ACTIVITY

The visual interpretation of the relative thermal activity and temperature distribution of the Ragged Hills area is based on the Fig. 5.18. The colors indicate special temperatures – the lighter the color the higher the temperature. Because the calibration of the thermal overview was not possible a quantitative analysis could not be achieved (section 4.2.4). The known water temperatures of the sampled hot springs give a first impression of the predominant temperatures, but normally more correction factors are necessary to correlate the colors with the corresponding true temperatures (section 4.2.4). Because the thermal overview pictures were taken in October 2003 only water temperatures measured in September and October were included in the interpretation (Planer-Friedrich 2004, U.S.G.S. hydrochemistry data 2003 unpublished, section 5.1).

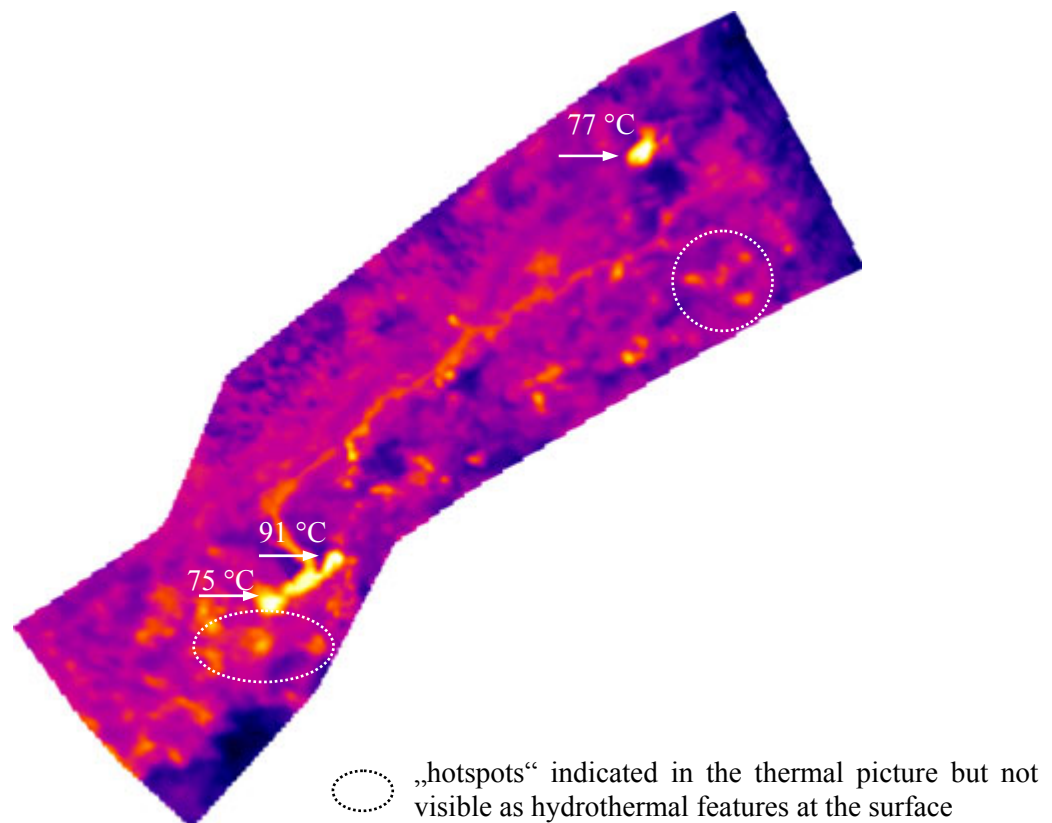


Fig. 5.18 Thermal overview Ragged Hills, October 2003

The attempt to compute a not-supervised classification (5 classes) by the methods “K-means” and “Fuzzy C-Means” with the program TNTmips didn’t result in helpful illustrations to interpret the overview in a better way (Fig. 5.19). Hydrothermal features with differences in water temperatures of about 20 °C were clustered in the same class. That wasn’t a calculating mistake but a problem of the thermal overview’s poor resolution.

It is difficult to identify both in Fig. 5.18 and in Fig. 5.19 but the highest water temperatures were measured at “Persnickety Geyser”, “Rainbow Growler” and YNPRH25 (sampling site Planer-Fiedrich) with around 90 °C. In this case both the thermography overview and the classified overview are irritating showing for example the features “Elk”, “Lifeboat” and “Titanic Spring” also with very high temperatures. But in contrast the measured water temperatures there were only around 70 °C (Fig. 5.18 and Fig. 5.19). Therefore a meaningful arrangement of temperature classes and thus a quantitative interpretation of the thermal overview were not obtained.

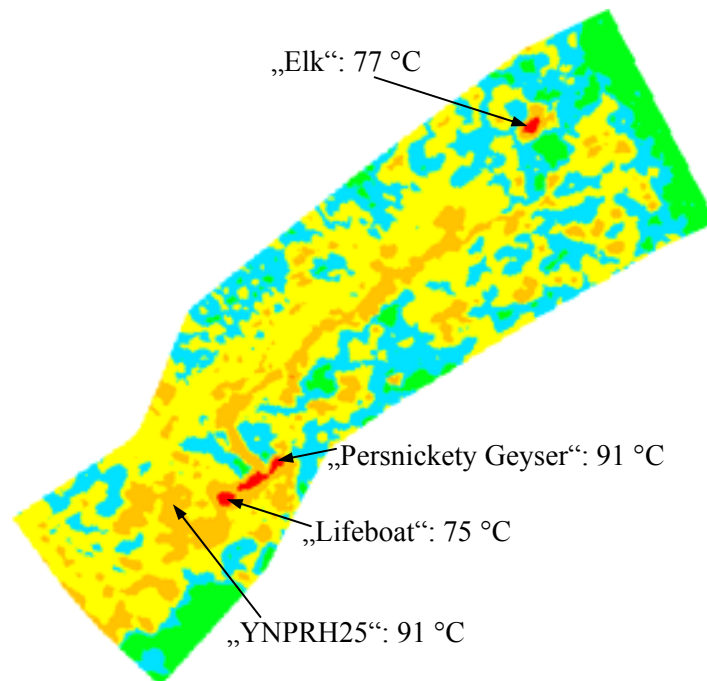


Fig. 5.19 Not-supervised classification (Fuzzy C-Means)

A supervised classification was not useful, because most of the hot springs with different water temperatures were not identifiable since the poor resolution. Thus defined reference points were too less.

Nevertheless the thermal overview enables qualitative conclusions about the thermal activity. For example The Gap area shows a more intensive geothermal activity than the northeastern plain (Fig. 5.18). Towards the river Tantalus Creek (not shown in the overview) the dark purple to blue color indicates colder subsoil. Furthermore, the main discharge is warmed up by the water draining from the hot springs. That is also proved by the green algae being typical for the warm acid streams. Also there are “hotspots” observable where no hydrothermal features exist at the surface yet (Fig. 5.18). In the aerial overview that regions are rich in precipitations and without vegetation.

To interpret the connection between the thermal activity and the gas activity a statistical correlation between the measured water temperature and the mapped gas activity of the hydrothermal features was done with the statistic program SPSS as well as with simple calculating processes (mean, standard deviation, median) by Excel. The bivariat

correlations computed by SPSS with “Kendall’s tau-b” and “Sperman” confirm the correlation between the gas activity of the hot springs and the measured water temperature on a significance level of 0.05. In contrast, the mean and the standard deviation of the water temperatures of the single gas activity groups calculated by Excel don’t show a correlation between temperature and gas activity (Tab. 5.7). It has to be pointed out that the data for the gas activity group 1 are not very reliable because 2 of the 3 cases could not be clearly identified regarding the gas activity. The remaining 4 groups record the trend that with increasing gas activity temperature is also growing but not vice versa. It is to presume that there is a correlation between temperature and gas activity, but only in the direction that the higher the gas activity the higher the temperature. A high temperature does not necessarily means a high gas activity. Because the gas activity was just estimated in a subjective way and can change over time the results of the statistic analyses are questionable.

Tab. 5.7 Statistics gas activity and temperature hot springs

| Gas activity | Cases | T (°C)_mean | T (°C)_deviation mean | T (°C)_median |
|---------------------|--------------|--------------------|------------------------------|----------------------|
| 1 | 3 | 52 | 23 | 65 |
| 2 | 20 | 61 | 20 | 69 |
| 3 | 17 | 72 | 14 | 74 |
| 4 | 5 | 85.4 | 4.48 | 86.1 |
| 5 | 3 | 88.8 | 1.78 | 87.5 |

5.3.2.3 TIME SERIES OF WATER CHEMISTRY

Because of the lack of data a statistic analysis of time series was not possible. Therefore the chemical development of only a few hydrothermal features will be reviewed by using Excel diagrams of the on-site parameters pH, T and EC as well the iron and arsenic species. Furthermore, the course of the predominant elements sulfate, sodium, silica, potassium, lithium, fluorine and chloride illustrated in the hydrochemistry layers of the digital atlas will be interpreted.

“Titanic Spring”

Remarkable is the great fluctuation of the water temperature of Titanic Spring. It decreased from September 1999 to May 2001 by nearly 20°C from 84°C to 67°C and three months later in September 2001 it increased again to 85°C ((1) in Fig. 5.20). After that maximum temperature fall once more till September 2003 to around 65 °C. Because the high water temperature of hot springs depends on the circulation from deeper, up-heated water resources the supply might have changed around that time. Also the pH value decreased from September 1999 to September 2001 from 5.63 to 2.87 ((2) in Fig. 5.20). It can be supposed that the deeper, neutral water from September 1999 was mixed with water near

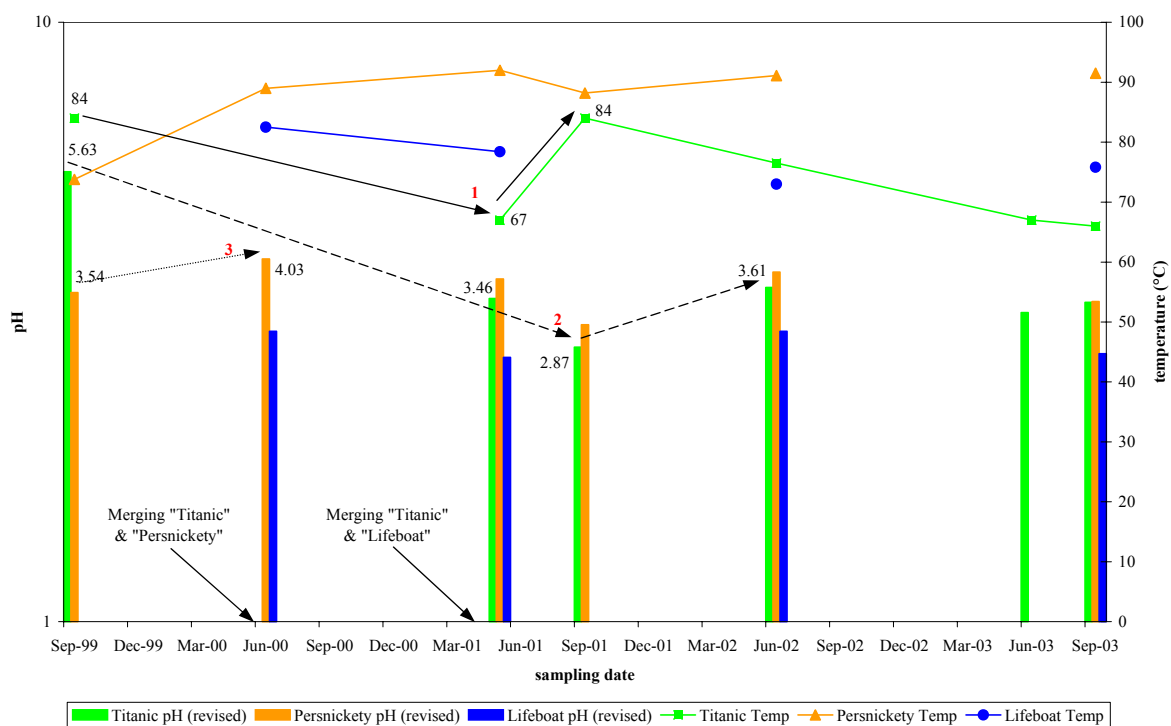


Fig. 5.20 Course of temperature and pH for „Titanic Spring“, „Persnickety Geyser“, and „Lifeboat“

the surface that is influenced by hydrogen sulfide gases oxidizing to sulfur which in turn oxidizes to sulfuric acid near the surface. Furthermore, the merging with “Persnickety Geyser” and “Lifeboat”, both with pH values around 3 to 4, may have influenced the decreasing pH value. Still, in 1999 “Titanic Spring” was not joined with the features “Persnickety Geyser” or “Lifeboat”. But already in June 2000 there was a surface connection between “Titanic Spring” and “Persnickety Geyser” and “Persnickety Geyser’s” pH value had slightly increased from 3.54 to 4.03 ((3) in Fig. 5.20). In May 2001, “Titanic Spring” and “Lifeboat” clearly joined, but it is to presume that again hydrogeochemical mixing occurred already before that time in the subsurface, because the

“Titanic Spring’s” pH-value had already decreased in June 2001 ((2) in Fig. 5.20). “Lifeboat’s” pH-values are more or less stable between 3.05 and 2.76 from 2000 to 2003.

The total iron concentrations of “Titanic Spring’s” water increased significantly from 0.07 mg/L in September 1999 to 9.91 mg/L in September 2001. As the correlation in Fig. 5.16 illustrates that is caused by the decreased pH value. The more acid water conditions mobilize iron from different iron reservoirs as clayey minerals and iron sulfides. After that peak the iron concentrations drop down to 1.16 and 1.85 mg/L. The Fe (II) concentration contributes 75 to 100 percent to the total iron concentrations. That indicates reducing conditions, also proved by the measured redox potential (Eh). Besides the peak of iron concentrations also a peak in total arsenic concentrations with 3.4 mg/L is observable in September 2001. Usually the arsenic concentrations range from 1.5 to 2.76 mg/L. Arsenite makes up 10 to nearly 100% of the total arsenic concentration.

The predominant elements vary only slightly. During the first sampling campaign in September 1999 minimum concentrations of sulfate (41 mg/L) were analyzed. Normally sulfate concentrations are around 100 mg/L without the peak in September 2001 of 150 mg/L. Maybe sulfate is mainly dissolved from iron sulfides because also Fe (II) has its maximum concentration in September 2001. The positive correlation (significance level 0.01, “Kendall’s tau-b”) of Fe (II) and (III) and the hydrogen activity (mmol/L) with sulfate supports that assumption.

The second most important element silica appears in high concentrations. It is a frequent mineral from the earth’s crust and stems from weathered quartz, clayey minerals and feldspar (volcanic ashes). Its solubility depends above all on temperature that influences

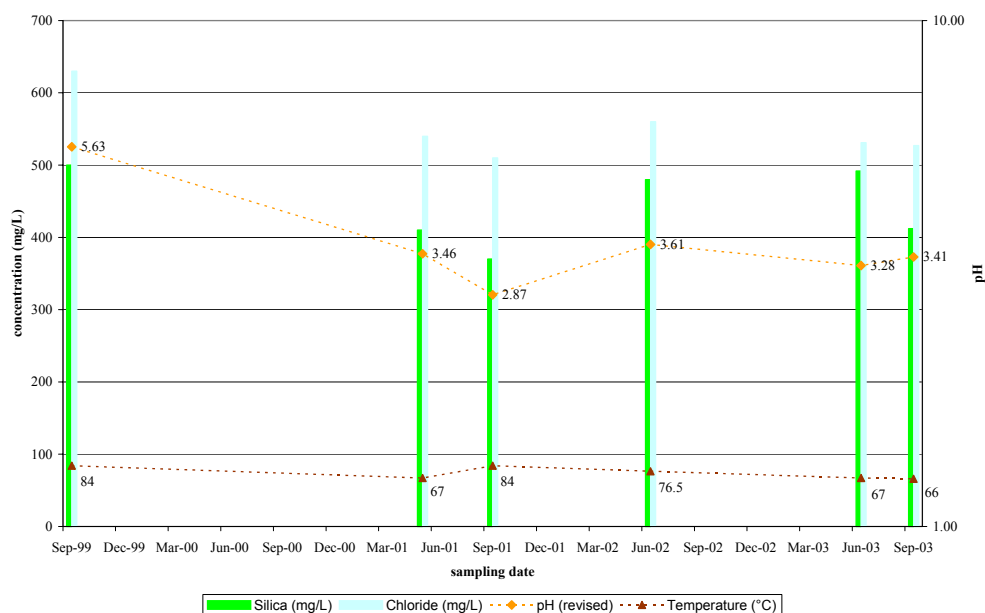


Fig. 5.21 Silica and chloride concentrations as well the course of the pH of „Titanic Spring“

the solubility of silica positively; high temperatures enable high solubility rates. Acid conditions support the solubility of clays and feldspar and thus the increasing concentrations of silica in the water. That silica is not infinitely soluble under acid conditions is shown by the inverse correlation computed regarding silica and the hydrogen activity. For example the solubility of quartz is more or less independent from the pH for a range of 7 to 1. That is also proved by the course of silica concentrations (Fig. 5.21).

Furthermore a positive correlation between the elements silica and chloride was computed (significance level 0.01, “Kendall’s tau-b”) (Fig. 5.21). Like silica chloride had its maximum in September 1999 with 630 mg/L and June 2002 with 560 mg/L. The remaining time it fluctuates around 510 to 540 mg/L. The halogen fluorine appearing in hydrothermal and in volcanic areas also belongs to the predominant elements of the water analyses. Fluorine had its maximum concentrations in June 2002 with 6.4 mg/L and September 1999 and 2003 with around 5.4 mg/L. The remaining time its concentration was around 4 mg/L. That proves the positive correlation of the halogen elements with each other (significant level 0.01, “Kendall’s tau-b”).

The alkaline metals sodium, potassium and lithium all have their maximum concentrations in September 1999. These trends are not always very distinct but nevertheless detectable. Stemming from silicates, halogen compounds and fluid inclusions the alkaline metals show positive correlations with silica, chloride and fluorine concentrations (significance level 0.01, “Kendall’s tau-b”). That is proved by the maximum concentrations of the alkaline metals in September 1999. The remaining time the alkaline metals sodium and potassium also fluctuate significantly as well as silica. Lithium decreased to a more or less stable concentration of around 3.6 mg/L in the last years.

“Persnickety Geyser”

The temperature of “Persnickety Geyser” increased by around 15°C from September 1999 to June 2000 and then leveled at about 90°C. That would correspond with the observations that “Persnickety Geyser” changed from a sub-boiling over a violently surging spring, to a small geyser in 2001 (Ball et al. 2002). Its conductivity increased from September 1999 to June 2000 by around 200 µS/cm to 2010 µS/cm and levels at 1930 to 1960 µS/cm during the next years. Maybe this increase followed the merging with “Titanic Spring” and its higher average conductivity from the muddy water (image page 123). The pH value fluctuates from 3.13 to 3.83 without the peak in June 2000 with 4.03. That might

be also a result of joining with “Titanic Spring” (see above “Titanic Spring”, Fig. 5.20). The total iron concentration peak in September 1999 (2.1 mg/L) then decrease to 0.38 mg/L in June 2000. That might be attributed to the increasing pH value in the merging process with “Titanic Spring” ((1) in Fig. 5.22). In September 2001, iron has its maximum concentration with 7.34 mg/L and levels then at around 1 mg/L between June 2001 and September 2003. The iron peak corresponds with the pH value of 3.13 (Fig. 5.22). The arsenic concentration of around 2 mg/L was stable through the whole time with the exception of the peak in September 2001 (5.82 mg/L, Fig. 5.22).

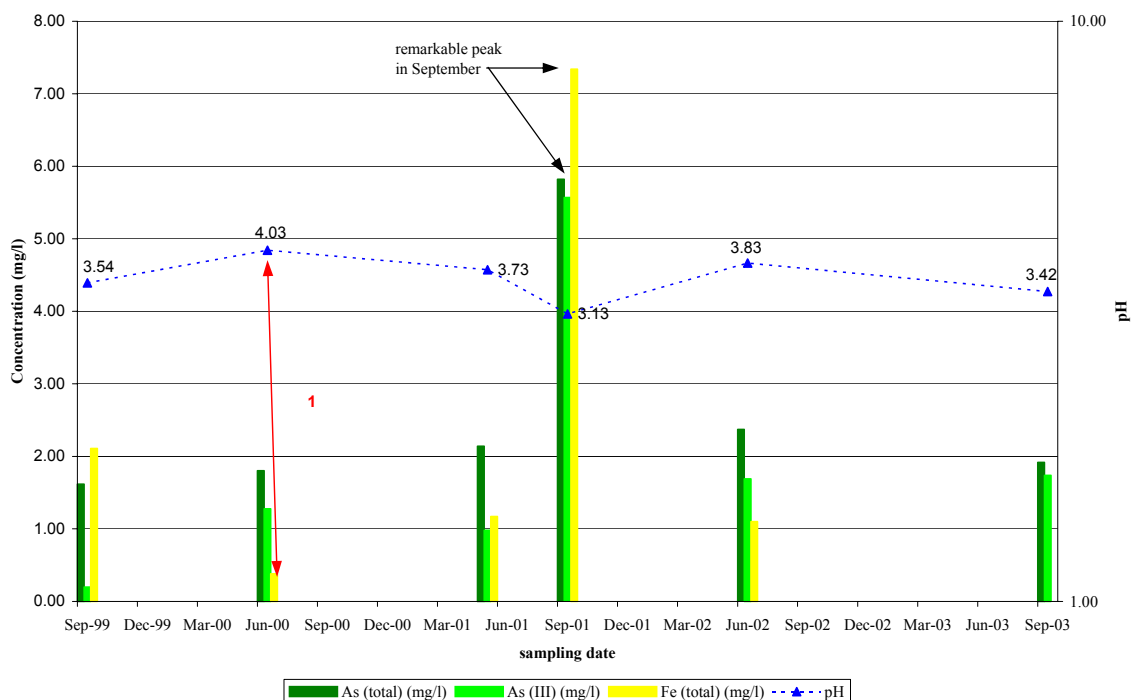


Fig. 5.22 Iron and arsenic concentrations of „Persnickety Geyser“

Like observed at “Titanic Spring” “Persnickety Geyser’s” sulfate concentrations doubled in September 2001 compared to other sampling times. The fact that the silica concentration was at a minimum of 400 mg/L at the same time, correspond with the calculated inverse correlation between silica and sulfate (significance level 0.05, “Kendall’s tau-b”). The halogen chloride fluctuated around 520 to 540 mg/L and had its maximum concentration in June 2000 with 580 mg/L corresponding to silica with 480 mg/L. Fluorine normally varied around 4.6 mg/L and had its maximum concentration of 6.6 mg/L in June 2002. The predominant elements sodium (minimum September 2001 with 300 mg/L), potassium (maximum in May 2001 with 64 mg/L) and lithium don’t vary remarkably between 1999 and 2003.

“Lifeboat”

The on-site parameters of the hot spring “Lifeboat” were more or less stable. The temperature ranged from 73°C to 83°C, the pH value changed only slightly around 3 and the conductivity was also stable with 2130 to 2200 $\mu\text{S}/\text{cm}$. Because of the low pH value it is to presume that the water has its source near the surface or is mixed to a significant part with surface water. The iron concentrations ranged from 2.25 mg/L (June 2000) to 0.75 mg/L (June 2001) and then leveled at around 1.4 to 1.6 mg/L. Because in September 2001 no sample was taken the peak observed at “Titanic Spring” and “Persnickety Geyser” can't be proved. Divalent iron made up 40 to 100 percent of the total iron concentrations. The arsenic concentrations normally leveled around 1 mg/L, only in June 2000 a maximum of 2.5 mg/L was noticed. The arsenite concentrations contributed between 5 and 82 percent of the total arsenic.

While sulfate had its maximum concentration in May 2001 (200 mg/L) silica showed minimum concentrations with 390 mg/L at the same time. Sodium decreased from June 2000 (380 mg/L) to May 2001 (270 mg/L) and then increased again. Also the halogen element chloride decreased from June 2000 (640 mg/L) to May 2001 with a minimum concentration of 440 mg/L. Following that decrease an increase was seen to June 2002 with 540 mg/L.

All in all the concentrations of total iron only differ slightly between the three hydrothermal features “Titanic Spring”, “Lifeboat” and “Persnickety Geyser” with 1 to 2 mg/L. Above all the time around September 2001 attracts attention by peaks of the on-site parameters or maximum concentrations of several elements. This will also be proved by the following descriptions of “Orpiment Puddle”. This phenomenon might be attributed to annual disturbances (section 3.2.2).

“Orpiment Puddle”

The water temperature as well the pH value do not show significant variations with 40 °C respectively 3.3, but both on-site parameters show a conspicuous peak in September 2001 with 85 °C and a pH of 4.89. The conductivity varies between 1300 to 1700 $\mu\text{S}/\text{cm}$ without the peak in September 2001 of 2200 $\mu\text{S}/\text{cm}$. The increasing pH value is also expressed in a decreasing concentration of total iron to 0.037 mg/L in September 2001 from normally 0.18 to 0.28 mg/L. All in all these iron concentrations are very low compared to “Titanic Spring”; “Persnickety Geyser” and “Lifeboat” with 1 to 2 mg/L. Divalent iron concentrations contribute nearly 100 percent of the total iron. The arsenic concentrations

range from 0.1 to 0.4 mg/L with a clear peak in September 2001 (2.1 mg/L). Arsenite seems to be always nearly 90 to 100 percent of the total arsenic concentrations.

The predominant elements show a different behavior. Sodium, silica, lithium, fluorine, potassium and chloride all had maximum concentrations in September 2001. Sulfate had a minimum concentration at the same time because of the increased pH value at that time.

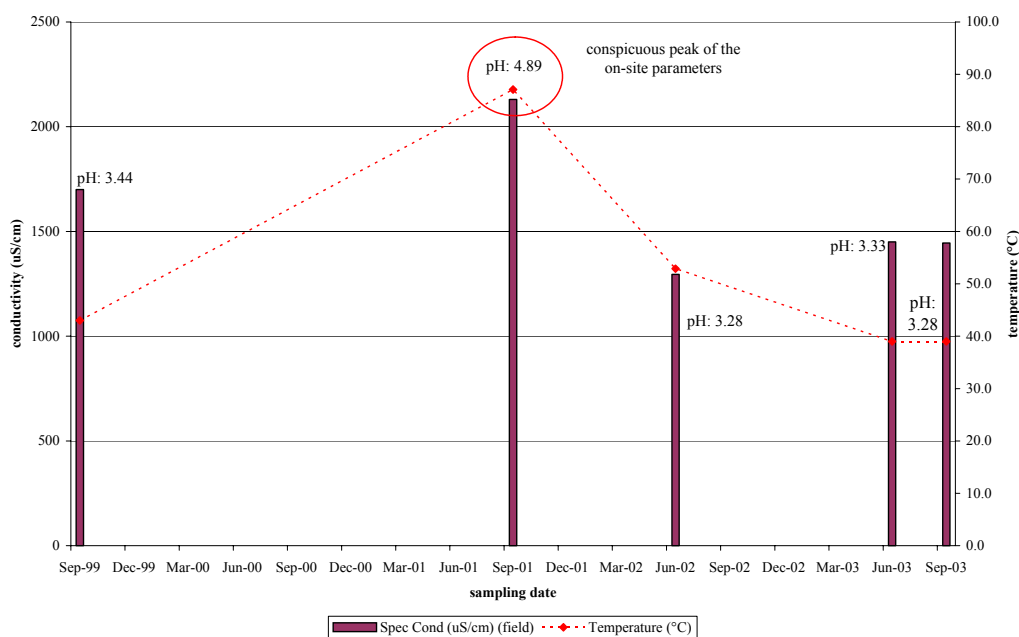


Fig. 5.23 Course of on-site parameters of „Orpiment Puddle“ with peak in September 2001

“Elk”

The water temperature is stable between 77 and 79 °C as well as the pH value around 4. The conductivity ranged between 2260 and 2410 μS/cm. Contrary to the expectations the conductivity increased from September 1999 to June 2000 although the water changed from muddy grey to clear blue. But the positive correlation between silica and the conductivity confirms this observation (significance level 0.01, “Kendall’s tau-b”). The iron concentrations ranged from 0.06 to 0.11 mg/L. Conspicuous is the fluctuating Fe (II) share to total iron with 13 and 98 percent. Changes in the redox conditions might be a reason. The arsenic concentrations were nearly stable around 3 mg/L, but also here the As (III) portion of the total arsenic fluctuated significantly between 8 to 88 percent. Again, changes in the redox conditions might be a reason.

The predominant element concentrations of sulfate, sodium, lithium and fluorine don’t show remarkable changes. Silica increased significantly from September 1999 (330 mg/L) to June 2000 (420 mg/L). That supports the observation of the change from grey muddy to clear blue water that is caused by the silica.

6 RECOMMENDATIONS

Ground survey - With a little practice it will be possible to skip the temporary marked stone-grid and start immediately with the stripes-grid and thus saving about 10 hours. Furthermore, if the ground control points are surveyed only by differential GPS and not additionally by theodolite that also cuts down time by 7 hours. A second advantage is that the differential GPS survey can be done by just 1 person. The higher deviation of the measured position from the true coordinates (± 2 to 5 m) is a disadvantage that should be known. Its acceptability depends on the general goal of the work.

For similar projects of mapping hydrothermal features the characteristics of the different gas activities should be described in greater detail and photos should be taken to illustrate the differences.

Aerial survey – To get sharp, unblurred images with the balloon aerial photography it is important to set an exposure time of 1/2000 and the manual focus to an infinite distance. The exposure time depends on the balloons movements mainly resulting from wind conditions and tether ropes. Because both cases can't be excluded at all the smallest exposure time that is possible in respect to the light conditions should be set. Furthermore it is recommended to decouple the camera construction from the balloon using a Picavet construction and therefore minimizing the transmitted movements.

Using a GPS is recommended if the area of interest is rugged or without remarkable signs. A GPS trekking will support the later georeferencing of the images. The mounting construction of the GPS should be stable and interactions with the balloon construction should be prevented. Mounting the GPS just by a simple rope at the balloons construction as it was done during this project isn't optimal. In the present case the GPS's rope was wrapped around the wire lines of the balloons construction at the end of the survey (Fig. 4.2).

Stronger tether lines and maybe two balloons hold together by a net instead of only one balloon secure the instrument against getting lost by flying away or damaged by crashing down. One balloon with a small parachute as used for weather balloons is a second securing possibility. Two tether ropes for the balloon survey are not only necessary to tether the balloon to the ground but also for directing it on the desired path, although it is to point out that an exact guiding of the balloon isn't possible.

To fill the balloon with helium it is suggested to use a vent fitting better towards the balloon's opening than the standard vent of the helium steels. To keep the helium filled balloon on site for two days or more a net or something similar could be used to fix it at the ground.

All in all it has to be concluded that balloon aerial photography is only possible during calm weather conditions. More than slight wind requires another low flying platform (section 2).

Taking images from the single engine airplane the flying route has to be exactly planned and several overflights have to be allowed for being sure that the target area is shown on the images. Exposure time again has to be at least 1/2000 to get sharp images. According to in general higher flight levels (minimum 500 ft) the pixel resolution of the camera must be better than for low flying platforms. Using a zoom is only an option to a certain extend while zooming increases the risk of blurred images.

Regarding future thermography aerial photography from low flying platforms better recognizable ground control points are required or a higher resolution of the images. That would enable an exact georeferencing of the images.

Digital atlas – A minimum of 1 week can be saved by georeferencing the digital images with the help of the program Geomatica that enables to assign the corresponding coordinates to a ground control point from a text file. The program TNTmips doesn't offer that possibility.

Knowing the interior and exterior orientation of the camera enables to process ortho images. This information should be possible to get from digital camera calibration software (Microsoft Research 2004).

While the mosaicking process it is recommended to use another overlap method than Last Raster because this method doesn't mix the colors of the mosaicked raster images. Using an overlap method that merges the overlapping areas would prevent visible borders between the images. Filtering should result in the same effect.

7 ACKNOWLEDGEMENT

For giving me the opportunity to work out a diploma thesis abroad, I am grateful to Britta Planer-Friedrich. Her engagement, enthusiasm and patient proof-reading helped me very much while working out this thesis. I also would like to thank Prof. Broder Merkel who supported this work not only by one week field work in the Yellowstone National Park but also by professional suggestions how to present the results in the best way and by proof-reading. As well, I am grateful to Prof. Irmgard Niemeyer for supporting me with professional advice regarding remote sensing problems, for providing me with literature and proof-reading. Every work has to be financed and therefore I would like to thank the Förderkreis Freiburger Geowissenschaften for their financial support.

Moreover, I would like to thank Henry Heasler and Christie Hendrix from the National Park Service, Yellowstone National Park for their support with the aerial survey permission that was required to realize our project. Furthermore, I appreciated the help of Steve Miller, GIS department of the National Park Service, during the survey field work and the evaluation of the GIS data. Thanks to Shannon Savage, National Park Service, for providing me with map material I looked for.

During the work in the Yellowstone National Park, I also got to know the work group of Dr. Kirk Nordstrom from the U.S. Geological Survey with Dr. James Ball and Blaine McCleskey. I really appreciated their answering my questions and sending material required to continue my work. Furthermore, the short-term cooperation with Dr Earl Mattson and Dr. Mitchell Plummer (INEEL) resulted in the thermography overview of the area Ragged Hills.

I still like to remember the instructive survey day with Steve Dill and Jerry Gitter (Western Federal Lands Highway Division), during which I learned to correctly use the theodolite and also got interesting information and views of the Park area. Moreover, I would like to thank Beate Böhme, a geo-ecology student from the TU Bergakademie Freiberg, who supported the field work during her practical training. Without her, the field work wouldn't be done in this short time.

In addition, I would like to express my thanks to Michelle Schneider from the Technical Service Center, Denver Service Center who provided the aerial overviews of Ragged Hills from 1986 and 1993.

To get more information about low-flying platforms, I contacted Prof. James S. Aber, Dr. Irene Marzolff, Les Beard, Jonathan E. Nyquist, Charles C. Benton and Bernard-Noel Chagny and they supported my work by sending articles and answering my questions regarding this chapter.

Finally, I would like to thank my family for financing my studies and the stay in the Yellowstone National Park and also for the permanent encouragement in times of less motivation. Many thanks to Ralf and my friends who helped me to get some distraction from my work if it was necessary or listened patiently to the problems I was confronted with.

8 REFERENCES

- Aber, J. S., Sobieske, R. J., Distler, D. A., Nowak, M. C. (1999): Kite aerial photography for environmental site investigations in Kansas. *Transactions of the Kansas Academy of Science*, vol. 102, no. 1-2, pp. 57-67
- Aber, J. S., Aber, S. W., Leffler, B. (2001): Challenge of Infrared Kite Aerial Photography. *Transactions of the Kansas Academy of Science*, vol. 104, no. 1/2 , pp. 18-27
- Aber, J. S., Aaviksoo, K., Karofeld, E. (2003). Kite aerial photography – tool for microstructural investigations of mire ecosystems. *Congress of the International Union for Quaternary Research*, vol. 16, pp. 185-186
- Aber, J. S. (2004a): Helium Balloons for SFAP.
<http://academic.emporia.edu/aberjame/airphoto/platform/balloon.htm>, last update 2003
- Aber, J. S. (2004b): History of Kite Aerial Photography.
<http://www.geospectra.net/kite/history/history.htm>, last update September 2003
- Aber, J. S., Aber, S. W. (2004c): Kite Aerial Photography equipment.
<http://www.geospectra.net/kite/equip/equip.htm>, last update July 2004
- Aber, J. S. (2004d): Lighter-than-air platforms for small-format aerial photography. *Transactions of the Kansas Academy of Science*, vol. 107, no. 1/2, pp. 39-44
- Aber, J. S. (2004e): Applications of small-format aerial photography in North Dakota. *NDGS Newsletter*, Winter 2003-04, vol. 30, no. 2, pp. 16-19
- Aerial Arts (2004): History of Aerial Photography - The Aerial Perspective.
<http://www.aerialarts.com/History/history.htm>
- Airship and Blimp resources (2004): Airship FAQ.
<http://www.myairship.com/faq/index.html>, last updated 2000
- Allstar - Aeronautics Learning Laboratory for Science, Technology, and Research (2004): Balloons and Airships. <http://www.allstar.fiu.edu/aero/balloon5.htm>, updated 23 March 2004
- Anthony, R. M., Anderson, W. H., Sedinger, J. S., McDonald L. L. (1995): Estimating populations of nesting brant using aerial videography. *Wildlife Society Bulletin*, vol. 23, no. 1, pp. 80-87
- Badekas, J., Peppes, E., Stambouloglou, E. (1980): Low altitude aerial photography. *International Archives of Photogrammetry*, vol.23, part B10, Commission V. (Committee 14th ICP, Hamburg 1980; Photogramm. Inst. Universitat Bonn), 1980, pp 1-20
- Ball, J. W., McCleskey, R. B., Nordstrom, D. K., Holloway, J. M., Verplanck P. L. (2002): Water-Chemistry Data for Selected Springs, Geysers, and Streams in Yellowstone National Park, Wyoming, 1999-2000. U.S.G.S., Open-File Report 02-382

- Bauer, M. (2003): Vermessung und Ortung mit Satelliten – GPS und andere satellitengestützte Navigationssysteme. 5. Auflage, Widmann, Heidelberg
- Benton, C. C. (2004): Soft Kites for Lifting.
<http://arch.ced.berkeley.edu/kap/equip/softkite.html>, revised: 02 August 1999
- Blimp History (2004): Blimp History.
<http://www.metlife.com/Applications/Corporate/WPS/CDA/PageGenerator/0,1674,P314,00.html>
- Boike, J., Yoshikawa, K. (2003): Mapping of Periglacial Geomorphology using Kite/Balloon Aerial Photography. *Permafrost and Periglacial Processes*, vol. 14, pp. 81-85
- Brock, T. B. (1994): Life at high temperatures. Yellowstone Association for Natural Science, History & Education, Inc. Yellowstone National Park, Wyoming
- Burch, R. (2004): History of Photogrammetry, The Center for Photogrammetric Training, Ferris State University,
www.ferris.edu/htmls/academics/course.offerings/burchr/sure340/notes/History.pdf
- Canon (2004): Power Shot G5.
http://www.canon.de/for_home/product_finder/cameras/digital/powershot_g5/index.asp
- Chase, T., E., Young, J., D. (1990): Detailed side and overhead views of geologic features from joint panoramic and blimp operations. *AAPG Bulletin*, vol.74, no.6, pp.964
- Christiansen, R. L. (1975): Geologic map of the Norris Junction quadrangle, Yellowstone National Park, Wyoming. U.S. Geological Survey Geologic Quadrangle Map GQ-1193, scale 1:62,500
- Christiansen, R. L. (2001a): Geologic map of the Yellowstone Plateau area. in *The Quaternary and Pliocene Yellowstone Plateau Volcanic Field of Wyoming, Idaho, and Montana*. U.S.G.S. Professional Paper 729-G
- Christiansen, R. L. (2001b): *The Quaternary and Pliocene Yellowstone Plateau Volcanic Field of Wyoming, Idaho, and Montana*. U.S.G.S. Professional Paper 729-G
- De Lange, N. (2002): *Geoinformatik in Theorie und Praxis*. Springer, Berlin Heidelberg
- Dzurisin, D., Wicks, C., Thatcher, W. (1999): Renewed uplift at the Yellowstone Caldera measured by leveling surveys and satellite radar interferometry. *Bulletin Volcanology*, vol. 61, pp. 349-355
- FLIR Systems (2004): ThermaCAM® Researcher.
http://www.flir.de/accessories/accessory/1135/accessory_category_id/1021/
- Fritz, W. J. (2003): *Roadside geology of the Yellowstone Country*. 10th ed., Mountain Press Publishing Company, Missoula
- Fuchs (2004): Aufhängevorrichtung für das KAP-Rig, mein Picavet # 1.
<http://members.fortunecity.de/kapmfs/pvet01.htm>, updated 20.08.2003
- Garmin (2004): GPS 12. www.garmin.de
- Gupta, R. P. (2003): *Remote Sensing Geology*. Springer, Berlin Heidelberg

- Harding, B. (1989): Model aircraft as survey platforms. *Photogrammetric Record*, vol. 13, no.74, pp. 237-240
- Hawkes (2004): HISTORY – The History and uses of the Aerial View. <http://www.jasonhawkes.com/history.html>
- Hutchinson, R. (1973): Annual Report Norris Geyser Basin
- Honkura, Y., Matsushima, M., Oshiman, N., Sasai, Y., Ohno, M., Tanaka, Y., Yamamoto, T., Ikeda, K., Wakino, Y. (1995): *Journal of Geomagnetism and Geoelectricity*, vol.47, no.2, pp.231-236
- Kiver, E. P., Harris, D. V. (1999): *Geology of U.S. Parklands*. 5th ed., John Wiley & Sons, Inc., New York
- Lewis, W. J. (1964): Thermal features of the Norris Geyser Basin. (Norris Geyser Basin Annual Report)
- Luhmann, T. (2000): *Nahbereichsphotogrammetrie – Grundlagen, Methoden und Anwendungen*. Wichmann, Heidelberg
- Makino, M., Okubo, Y., Morijiri, R., Nakatsuka, T., Honkura, Y. (1991): An Attempt of Geomagnetic Field Measurement with a Radio-Controlled Blimp in the Vicinity of the Tanna Fault. *Journal of Geomagnetism and Geoelectricity*, 43, pp. 951-956
- Marzolf, I., Ries, J., B. (2000): Großmaßstäbiges Luftbild-Monitoring mit einem ferngesteuerten Heißluftzeppelin. *Petermanns Geographische Mitteilungen*, vol. 6, pp. 4-5
- Marzolf, I., Ries, J., B., Albert, K.-D. (2002): Kite aerial photography for gully monitoring in sahelian landscapes. *Proceedings of the Second Workshop of the EARSeL Special Interest Group on Remote Sensing for Developing Countries*, 18 – 20 September 2002, Bonn, Germany, pp. 2-13
- Matthews, Noble, Titus, Foster, Smith, Breithaupt, Kett (2002a): Tracking dinosaurs using low-altitude aerial photography at the Twentymile Wash dinosaur tracksite, Grand Staircase Escalante National Monument, Utah. *Abstract with Programs – Geological Society of America*, vol.34, no. 4, pp.6
- Matthews, Neffra, Noble, Breithaupt (2002b): An integrated approach to 3-dimensional data collection at dinosaur sites in the Rocky Mountain West. *Abstract with Programs - Geological Society of America*, vol.34, no.6, pp.204
- Mason, S., Rüther, H., Smit, J. (1997): Investigation of the Kodak DCS460 digital camera for small-aera mapping. *ISPRS Journal of Photogrammetry & Remote Sensing* 52, pp. 202-214
- McCleskey, B., Ball, J. W., Nordstrom, D. K., Holloway, J. M., Taylor, H. E. (2004): *Water-Chemistry Data for Selected Springs, Geysers, and Streams in Yellowstone National Park, Wyoming, 2001-2002*. U.S.G.S. Open-File Report 2004-1316
- Microsoft Research (2004): A Flexible New Technique for Camera Calibration. www.research.microsoft.com/~zhang/calib/

- National Park Service Water Resources Division (2001): Yellowstone National Park Small-Scale Base GIS Data. Fort Collins, CO
- NESPAL – National Environmentally Sound Production Agriculture Laboratory (2004): Developing an Airborne Digital Camera System. <http://nepsal.cpes.peachnet.edu/PrecAg/mpsphoto.asp>
- Nyquist, J. E. (1994): A “model” geophysics program, Proceedings of the Symposium on the Application of Geophysics to Environmental and Engineering Problems (SAGEEP). vol.1994, pp.817-824
- Palacio-Prieto, J. L., López-Blanco, J. (1994): Using video imagery for gully erosion evaluation. *Zeitschrift für Geomorphologie N. F.*, vol. 38, no. 1, pp. 33-43
- PCI Geomatics Enterprises Inc. (2003): Geomatica OrthoEngine. User Guide. Version 9.1, Richmond Hill
- Pittenger, T. (1977): Norris Geyser Basin Annual Report
- Planer-Friedrich, B. (2004): Volatile arsenic in aquatic environments. unpublished PhD thesis Technische Universität Bergakademie Freiberg
- Ries and Marzloff (2003): Monitoring of gully erosion in the Central Ebro Basin by large-scale aerial photography taken from a remotely controlled blimp. *CATENA*, vol. 50, Issues 2-4, pp 309-328
- Rinehart, J. S. (1976): A guide to geyser gazing. Hyper Dynamics, Santa Fe
- Rocco, P. (1984): Report on the Norris Geyser Basin 1984
- Rumerman, J. (2004): Modern-Day Airships. U.S. Centennial of Flight Commission, http://www.centennialofflight.gov/essay/Lighter_than_air/modern_airships/LTA18.htm
- Schreier, C. (1999): A Field Guide to Yellowstone’s Geysers, Hot Springs and Fumaroles. Homestead Publishing, Moose, Wyoming
- Smith, R. B., Siegel, L. J. (2000): Windows into the Earth – The Geologic story of Yellowstone and Grand Teton National Park. Oxford University Press, New York
- Spatial Analysis Center, Yellowstone National Park (1995): Boundary of Yellowstone National Park, Wyoming, Montana, Idaho. unpublished material
- Spatial Analysis Center, Yellowstone National Park (1997): Major Roads of Yellowstone National Park, Wyoming, Montana, Idaho. unpublished material
- Spatial Analysis Center, Yellowstone National Park (1998): 10m Digital Elevation Model for Yellowstone National Park, Wyoming, Montana, Idaho. unpublished material
- Spatial Analysis Center, Yellowstone National Park (2000): Major Lakes of Yellowstone National Park, Wyoming, Montana, Idaho (1:24,000).
- Technical Information Center, Denver Service Center (2004): Aerial photos from 1986 and 1993. written communication with Michelle Schneider (Michelle_Schneider@nps.gov)

- Thome, D. M., Thome, T. M. (2000): Radio-controlled model airplanes: inexpensive tools for low-level aerial photography. *Wildlife Society Bulletin*, vol. 28, no. 2; pp. 343-346
- Trimble (2004): Reflectorless total stations - LEICA TCR303 / 305 / 307. <http://www.leica-geosystems.com/surveying/product/totalstations/tcr300.htm>
- Tulsa World (2004): It's geek-meets-grape as wine producers get wired. newspaper, 21. April 2004
- Warner, W. S., Graham, R. W., Read, R. E. (1996): *Small format aerial photography*. Whittles Publishing
- Weilerwelding (2004): Chemical Product and Company Identification. www.weilerwelding.com/MSDS/helium.html
- Wester-Ebbinghaus, W. (1980): Aerial photography by radio controlled model helicopter. *Photogrammetrie Record*, vol. 10, no. 55, pp. 85-92
- WGIAC - Wyoming Geographic Information Advisory Council (2004): Topography maps. http://wgiac2.state.wy.us/scripts/drgemap/drge_Block.aspx?Lat=44&Long=110
- White, D. E., Hutchinson, R. A., Keith, T. E. C. (1988): *The Geology and Remarkable Thermal Activity of Norris Geyser Basin, Yellowstone National Park, Wyoming*. U.S.G.S. Professional Paper 1456
- Whittlesey, L.H. (1995): *Wonderful Nomenclature: A history of the place names of Yellowstone National Park, being a description of and guidebook to its most important natural features together with appendices of related elements*. Helena, MT, Montana Historical Society Press, 867 p.

9 APPENDIX

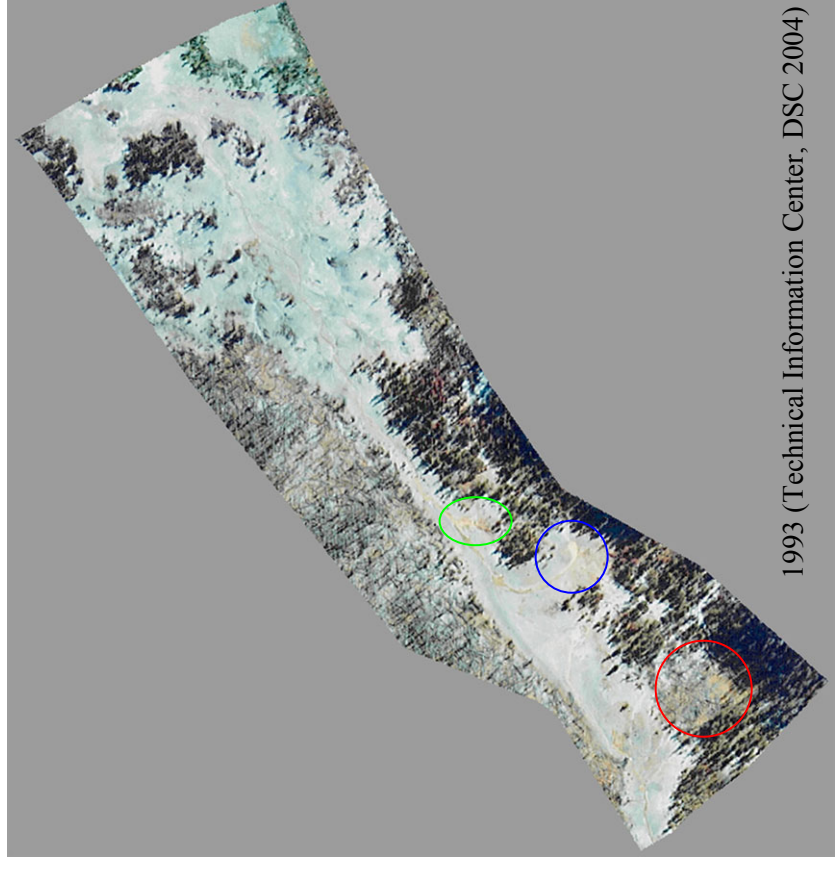
Appendix No. 9.1 Summary of water chemistry measurements and determined elements (Planer-Friedrich 2004)

| | Technique in the field/laboratory | Analyzed parameters (Detection Limit in mg/L) |
|---|--|---|
| In the field – On site parameters | WTW MultiLine P4, SenTix 97/T pH electrode, TetraCon 325 conductivity cell, redox Pt 4805/S7 probe, CellOx 325 probe | pH, EC, redox potential, dissolved oxygen, temperature |
| In the field – photometry | HACH photometer DR/890 | Total Fe, Fe ²⁺ , SiO ₂ , and S ²⁻ |
| In the field – Arsenic specification | Commercial cation (from Alltech) and anion (from Supelco) exchangers | As(III), As(V), MMAA, DMAA |
| Laboratory – TU Bergakademie Freiberg, Germany | LiquiTOC (Elementar Analysensysteme GmbH) | Total inorganic carbon (TIC), total organic carbon (TOC) (0.1) |
| | IC Merck Hitachi D 6000 (conductivity detector) | Cations: Mg ²⁺ (0.4), Ca ²⁺ (1.6), Na ⁺ (0.2), K ⁺ (1.0), Li ⁺ (0.1); Anions: Cl ⁻ (0.7), SO ₄ ²⁻ (2.0), F ⁻ (0.3), Br ⁻ (0.5), and NO ₃ ⁻ (0.5) |
| | Zeiss AAS EA4 using graphite furnace with platform technique | From ion exchangers: As(III), As(V), MMAA, DMAA From filtered, acidified sample: total As (1.5 µ/L) |
| Laboratory – U.S.G.S. Laboratories in Boulder, Colorado, USA | IC (Dionex model 2010i ion chromatograph) | Cl ⁻ (0.25), SO ₄ ²⁻ (1), F ⁻ (0.1), Br ⁻ (0.08), and NO ₃ ⁻ (0.06) |
| | ICP-AES (Leeman Labs Direct Reading Echelle) | As (0.04), Al (0.06), B (0.01), Ba (0.0008), Be (0.001), Ca (0.4), Cd (0.001), Co (0.002), Cr (0.002), Cu (0.003), Fe (0.007), K (0.04), Li (0.001), Mg (0.04), Mn (0.001), Mo (0.007), Na (0.1), Ni (0.002), Pb (0.008), Si (0.06), Se (0.04), Sr (0.0003), V (0.005), and Zn (0.004) |
| | PS Analytical, model Galahad (Cold Vapor Atomic Fluorescence Spectrophotometry) | Hg |
| Laboratory – Activation Laboratories, Canada (accredited by ISO 17025) | ICP-MS | Li, Be, Na, Mg, Al, Si, K, Ca, Sc, Ti, V, Cr, Mn, Fe, Co, Ni, Cu, Zn, Ga, Ge, As, Se, Br, Rb, Sr, Y, Zr, Nb, Mo, Ru, Pd, Ag, Cd, In, Sn, Sb, Te, I, Cs, Ba, La, Ce, Pr, Nd, Sm, Eu, Gd, Tb, Dy, Ho, Er, Tm, Yb, Lu, Hf, Ta, W, Re, Os, Pt, Au, Hg, Tl, Pb, Bi, Th, and U |

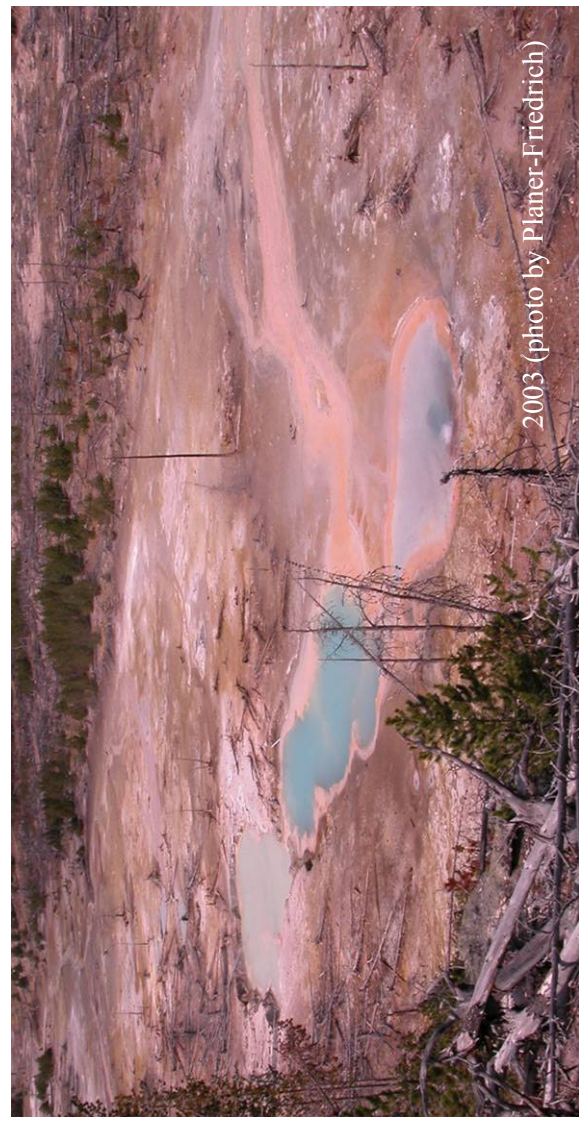
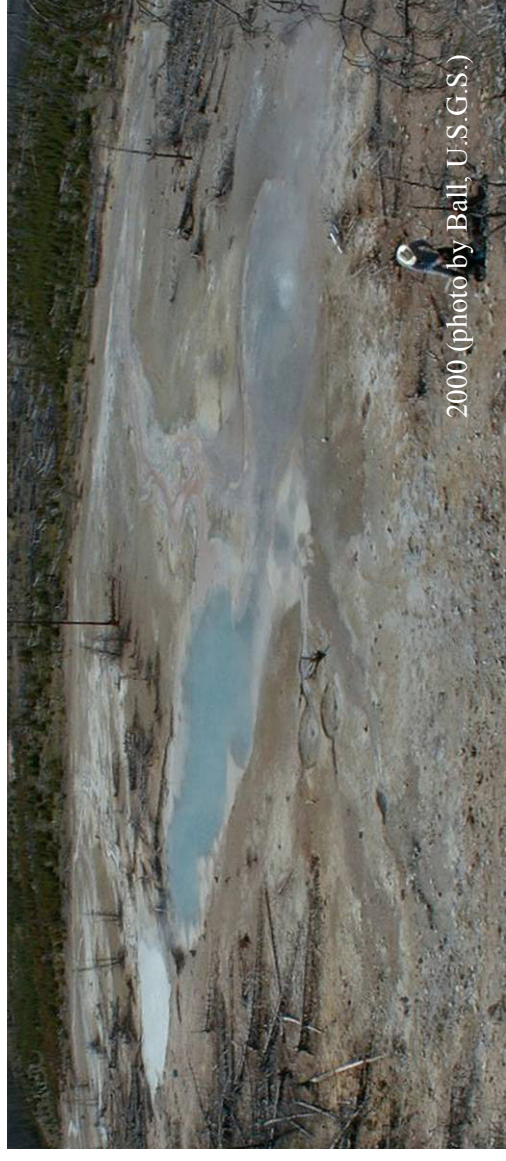
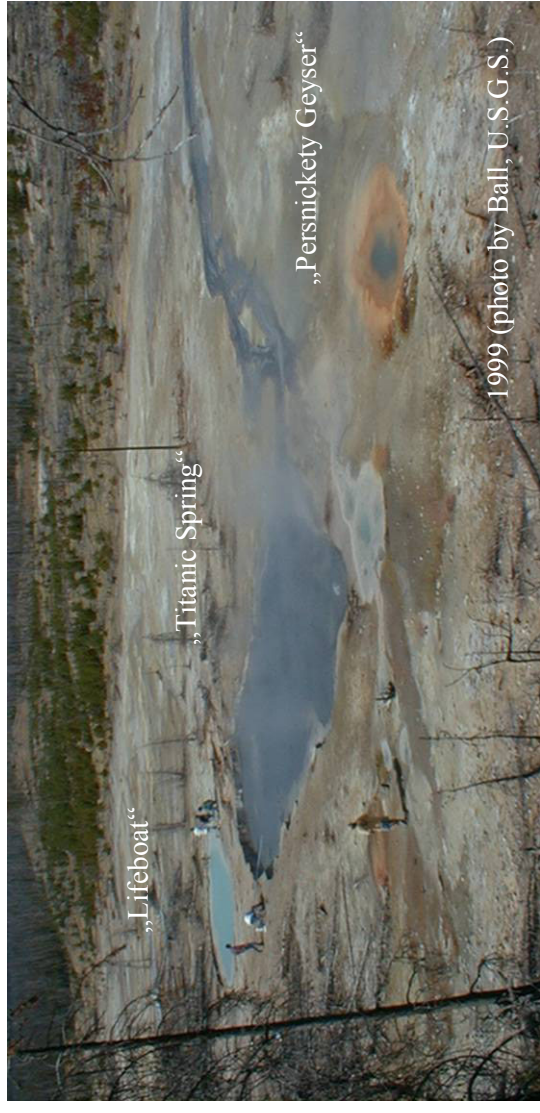
Appendix No. 9.3 Legend (part B) of the geological map in the section “Situation of Ragged Hills in the YNP (overview)”

| LIST OF MAP UNITS | |
|---|--|
| [See text for complete description of map units] | |
| Surficial deposits (Holocene and Pleistocene)—Age ranges of individual units overlap | |
| | Detrital deposits |
| | Hot-spring deposits |
| | Cemented ice-contact deposits localized by hot springs |
| | Hydrothermal-explosion deposits |
| Plateau Rhyolite (Pleistocene) | |
| Central Plateau Member | |
| | Pitchstone Plateau flow |
| | Grants Pass flow |
| | Moose Falls flow |
| | West Yellowstone flow |
| | Trischman Knob dome |
| | Douglas Knob dome |
| | Tuff of Cold Mountain Creek |
| | Solfatara Plateau flow |
| | Hayden Valley flow |
| | Bechler River flow |
| | Summit Lake flow |
| | Buffalo Lake flow |
| | Spring Creek flow |
| | Nez Perce Creek flow |
| | Spruce Creek flow |
| | Elephant Back flow |
| | West Thumb flow |
| | Aster Creek flow |
| | Tuff of Bluff Point |
| | Mary Lake flow |
| | Dry Creek flow |
| Roaring Mountain Member | |
| | Crystal Spring flow |
| | Gibbon River flow |
| | Obsidian Cliff flow |
| | Cougar Creek dome |
| | Riverside flow |
| Mallard Lake Member | |
| | Mallard Lake flow |
| Obsidian Creek Member | |
| | Gibbon Hill dome |
| | Paintpot Hill dome |
| | Willow Park dome |
| | Apollinaris Spring dome |
| | Landmark dome |
| | Rhyolite-basalt mixed lavas of Gardner River |
| | Rhyolite-basalt mixed lavas of Grizzly Lake |
| Upper Basin Member | |
| | Scaup Lake flow |
| | Biscuit Basin flow |
| | Dunraven Road flow |
| | Canyon flow |
| | Tuff of Sulphur Creek |
| | Tuff of Uncle Tom's Trail |
| | Gerrit Basalt (Pleistocene) |
| | Osprey Basalt (Pleistocene)—Includes some gravel |
| | Madison River Basalt (Pleistocene) |
| | Sediments (Pleistocene)—Interlayered with Plateau Rhyolite |
| | Falls River Basalt (Pleistocene) |
| | Swan Lake Flat Basalt (Pleistocene) |
| | Basalt of Geode Creek (Pleistocene) |
| | Basalt of Mariposa Lake (Pleistocene) |
| Lava Creek Tuff (Pleistocene) | |
| | Member B |
| | Member A |
| | Undine Falls Basalt (Pleistocene)—Includes some gravel |
| Mount Jackson Rhyolite (Pleistocene) | |
| | Mount Haynes flow |
| | Big Bear Lake flow |
| | Harlequin Lake flow |
| | Flat Mountain flow |
| | Wapiti Lake flow |
| | Moose Creek Butte flow |
| | Lewis Canyon Rhyolite (Pleistocene) |
| | Basalt of Warm River (Pleistocene) |
| Island Park Rhyolite (Pleistocene) | |
| | Warm River Butte dome |
| | Mesa Falls Tuff (Pleistocene) |
| | Sediments and basalts of The Narrows (Pleistocene) |
| Huckleberry Ridge Tuff (Pliocene) | |
| | Member C |
| | Member B |
| | Member A |
| | Junction Butte Basalt (Pliocene)—Includes some gravel |
| | Conant Creek Tuff and tuff of Kilgore (Pliocene) |
| | Gravel of Mount Everts (Pliocene) |
| | Heart Lake Conglomerate (Pliocene) |
| | Intrusive rocks (Tertiary) |
| | Volcanic rocks (Tertiary) |
| | Sedimentary rocks (Paleocene and Mesozoic) |
| | Sedimentary rocks (Paleozoic) |
| | Metamorphic rocks (Precambrian) |
| Contact—Dotted where concealed | |
| | Lava-flow front—Hachures on side of younger flow; dotted where concealed |
| Lava-flow form lines | |
| Faults—Dotted where concealed | |
| | Normal—Bar and ball on downthrown side |
| | Reverse—Teeth on overriding block |
| | Reverse (with later normal movement)—Teeth on overriding block of reverse fault; bar and ball on downthrown side of normal fault |
| | Low angle fault—Sawteeth on upper plate |
| Strike and dip of bedding | |
| | Inclined—Angle of dip shown where known |
| | Horizontal |
| | Overturned—Angle of dip shown where known |
| | Area of hydrothermal acid alteration |
| | Volcanic vent |
| | Localities of analysed sample—See table 4 |
| | Drill hole locality |

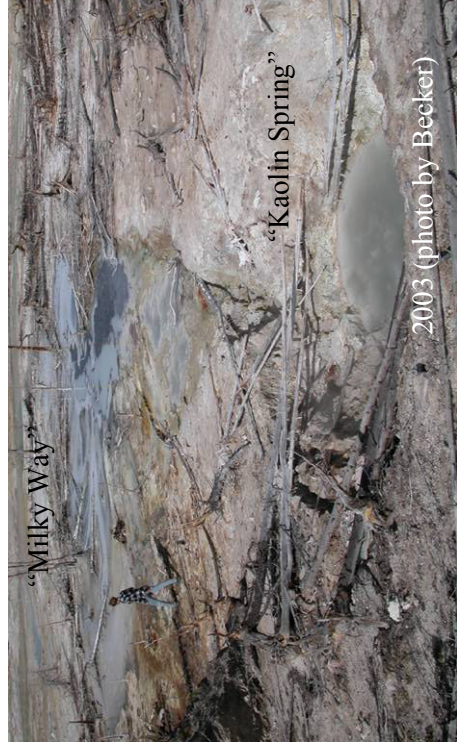
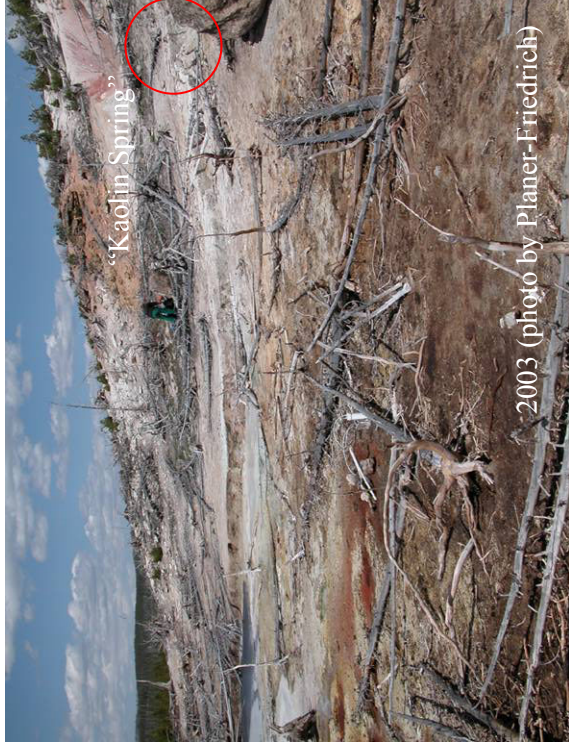
Appendix No. 9.4 Overview aerial photos 1986 and 1993



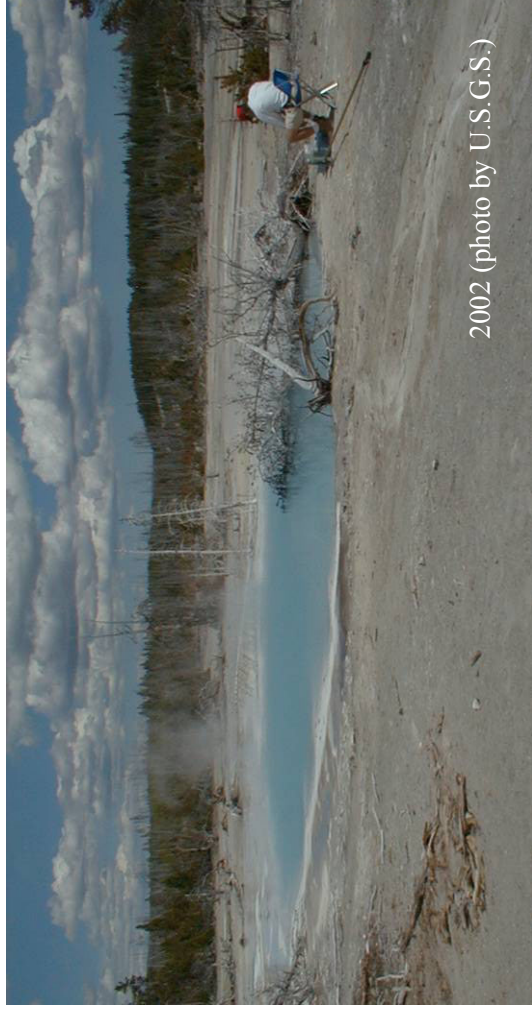
Appendix No. 9.5 Overview “Persnickety Geyser”, “Titanic Spring”, and “Lifeboat”



Appendix No. 9.6 Overview “Kaolin Spring” and “Milky Way”



Appendix No. 9.7 Overview "Elk"



Appendix No. 9.8 Overview "Rainbow Growler"

